SYNTHETIC MODIFICATION OF POLY(AMIDOAMINE) STARBURST DENDRIMERS BY ACYLATION AND A STUDY OF THEIR NMR AND VIBRATIONAL SPECTRA

A Thesis

Presented in Partial Fulfillment of the Requirements for

the Degree Master of Science in the

Graduate School of The Ohio State University

By

Anthony Paul Davis, B.S.

*****

The Ohio State University
2002

Master's Examination Committee:

Dr. Heather C. Allen, Adviser

Dr. Jonathan R. Parquette

Approved by

_____

Adviser
Department of Chemistry

ABSTRACT

A commercially available dendrimer, poly(amidoamine) (PAMAM) is studied at the G0 and G1 levels, first by ^{1}H and ^{13}C NMR for characterization purposes. Bulk vibrational IR and Raman spectra are presented and compared to calculated vibrational predictions. The G0 dendrimer is modified by acylation with both acetic anhydride and d_6-acetic anhydride, and the NMR and bulk vibrational spectra of these compounds are also presented and compared to calculated vibrational predictions. Finally, the surface properties of the PAMAM dendrimers and of the acylated PAMAM dendrimers are probed with sum frequency generation.

The ^{1}H NMR spectra of the PAMAM and acylated PAMAM dendrimers are consistent with the structures. A comparison between G0 and G1 ^{1}H NMR spectra indicates that as the generations increase, each new branch is nearly chemically equivalent to the branches of the preceding generation. Differences occur only in that as the terminating groups move outward in generation, the previous generation shifts in relation to the generation or core that preceded it, and the unique chemical shifts representing the terminating groups represent the outer generation only. The ^{13}C NMR spectra represented only the number of chemically equivalent carbons in each molecule.

The vibrational mode calculations were limited to the C-H and N-H stretching regions because the wavelengths provided by our instruments for sum frequency generation are resonant with the frequencies found in that region of the vibrational

spectrum. The calculated predictions indicated several mixed bands of vibrational modes in the CH_2/CH_3 stretching region and three bands in the NH/NH_2 region, representing N-H stretches, NH_2 symmetric stretches, and NH_2 asymmetric stretches. IR studies revealed broad C-H absorptions and two resolvable absorptions in the N-H region. Raman studies were limited to the C-H region due to molecular fluorescence and detector limits, but three resolvable peaks were recorded. Preliminary sum frequency generation studies at the air-dendrimer interfaces indicated a randomly skewed surface orientation of the dendrimer branches in a distribution about the surface normal.

Dedicated to the memory of James Oliver Edward Davis

May 2, 1918 – March 3, 2001

ACKNOWLEDGMENTS

I wish to thank my adviser, Dr. Heather Allen, for being my adviser. I would also like to thank Drs. Susan Olesik and Terry Gustafson for participating on my Advisory Committee.

I wish to thank all of the past and present members of the Allen Research Group for their collaborative help, but in particular, I would like to thank Dr. Gang Ma for his hard work and invaluable assistance.

I wish to thank Dr. Jonathan Parquette and Noel Paul of the Parquette Research Group for their tremendous help with the organic synthesis portion of this project. Also, I would like to thank all of the present members of the Parquette Research Group who lent their assistance on this project.

I wish to thank Dr. Chris Hadad and John Merle of the Hadad Research Group for their help with the computational portion of this project. Also, Dr. Jim Coe and Shaun Williams of the Coe Research Group lent their assistance in this area, and Dr. Terry Gustafson and Frank DeLucia of the Gustafson Research Group provided computer resources from their research lab. Computational funding was provided by a resource grant from the Ohio Supercomputer Center.

I wish to thank Dr. Richard McCreery and Belinda Hurley of the McCreery Research Group for the use of the Laser Spectroscopy Center and for Belinda's technical assistance.

I would like to acknowledge Dr. Michael Freitas for the use of a C-language computer program he issued as an homework assignment in his course, *Principles of Analytical Processes*, as the shell for the VibSpec 1.1 computer program found in Appendix A.

I would like to thank InPhotonics, Inc., and Process Instruments, Inc., for the use of the 785 nm diode laser/Raman probe setup.

I would like to thank Dr. Gordon Renkes for his technical advice and assistance, and also Leah Blatzer of the Turro Research Group for her technical assistance.

I wish to thank the United States Coast Guard for the support and funding of this program, but in particular, I would like to thank: Dr. Thomas Haas, CAPT, USCG (Ret.) for his mentorship; CAPT Richard Gaines, USCG, for selecting me into the Advanced Education Program; and CAPT Jerzy Kichner, USCG, for his support during the selection process and during my academic preparation for this program.

Lastly, I would like to thank my family and friends for the support provided to me throughout this program – above all others: my wife, Kimberly, and my father and stepmother, James and Connie Davis. Thank you all.

VITA

October 15, 1972	Born – Lawrenceburg, Indiana
1994	B.S. (with High Honors), Marine Science, United States Coast Guard Academy.

FIELDS OF STUDY

Major Field: Chemistry

TABLE OF CONTENTS

LIST OF TABLES

LIST OF FIGURES

LIST OF ABBREVIATIONS

Abbreviation	Definition
^{1}H	hydrogen (atomic mass = 1 amu)
^{13}C	carbon-13 (atomic mass = 13 amu)
3-D	three-dimensional
Ac	acetyl group (CH_3CO-)
AcPAMAM	acetylated poly(amidoamine) starburst dendrimer
AES	Auger electron spectroscopy
AFM	atomic force microscopy
amu	atomic mass units
as	asymmetric stretch
BBSFG	broadband sum frequency generation
°C	degrees Celsius (centigrade)
CCD	charge-coupled device
cm^{-1}	wavenumbers
CW	continuous wave
d-	deuterated (subscript denotes number of deuterons)
DFG	difference frequency generation
DMAP	4-dimethylaminopyridine
DMF	dimethylformamide
DNA	deoxyribonucleic acid

En	ethylenediamine
fr	Fermi resonance
fs	femtosecond
FTIR	Fourier transform infrared absorption spectroscopy
g	gram
g/mm	grooves per millimeter
G#	generation (# number denotes generation level)
HPLC	high-performance liquid chromatography
IR	infrared
kHz	kilohertz
M	molarity (moles per liter)
mg	milligram
MHz	megahertz
mL	milliliter
μJ	microjoule
μm	micrometer
mm	millimeter
mmol	millimole
MΩ	megaohm
Mw	megaword
mW	milliwatt
nm	nanometer
NMR	nuclear magnetic resonance spectroscopy
NSOM	near-field scanning optical microscopy

OPA	optical parametric amplifier
PAMAM	poly(amidoamine) starburst dendrimer
ppm	parts per million
ps	picosecond
PVP	poly(4-vinylpyridine) polymer
RMS	root mean square
rpm	revolutions per minute
SDS	sodium dodecyl sulfate
SFG	sum frequency generation
SHG	second harmonic generation
ss	symmetric stretch
TLC	thin layer chromatography
UV	ultraviolet
vol %	volume percent
wt %	weight percent
XPS	X-ray photoelectron spectroscopy

CHAPTER 1

SYNTHETIC MODIFICATION OF PAMAM DENDRIMERS BY ACYLATION

1.1: Introduction.

1.1.1: Background. The broad description of molecules included in the category of polymeric molecules fails to capture the virtually infinite combinations of compounds possible for use in research and technology. Generally, when one considers the term "polymer", a simplistic image of a straight-chain molecule of one or two repeating units comes to mind, in the manner of a compound like polyethylene or polystyrene. However, with a small amount of imagination, one can see that polymers could become much more complex, with branching units and/or multiple linkages.

All polymers can be subdivided into four categories: linear, cross-linked, branched, and dendritic (Figure 1.1) (Esfand and Tomalia 2001). Linear polymers are simply straight-chain polymers made up of any number of monomers linked end-to-end. It is also possible to construct a linear polymer with certain functionalities that are capable of cross-linking into a mesh-like molecule by either covalent and/or hydrogen bonding. These cross-linked polymers comprise the second category of polymers and generally become denser as the cross-linked bonds increase in number and strength. The third category, branched polymers, is composed of polymers constructed from monomeric units bearing a non-polymerizing molecular branch; the resulting molecule is

essentially a linear polymer with any number of branches, as the name implies. Extending this idea generates the fourth and final category; if the molecular branches are capable of additional polymerization, a "hyperbranched" molecule would be the result. These extra branches could be regular or random throughout the molecule, and it is conceivable for any branch to have additional branches. The category of hyperbranched molecules is referred to as the dendritic polymers, owing to their similarity to the branches of a tree (Tomalia 1995).

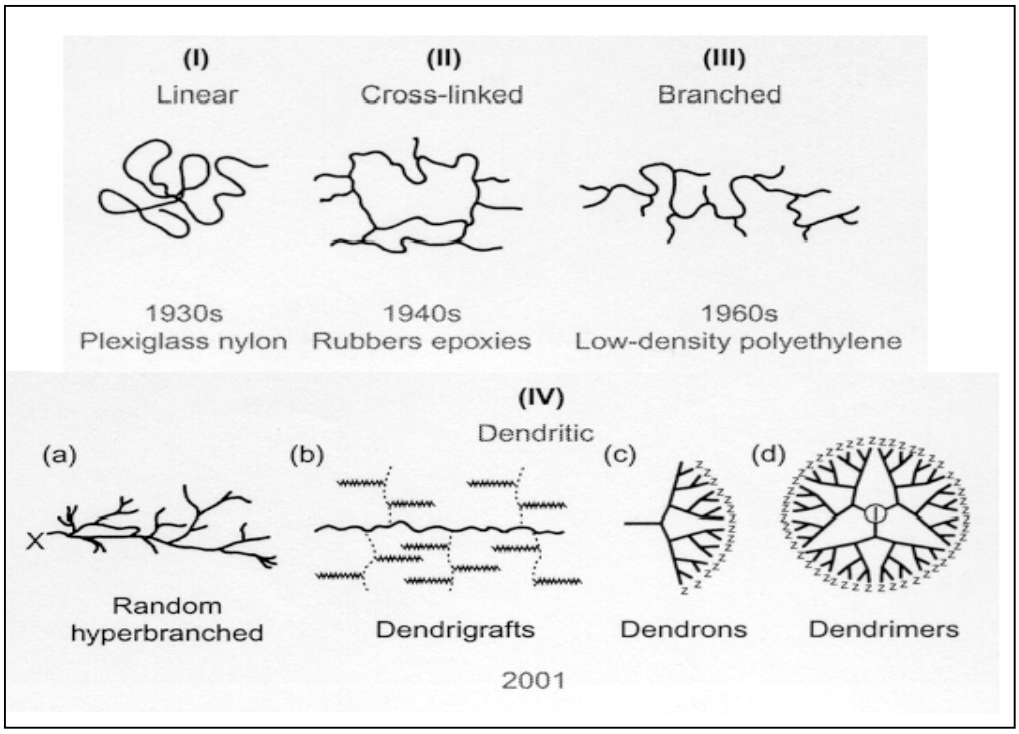

Figure 1.1: A pictorial description of the various categories of polymeric molecules (Esfand and Tomalia 2001).

A unique class of dendritic molecules has been subdivided from the category of hyperbranched molecules. These molecules are distinguished from randomly

hyperbranched dendritic polymers in that each monomer joins the polymer at one site and adds two or more additional sites for further polymerization. In this way, the molecule expands in an extremely ordered, exponentially geometric fashion with each successive generation of monomeric units. A molecule constructed this way into a single branch or fan is referred to as a "dendron"; when two or more dendrons are bonded to a core molecule, such as ammonia or ethylenediamine, the polymer is referred to as a "dendrimer."

The invention of the dendrimer is attributed to Donald Tomalia, who first published his report of poly(amidoamine) dendrimer synthesis in 1979 from his laboratory at the Michigan Molecular Institute in Midland, Michigan (Tomalia 1995). His first poly(amidoamine) dendrimer was the result of reacting three methylacrylate molecules to an ammonia core, followed by the addition of three ethylenediamine molecules to form the G0 amidoamine. By continuing this two-step process of methylacrylate/ethylenediamine addition, successive amidoamine generations are produced, doubling the number of terminal amine groups each time (Tomalia 1995). Concurrently, Fritz Vögtle of the University of Bonn published his own dendrimer synthesis consisting of ammonia derivatives with acrylonitrile. Later, George Newkome would publish an alternative synthesis of similar molecules that he called "arborols," after the tree-like symmetry, but his 1985 discovery would be largely overshadowed four years later when a collaboration between Cornell University and AT&T Laboratories would revolutionize dendrimer synthesis, setting off an explosion of dendrimer research around the globe (Tomalia 1995).

The synthesis published by Tomalia began at the initiating core and expanded outward in a divergent manner with each generation, creating the term "divergent synthesis." This divergent synthesis created several problems with impurities that compound themselves with the addition of each generation. First, as with any reaction, the desired product almost never occurs 100% of the time. In dendrimer synthesis, the successful addition of a generation requires several reactions on each molecule; even for a reaction that succeeds 99.9% of the time, the number of defective molecules produced becomes significant as the required number of successful reactions per molecule increases exponentially with each generation. In the case of poly(amidoamine), ethylenediamine is equally reactive at both ends; during the second step of the amidoamine synthesis, ethylenediamine is capable of bonding once, looping two dendrimer branches together, or linking two dendrimer molecules together. A large excess of ethylenediamine can reduce the occurrence of these defects, but they cannot be eliminated. In addition, ethylenediamine has replaced ammonia as the initiator core molecule in PAMAM synthesis. Because such a large excess of ethylenediamine is required in the second step, it is impossible to completely remove every residual molecule during the synthetic work-up. When PAMAM G0 is subjected to the two-step synthesis to create G1, any residual ethylenediamine acts as a new initiator core and becomes a G0 molecule. When PAMAM G1 is made into generation 2, the G0 molecules become G1, and the residual ethylenediamine becomes G0. This pattern continues such that in every generational batch of PAMAM, every lower generation is represented as an impurity referred to as "trailing generations."

In 1989, Jean Fréchet of Cornell University and Timothy Miller of AT&T Laboratories jointly developed a convergent synthesis for producing dendrimers. Rather than beginning with a core molecule and building each generation onto the core outwardly, Fréchet and Miller were able to begin with the dendrimer periphery and inserted the molecular core as the last step. In this manner, high-purity dendrons of the desired generation could be synthesized, and then by reacting these dendrons with the core molecule, dendrimers could be produced with the same high purity. Prior to the development of convergent dendrimer synthesis, only a handful of scientific papers had been published on dendrimer research; in the five years that followed, dendrimer research literally exploded within the scientific community (Tomalia 1995).

Because of their early discovery and thus the amount of research that has been conducted with them (Bosman, Janssen et al. 1999), PAMAM dendrimers are among the very few commercially available dendrimers, available in generations 0 to 10 from Aldrich, Inc. PAMAM G0 ($[\text{-}CH_2N(CH_2CH_2CONHCH_2CH_2NH_2)_2]_2$) and PAMAM G1 ($[\text{-}CH_2N[CH_2CH_2CONHCH_2CH_2N(CH_2CH_2CONHCH_2CH_2NH_2)_2]_2]_2$) are both packaged as a 20 wt % solution in methanol. Because dendrimers increase their molar mass by a factor of approximately two with each successive generation, a 20 wt % solution results in increasingly smaller concentrations of each generation for the same quantity purchased. For example, a 5-g bottle of PAMAM G0 20 wt % in methanol contains 1.94 mmol of dendrimer, while a 5-g bottle of PAMAM G1 20 wt % in methanol contains 0.699 mmol of dendrimer, or very roughly one-half of the stoichiometric quantity of the preceding generation. The PAMAM dendrimers available from Aldrich, Inc., are prepared by a divergent synthesis.

There are three simple formulae for calculating dendrimer properties as a function of generation. The first formula calculates the number of surface groups, Z, as a function of generation, G:

$$Z(G) = N_c \cdot N_b^G \qquad (1)$$

where N_c represents the number of reactive sites on the initiator core molecule, and N_b represents the number of reactive sites at the end of each repeating branch (Esfand and Tomalia 2001). For PAMAM, N_c is four for the ethylenediamine core, and N_b is two for the terminating amine on each amidoamine branch (Table 1.1). N_b^G equates to the number of surface groups per dendron, and N_c is essentially a multiplier representing the number of dendrons bonded to the core. The second formula calculates the number of non-terminating branch cells, BC, as a function of generation, G:

$$BC(G) = N_c \cdot \left[\frac{N_b^G - 1}{N_b - 1} \right] \qquad (2)$$

The expression in parentheses represents the number of branch cells per dendron (Esfand and Tomalia 2001). The expression can be explained by noting that the numerator contains the number of surface groups per dendron minus one, and the denominator contains one less than the number of reactive sites at the end of each repeating branch. Each surface group is attached to the end of a terminating branch, which is not counted as a branch cell. For the dendrimer where N_b equals two, as in PAMAM, there must be one half the number of branch cells from the preceding generation to support the number of terminating branches, or N_b^G. In addition, there must be one half as many branch cells in the generation before that to support those branch cells, and so on. For a molecule in the third generation, N_b^G would be 2^3, or eight surface groups per dendron. To support eight

terminating branches, four branch cells are required from generation two, which require two branch cells from generation one, which require one branch cell from generation zero. This requirement totals seven branch groups, or $N_b^G - 1$. To account for dendrimers with N_b values of three or more, the $N_b - 1$ term is placed in the denominator. The utility of equation (2) is found in equation (3), the formula for molecular weight, MW:

$$MW(G) = M_c + N_c \cdot \left[M_{bc} \cdot \left(\frac{N_b^G - 1}{N_b - 1} \right) + M_{tb} \cdot N_b^G \right] \qquad (3)$$

where M_c is the molar mass of the initiator core, M_{bc} is the molar mass of one branch cell, and M_{tb} is the molar mass of one terminating branch (Esfand and Tomalia 2001). It is important to note that the correct molar masses may be slightly lower than first assumed; for example, M_c for PAMAM is 56 g/mol, four g/mol less than a complete ethylenediamine molecule due to the loss of four hydrogen atoms from the initiator core molecule in bonding. Using the above equation in Table 1.2, it can be shown that as the generational number increases, the increase in molecular weight between generations approaches a factor of two.

N_c	4
N_b	2
M_c	56.068 g/mol
M_{bc}	113.140 g/mol
M_{tb}	115.156 g/mol

Table 1.1: Values for dendrimer equation variables as they apply to PAMAM dendrimers.

G	Z(G)	BC(G)	MW(G)	MW Increase
0	4	0	516.692 g/mol	----------
1	8	4	1.430×10^{3} g/mol	× 2.767
2	16	12	3.256×10^{3} g/mol	× 2.277
3	32	28	6.909×10^{3} g/mol	× 2.122
4	64	60	1.421×10^{4} g/mol	× 2.057
5	128	124	2.883×10^{4} g/mol	× 2.028
6	256	252	5.805×10^{4} g/mol	× 2.014
7	512	508	1.165×10^{5} g/mol	× 2.007
8	1,024	1,020	2.334×10^{5} g/mol	× 2.003
9	2,048	2,044	4.672×10^{5} g/mol	× 2.002
10	4,096	4,092	9.347×10^{5} g/mol	× 2.001

Table 1.2: Values for dendrimer equations as they apply to PAMAM dendrimers from generation 0 to 10. G: generation; Z: number of terminating groups; BC: number of branch cells; MW: molecular weight

The potential for new dendrimer applications is as diverse as the very nature of the chemical versatility of dendrimers. They are well suited for new avenues in materials science in keeping with their characterization as polymers, but due to their uniquely uniform structure, there are many other promising areas for which dendritic molecules are being developed. For example, as dendrimers grow generationally, they quickly become macromolecular in size; this fact could be used to mechanically remove them from a solution by filtration. Often, expensive catalysts are unrecoverable during the product work-up after a chemical reaction. A macromolecular dendrimer modified at the periphery with an appropriate catalyst could be recovered from a reaction mixture by filtration and recycled (Service 1995). Another important application is in the area of biomimicry. Many biologically significant molecules, including insulin, cytochrome C, and hemoglobin, are of the same spherical shape and diameter as certain dendrimer molecules (Sayed-Sweet, Hedstrand et al. 1997). There is hope that dendrimer molecules could be developed to carry out therapeutic functions by blending in with these important natural molecules. Dendrimers have already been used to successfully mimic histone, a molecule used by the body to coil strands of DNA, in gene therapy research on laboratory rats (Service 1995). Yet another area of prolific dendrimer research is that of drug delivery. Dendrimers of fourth or fifth generation tend to become rigid as the molecular periphery becomes highly populated and sterically crowded; likewise, the interior regions of these molecules are relatively hollow, providing protected space for a potentially sensitive drug molecule. A dendrimer could be developed to protectively carry a drug to a particular site in the body before it is chemically released to carry out its function (Esfand and Tomalia 2001).

1.1.2: Motivation for research. With the many exciting prospects ahead for the future of dendritic polymers, organic and bioorganic chemists have their work cut out for them in designing and synthesizing novel new dendrimers. But in order to find molecules that perform their intended functions, a great deal of research into their physical properties must be completed to understand how they behave. This inevitably requires developing analytical techniques to investigate these properties.

Among the physical properties of dendrimers that have garnished the most attention are molecular dimensions, uniformity of size and shape, degree of rigidity, location of terminating groups, and behavior on liquid and solid surfaces (Bosman, Janssen et al. 1999). In the younger generations of dendrimers, one would expect that their physical properties would parallel conventional molecules in that their size, shape, and relative complexity are not very different from other molecules. As the generation increases to generations two, three, and four, dendrimers begin to expand rapidly in size and mass. Further, while the dendritic branches may still be relatively free in motion, the periphery of the molecule becomes more crowded until the molecule can no longer "lie flat"; even in the least energetic conformation, the molecules are forced to take on a macromolecular, three-dimensional shape. Above generation four, dendrimers like PAMAM are considered to be globular and/or spherical in shape, and as the generations progress upward, the molecules become more rigid until the molecules cannot accept the addition of another complete generation (Bosman, Janssen et al. 1999). Various studies have begun to disclose other unique behaviors of dendrimers. For example, studies at the Michigan Molecular Institute indicate that the size and dimensions of higher-generation PAMAM remain constant over changes of temperature and solvent quality, refuting the

idea that these molecules might unravel to some extent under favorable conditions (Topp, Bauer et al. 1999). On the other hand, according to research at Columbia University, PAMAM dendrimers may undergo pH-dependent internal conformational changes as the amines become protonated and carry a positive charge. Theoretically, the electrostatic repulsion between internal amines would drive the molecule into a more expanded configuration, encouraging the branches to spread out (Chen, Tomalia et al. 2000).

Although there is much left to be done with bulk and solution studies such as these, molecular behavior at surfaces and interfaces can be quite unique. Changes in interfacial behavior can potentially influence a compound's practical applications in that surface activity can alter molecular uptake by a surrounding environment, or perhaps a tendency toward monolayer self-assembly could lead to coating, film, and/or membrane applications. Studying surfaces and interfaces ushers in completely different challenges, as there are few analytical techniques that can differentiate between a surface or interface and the bulk properties of a substance. Three of the most important surface analysis methods are X-ray photoelectron spectroscopy (XPS), Auger electron spectroscopy (AES), and electron microscopy. The first two techniques provide information about the elemental composition of a surface, and to discriminate between surfaces and bulk, they both rely on the inability of electrons to escape more than a few atomic layers. The third technique, electron microscopy, while highly developed for different applications, can rarely be expanded beyond topographical imaging (Skoog and Leary 1992). Near-field scanning optical microscopy (NSOM) is capable of spectroscopically acquiring chemical information at surfaces by combining electron microscopy technology with specially fabricated, ultra-fine fiber optics. However, NSOM is currently limited by issues relating

to the cost of tip manufacture, to methods of providing surface-tip feedback (Dunn 1999), and to its inability to probe subsurface interfaces.

Another surface-specific optical technique that has been gaining prominence in the past twenty years is second-order nonlinear spectroscopy, namely second harmonic, sum frequency, and difference frequency generation. Rather than depending on penetration depths, as with an evanescent wave, or upon absorption by the bulk, as with XPS and AES, second-order nonlinear methods depend upon lack of inversion symmetry for signal intensity. While many crystalline substances possess asymmetry about a center of inversion, all substances are asymmetrical at a surface, or more appropriately, an air-liquid, air-solid, liquid-liquid, liquid-solid, or solid-solid interface. To date, no work to our knowledge has been published investigating the surface behavior of dendrimers by second-order nonlinear spectroscopic methods. Atomic force microscopy has been used extensively to study molecular dimensions, shape, and orientation of dendrimers on surfaces (Hierlemann, Campbell et al. 1998; Lackowski, Campbell et al. 1999; Imae, Ito et al. 2000; Li, Piehler et al. 2000; Sui, Micic et al. 2000; Betley, Holl et al. 2001). A plethora of other studies exist probing various surface dendrimer properties, such as measuring adsorption with a quartz crystal microbalance (Rahman, Durning et al. 2000), testing chemical sensor potential with a surface acoustic wave mass balance (Wells and Crooks 1996), observing dendrimer adsorption onto a self-assembled monolayer by attenuated total reflectance surface enhanced infrared absorption spectroscopy (Nagaoka and Imae 2001), and another study that combined some of these techniques with ellipsometry, contact-angle measurements, ac-impedance spectroscopy, and cyclic voltammetry to observe the orientation of PAMAM dendrimers on different types of

surfaces (Tokuhisa, Zhou et al. 1998). But a recent review by Tully and Fréchet concluded that the current expense of dendrimer production made them well suited for interfacial applications where only small amounts are required (Tully and Fréchet 2001), and thus any new analytical technique that can help to better explain the behavior of these unique molecules at interfaces would be of considerable benefit. The challenge for second-order nonlinear spectroscopy in this arena is in developing a way to add specific spectroscopic contrast to dendrimers.

Much of the work that has been published involves modifying dendrimer molecules, synthetically or otherwise, to make them detectable by some well-established analytical method. In Manchester, England, researchers reacted 4-acetamidobenzene sulphonyl chloride with PAMAM G2 to yield a fully substituted sulphonamide. This compound was hydrolyzed to the sulphanilamide hydrochloride, diazotised, and coupled with 2-naphthol-3,6-disulphonic acid disodium salt, to yield an orange dye (Ahmed, Budd et al. 2001), making it detectable by UV-visible absorption spectroscopy. Other UV-visible spectroscopy work is being combined with fluorescence lifetime measurements at the University of Missouri-Columbia, where the solvatochromic probe phenol blue was used to "stain" regions of poly(propyleneimine) and PAMAM dendrimers to study the physical behavior of the moderately hollow microcavities believed to lie near the dendrimer core (Richter-Egger, Tesfai et al. 2001). The same group in Missouri has investigated the theoretical molecular micelle properties of carboxylate-terminated (half-generation) PAMAM using fluorescent polyaromatic hydrocarbons in tandem with nitromethane, a known selective quenching agent for the hydrocarbons (Wade, Torres et al. 1999). At the University of South Florida, researchers

have synthesized a novel series of structured dendritic macromolecules incorporating covalently linked electroactive diaminoanthraquinones (Newkome, Narayanan et al. 1997), opening the door to the use of electrochemical analysis. A more technical analysis was conducted by the laboratories at the National Institute of Standards and Technology to calculate the radius of gyration of the terminal groups of PAMAM dendrimers. By using small-angle neutron scattering with deuterium labeling and scattering contrast variation, they determined that PAMAM G7 terminal groups concentrate at the periphery, rather than fold back, as calculations suggest (Topp, Bauer et al. 1999). Because the frequencies employed in the sum frequency generation setup in our research lab are in the infrared, a reasonable approach to providing second-order nonlinear spectroscopic contrast to dendrimer molecules would be to modify them in such a way as to alter their vibrational spectrum. One method that was suggested was to append a deuterated methyl functionality to the periphery of the PAMAM molecules, so that the methyl C-H stretching frequencies would be red-shifted away from the large aliphatic C-H stretch absorption centered around 2900 cm^{-1}. Considering the size of dendrimer molecules and the abundance of methylene groups, their vibrational spectra must have numerous vibrational modes in the aliphatic C-H stretch region. Even PAMAM G0, the smallest PAMAM dendrimer, has 246 vibrational modes and eighteen methylene groups; thirty-six of the vibrational modes are found in the C-H stretch region (Appendix B).

The creativity of the synthetic chemist has underscored the seemingly infinite ways in which dendritic molecules can be manipulated to express different properties. At the Michigan Molecular Institute, where Tomalia developed his first dendrimers, researchers have shown that dendrimer generations can be alternated or radially layered,

in this case between hydrophilic amidoamine and hydrophobic organosilicon (Dvornic, de Leuze-Jallouli et al. 2000). Chemical engineers at the State University of New York at Buffalo synthesized a complexing inorganic/organic SiO_2-PAMAM dendrimer hybrid (Ruckenstein and Yin 2000). In a utilitarian approach to dendrimer functionality, the Materials Science Center at the Indian Institute of Technology, Kharagpur, India, synthesized a photoresponsive, photoswitching PAMAM using a convergent synthesis to an azobenzene *trans/cis*-switching central core (Ghosh and Banthia 2001). Here at the Ohio State University, dendritic conformational structure was controlled by synthesizing dendrons capable of intramolecular hydrogen bonding (Huang and Parquette 2000), creating a conformational dependence on solvent, temperature, and generation (Recker, Tomcik et al. 2000). And finally, chemists at Sheffield University in the United Kingdom used protecting groups in both divergent/convergent and divergent/divergent syntheses of unsymmetrical dendrimers with two, three, and even four different functionalities in one molecule (Martin and Twyman 2001). The imagination is apparently the limit to how dendrimers can be crafted to suit various research needs.

1.1.3: Synthetic Approach. There are several possible mechanisms capable of appending a methyl functionality to the terminating groups of a PAMAM dendrimer. In addition, PAMAM dendrimers are available both as amine-terminated generations and as carboxylate-terminated half-generations. As an amine, PAMAM could either be alkylated by reacting with ethyl bromide or acylated with acetic chloride or acetic anhydride. Alternatively, as a carboxylic acid, half-generation PAMAM could be converted to an ester by methanol or diazomethane, made into an amide by methyl/ethylamine, or made into a lithium carboxylate to be alkylated by methyl/ethyl

lithium (Wade 1999). Considering both ease and reliability of the reactions, as well as the cost of the deuterated forms of the reagents, it was recommended that amine-terminated PAMAM be acylated by acetic anhydride to leave an -$NHCOCH_3$ terminating group on each dendritic branch. Acylation reactions tend to produce high yield, rarely overacylate, and d_6-acetic anhydride was both available and reasonably priced. Acetic anhydride was chosen over acetic chloride because it is less sensitive than acetic chloride and because it can be used in tandem with 4-(dimethylamino)pyridine (DMAP), an acyl transfer catalyst (Steglich and Hoefle 1969).

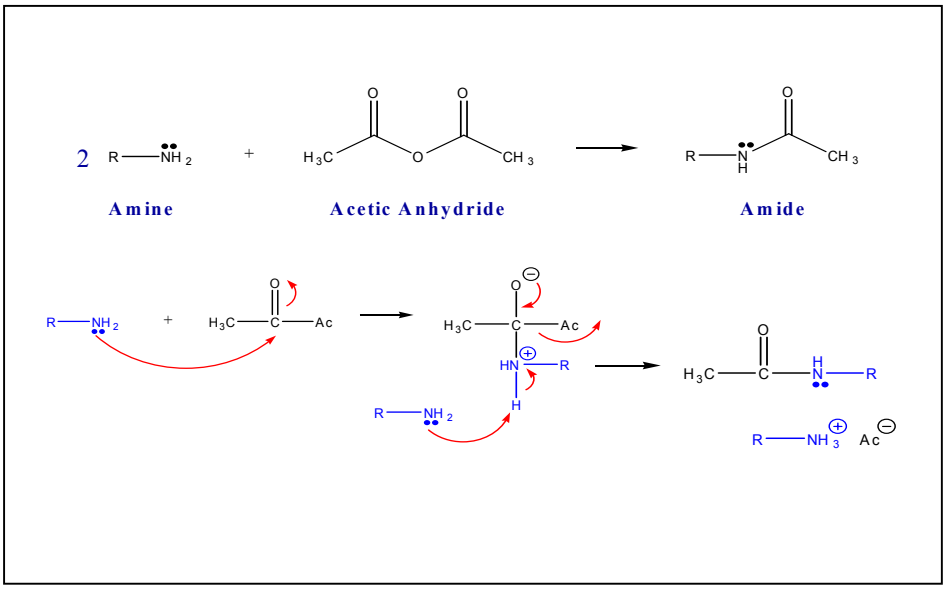

Figure 1.2: Accepted mechanism for nucleophilic acyl substitution by acetic anhydride (Wade 1999).

Acylation is a shortened name for nucleophilic acyl substitution, the replacement of a leaving group on a carbonyl carbon by a nucleophile. As outlined in figure 1.2, the nucleophilic lone pair of a primary amine attacks the carbonyl of the acetic anhydride,

forming a tetrahedral intermediate. The acetate ion, stabilized by resonance, becomes the preferred leaving group and dissociates, restoring the carbonyl to create a protonated amide. A second nucleophile accepts the additional proton as a Brønsted-Lowry base, and the reaction is complete. The amide, also stabilized by a resonance structure between

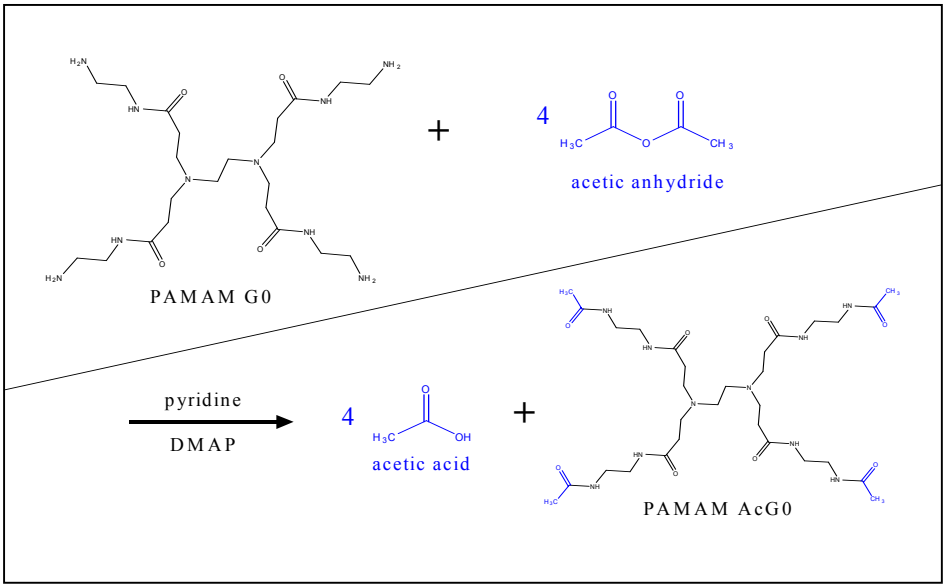

Figure 1.3: Proposed reaction for the synthetic modification of PAMAM G0 by acylation with acetic anhydride.

the carbonyl and the nonbonding electrons on nitrogen, is much less basic and nucleophilic than an amine, which prevents further acylation (Wade 1999). Following this mechanism, reaction of PAMAM G0 with four equivalents of acetic anhydride should produce AcPAMAM G0 and four equivalents of acetic acid (Figure 1.3). By using pyridine as a solvent, the extra protons lost in the conversion of the amines to amides will largely be taken up by the pyridine, eliminating the creation of the PAMAM

acetate salts that are suggested by the mechanism in figure 1.2. DMAP, as stated before, is an acyl transfer catalyst (Steglich and Hoefle 1969), and acetic anhydride will be used in excess to aid in the complete tetra-acylation of the dendrimer molecules.

1.2: Synthetic modification attempts prior to successful synthesis. While acylation is a fairly straightforward, one-step process, purification of any product can be a challenge to any chemist. None of the attempts recorded in this section (1.2) successfully produced a viable product, but they are included in this report as a record of the attempted procedures. All science is a process of trial-and-error, and adequate documentation can prevent future researchers from wasting time repeating the same mistakes. The reader looking for the final synthesis may wish to skip ahead to section 1.5, which incorporates the final working synthesis with several crucial improvements.

1.2.1: Initial attempt: Aqueous work-up. The first procedure attempted for the synthetic PAMAM modification followed a common route for conducting a synthetic organic acylation. Dissolving the product in an organic solvent and washing several times with various aqueous solutions (acid, base, and saturated NaCl) should purify the product. This procedure failed to produce a viable product, seemingly due to the solubility of the product in water.

PAMAM G0 20 wt % in methanol was commercially procured from Aldrich, Inc., and approximately 0.5 mL of the solution was placed into a cleaned, flame-dried, argon-filled, 10-mL cone-bottom flask with a magnetic stir bar. The flask was placed under a rotary evaporator in a warm water bath until the methanol appeared to be evaporated, and then the flask was put on a vacuum pump and evacuated overnight to remove any residual methanol or moisture. The flask was then filled with argon and sealed with a

rubber septum. The starting material was weighed to be 90.1 mg (0.174 mmol). About 1.6 mL of pyridine (Figure 1.4a) was collected by distillation into a separate vial, to which 4.1 mg DMAP (Figure 1.4b), the acyl transfer catalyst (Steglich and Hoefle 1969), was added. The pyridine/DMAP mixture was added to the reaction flask to dissolve the PAMAM G0. The flask was then moved to an ice bath and set to stir, while maintaining positive pressure with an argon-filled balloon. After allowing a few minutes for the contents to thermally equilibrate, 0.25 mL of acetic anhydride (3× excess) was added drop-wise by a hypodermic needle and syringe. The reaction was allowed to run overnight while stirring, and the ice bath was allowed to melt to room temperature.

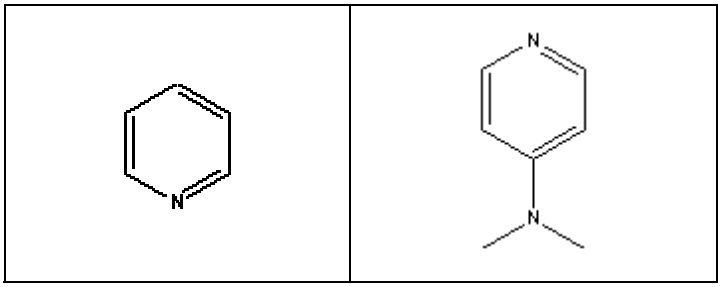

(a) (b)

Figure 1.4: Structural formulae of (a) pyridine and (b) 4-(dimethylamino)pyridine (DMAP).

After running overnight, the reaction flask contained a small amount of liquid at the bottom, and a large amount of a cloudy white gel was caked around the top of the flask. The gel was rinsed down into the flask with ethyl acetate ($CH_3COOCH_2CH_3$), and then the majority of the solvents were removed by evaporation. The crude product was then dried under high vacuum. The crude product was transferred to a test tube with methylene chloride (CH_2Cl_2) and then 10 vol % aqueous sulfuric acid. The organic layer

that developed in the test tube was washed with equivalent portions of first 10 vol % aqueous sulfuric acid (H_2SO_4), then with saturated aqueous sodium bicarbonate ($NaHCO_3$), and finally with saturated aqueous sodium chloride (NaCl). The organic layer was dried with magnesium sulfate ($MgSO_4$), filtered through a pipette, and placed into a 100-mL round-bottom flask. The methylene chloride was evacuated from the flask by a rotary evaporator, and then the flask was dried under a high vacuum pump. The flask appeared to be empty by visual inspection, but the mass had increased by 31.8 mg from the tare weight. Assuming that the reaction had gone to completion, it seemed that methylene chloride was a poor solvent for the acylated product. Considering that the PAMAM starting material had been shipped in methanol, it was believed that the product preferred the polarity of the aqueous layers to the nonpolar methylene chloride. These layers had been retained and segregated into two flasks: acid washes and base/salt washes.

Extractions were performed on the two aqueous layer flasks with equivalent portions of ethyl acetate. Ethyl acetate was chosen for three reasons; it is more polar than methylene chloride, it has the acetyl functionality in common with the AcPAMAM product, and it is immiscible in water. After completing three extractions on each aqueous layer, the ethyl acetate layers were dried with magnesium sulfate and filtered into a 250-mL round-bottom flask. The ethyl acetate was removed with a rotary evaporator, and a reddish-brown residue that emanated an odor resembling acetic acid (CH_3COOH) remained. Acetic acid is not only a byproduct from the reaction, but it would also result from the hydration of excess acetic anhydride during the aqueous washes. It is also reasonable to assume that ethyl acetate would extract a portion of

acetic acid from the aqueous layers, causing the odor emanating from the residue in the flask. In order to remove any acetic acid present, the reddish-brown residue was transferred to a test tube in a small amount of ethyl acetate and washed three times with 4-mL portions of saturated aqueous sodium bicarbonate. With each washing, the organic layer faded from the reddish-brown color to a slight yellow color. In addition, a solid material, possibly sodium bicarbonate, seemed to precipitate out of the aqueous layer into the phase boundary between layers and into the ethyl acetate, which was becoming cloudy. The ethyl acetate was washed twice with distilled water, which removed some of the cloudiness and did not appear to change the yellow color. The organic layer was removed, dried with magnesium sulfate, and vacuum-filtered into a 250-mL round-bottom flask. The ethyl acetate flask contents were compared by TLC to the contents of the first flask evaporated from methylene chloride extraction, which indicated that the two flasks contained the same compound. The contents of both flasks were combined; the solvents were removed with a rotary evaporator; and the contents of the flask were weighed. The crude product mass was now 40.5 mg, which was a 7% improvement in yield; however, the product had yet to be purified.

A liquid chromatographic column was prepared with approximately 2.5 g of gravity silica (43 – 75 μm) in a slurry of methylene chloride. The crude product was transferred to the top of the column in methylene chloride and loaded onto the column with three methylene chloride rinses. Two small vials of methylene chloride were eluted, and then a 1:1 ratio methylene chloride/methanol mixture was loaded onto the top of the column. The methylene chloride/methanol mixture was flashed through the column, and the yellow-colored portion of the product eluted immediately. A TLC comparison of the

eluted product with the crude product made it appear that the product had been purified by the silica column, but a ^{1}H NMR spectrum taken on a Bruker DPX-400 MHz NMR spectrometer, calibrated to the d-chloroform ($CDCl_3$) singlet at 7.26 ppm (Gottlieb, Kotlyar et al. 1997), did not indicate that the desired product had been isolated in the flask (Figure 1.5). However, a sample submitted for electrospray ionization mass spectrometry (Kallos, Tomalia et al. 1991) did detect a sodiated ion peak at 707.41916 amu, which corresponds to the desired tetra-acetyl product.

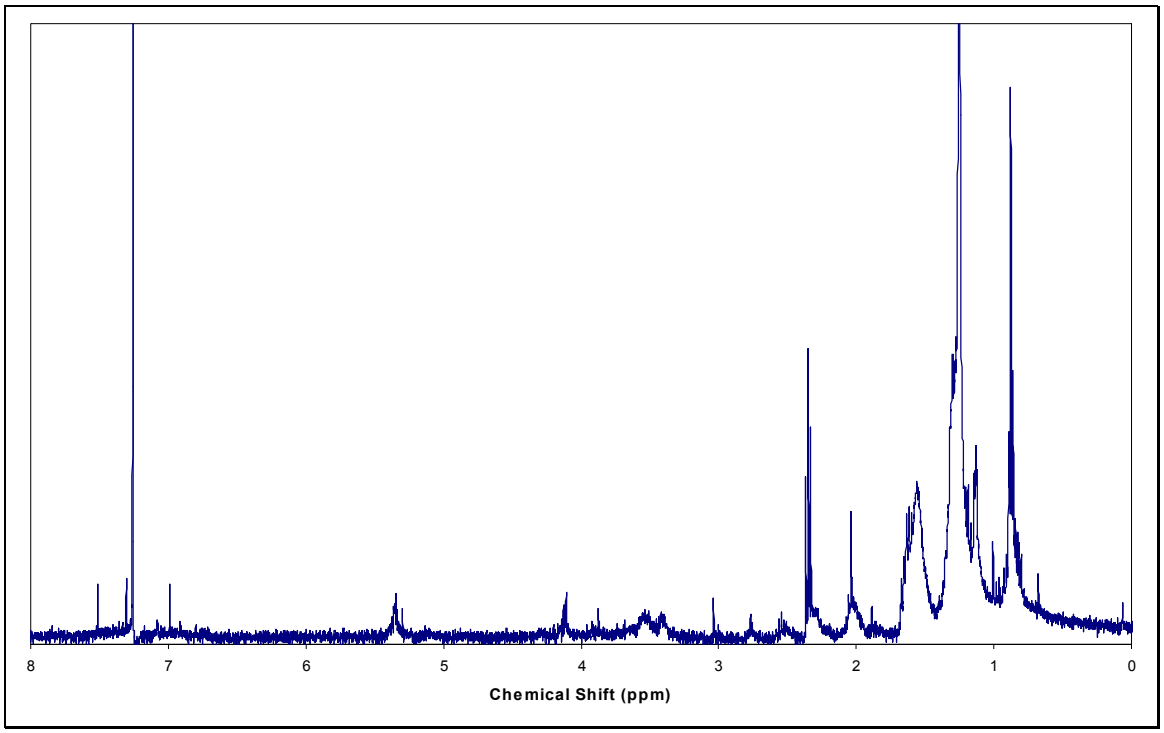

Figure 1.5: ^{1}H NMR spectrum of chromatographic eluent of product after an aqueous work-up.

1.2.2: Second attempt: Liquid chromatography work-up. While the aqueous work-up procedure seemed to be somewhat successful, utilizing aqueous washes turned

out to be a disaster. Methylene chloride may be considered a universal solvent to the organic chemist, but hindsight would show that it was folly to attempt aqueous washes with a product that is suspected to favor a solvent as polar as methanol. It was concluded that the crude product should be loaded directly onto a silica column without first being washed. In addition, it was concluded that due to the acetic anhydride excess, it was not necessary to be overly cautious in keeping moisture away from the reaction. The next step would be to repeat the reaction, scaling up by a factor of two and attempting to isolate the desired product without using aqueous washes. Unfortunately, this modified procedure failed to produce the desired product as well.

Approximately 1.0 mL of PAMAM G0 20 wt % in methanol solution was placed into a cleaned, flame-dried, argon-filled, and 25-mL cone-bottom flask with a magnetic stir bar. The flask was placed under a rotary evaporator in a warm water bath until the methanol appeared to be evaporated, and then the flask was put on a high vacuum pump and evacuated overnight. The flask was then filled with argon and sealed with a rubber septum. The starting material was weighed to be 183.4 mg (0.355 mmol). About 3.0 mL of pyridine was collected by distillation and added, along with 26.7 mg of DMAP, to the flask to dissolve the PAMAM G0. The flask was then covered with a rubber septum, evacuated by a vacuum pump, filled with argon, moved to an ice bath, and set to stir while maintaining positive pressure with an argon-filled balloon. After allowing a few minutes for the contents to thermally equilibrate, 0.5 mL of acetic anhydride (3× excess) was added by syringe drop-wise. After five hours, the solution had turned orange-yellow and began to gel around the sides of the flask. An additional 2 mL of pyridine was added, and the flask was swirled to dissolve the gel. The flask was then returned to the

water bath and magnetic stirrer. After 7 hours, the solution was still orange-yellow and coagulating on the walls of the flask. The flask sides were rinsed down with methylene chloride, the solvents were removed with a rotary evaporator, and the product was dried overnight with a high vacuum pump.

The dried crude product was mostly yellow in color, with some white material and a small amount of brown material. A liquid chromatographic column was prepared with approximately 5.4 g of gravity silica (43 – 75 μm) in a slurry of methylene chloride. The crude product was transferred to the top of the column in methylene chloride and loaded onto the column with methylene chloride rinses. However, a large amount of a white, flaky solid, presumably pyridinium acetate salts, failed to dissolve in the methylene chloride and formed a solid plug at the column head. This solid was removed from the column head mechanically, rinsed and vacuum filtered with methylene chloride, and disposed of. The mother liquor from the vacuum filtration was then reduced by a rotary evaporator and reloaded onto the column head. The column was then filled with methylene chloride and flashed into a clean flask, leaving only 2 cm of solvent above the column head, washing the most nonpolar impurities from the crude product. The column was then filled with a 1:1 mixture of methylene chloride/methanol and flashed into a separate flask. The yellow portion of the product moved readily through the column with the methanol. This procedure was then repeated with 100% methanol and collected as a third fraction. A TLC analysis of the three column fractions indicated that only the second fraction, the yellow portion of the eluent, contained any detectable compounds. The analysis of fraction two displayed two chromatographic bands in addition to the baseline spot, which ran only slightly. It was presumed that this was an indication that

the reaction had not run to completion; the PAMAM starting material was known to remain on the baseline, so ideally, the acylated products would separate out, possibly as separate bands. It was decided to return the crude product to the reaction vessel to attempt to drive the reaction further to completion.

The crude product material was dried of solvent then dissolved in 5 mL of distilled pyridine with 90 mg of DMAP in a 25-mL cone-bottom flask. The flask was placed in an ice bath with a stir bar and set to stir. A vacuum pump was used to evacuate the flask, and then the flask was backfilled with argon and sealed with a rubber septum. After allowing a few minutes for the solution to thermally equilibrate, about 0.5 mL of acetic anhydride was added to the flask, the flask was returned to an argon atmosphere, and the reaction was left to stir overnight. After eighteen hours, the solution had turned a dark, reddish-brown color, similar to the previous experiment. The solvent was removed from the flask by rotary evaporation and then left overnight on a vacuum pump to dry completely. TLC conducted in methanol demonstrated that the crude product mixture still contained three components. A liquid chromatography column was constructed in a similar fashion to that which was used earlier in this trial, and the crude product was run through the column with 60-mL portions of 100% methylene chloride. A yellow band moved through the column, and spotting with TLC showed that the first of the three bands was eluting with 100% methylene chloride. After collecting about 200 mL of methylene chloride from the column, the column was loaded with a 19:1 mixture of methylene chloride/methanol. As this mixture was run through the column, a yellow-orange band began eluting from the column, and 5-mL fractions were collected in test tubes until the color was no longer visible at the column tip. The eluent was then

changed to a 1:1 mixture of methylene chloride/methanol, and two 125-mL flasks were collected, the first one being orange in color and the second being yellow. The eluent was then changed to 100% methanol, and four 125-mL flasks were collected to flush out the column. All of the colored test tube fractions were combined into one round-bottom flask labeled as fraction two. Any fraction collected prior to the colored fractions were combined into a second round-bottom flask labeled as fraction one, and the fractions collected after the colored fractions were combined into a third round-bottom flask labeled as fraction three. TLC in methanol indicated that the three fractions contained one each of the three separate chromatographic bands observed previously in the crude product mixture, but fraction three clearly contained more than one component.

The question that posed itself at this point was into which fraction the desired product had gone. For ease of purification, it was hoped that the product had eluted as fraction two, the part-methanol elution that came off cleanly before the baseline products in fraction three. In order to find the desired product, both 400-MHz ^{1}H NMR and FTIR spectra were acquired on each fraction, as well as 400-MHz ^{1}H NMR spectra of both the PAMAM G0 and acetic anhydride starting materials. All NMR spectra were taken on a Bruker DPX-400 MHz spectrometer calibrated to the d-chloroform singlet at 7.26 ppm (Gottlieb, Kotlyar et al. 1997), and all of the FTIR spectra were taken as thin films on NaCl windows with a Mattson Cygnus 100 FTIR spectrophotometer. The fraction that contained the desired product should display chemical shifts in its NMR spectrum similar to those of PAMAM G0 as well as N-H amide stretches between 3000 – 3500 cm^{-1} and an amide carbonyl C=O stretch around 1660 cm^{-1} on its FTIR spectrum; however, all of the acquired spectra were inconclusive. The NMR spectra were filled with unidentifiable

peaks, none of which resembled the PAMAM G0 starting material spectrum, and two of the three FTIR spectra were largely overshadowed by a broad, O-H stretch absorption from 2500 – 3900 cm^{-1}, obscuring any possibility of detecting N-H amide stretches. The FTIR spectrum for fraction one (Figure 1.6), which had been eluted in methylene chloride, did not have the O-H stretch and displayed both aliphatic C-H stretches just below 3000 cm^{-1} and a small absorbance resembling an N-H stretch just above 3000 cm^{-1}. The FTIR spectrum for fraction two, which had been eluted in 19:1 methylene chloride/methanol, was partially obscured by a broad O-H stretch from 2700 – 3700 cm^{-1}, so that no conclusive N-H stretches could be observed. The spectrum for fraction three, which was eluted from 100% methanol, was completely obscured from 1800 – 3800 cm^{-1} by a very broad O-H stretch. Suspecting that methanol was the source of the O-H stretches in fractions two and three, both flasks were dried overnight on a vacuum pump, and new spectra were taken the next day. Fraction two was much improved after drying, and seemed to show a very characteristic NH stretch absorbance from 3000 – 3700 cm^{-1} (Figure 1.7). Fraction three, on the other hand, was much improved but still inconclusive (Figure 1.8). Without a definitive identification made of the desired product, these three fractions were set aside for later analysis.

1.2.3: Third attempt: Increased excess and trituration work-up. Under advisement, a third acylation trial was begun, this time using 10× excess acetic anhydride and taking particular caution to remove all methanol from the starting material PAMAM. It was hypothesized that the previous reactions may have been hindered from going to completion if excess methanol was reacting with the acetic anhydride. Also, if other sources of environmental contamination (moisture, etc.) were also competing with the

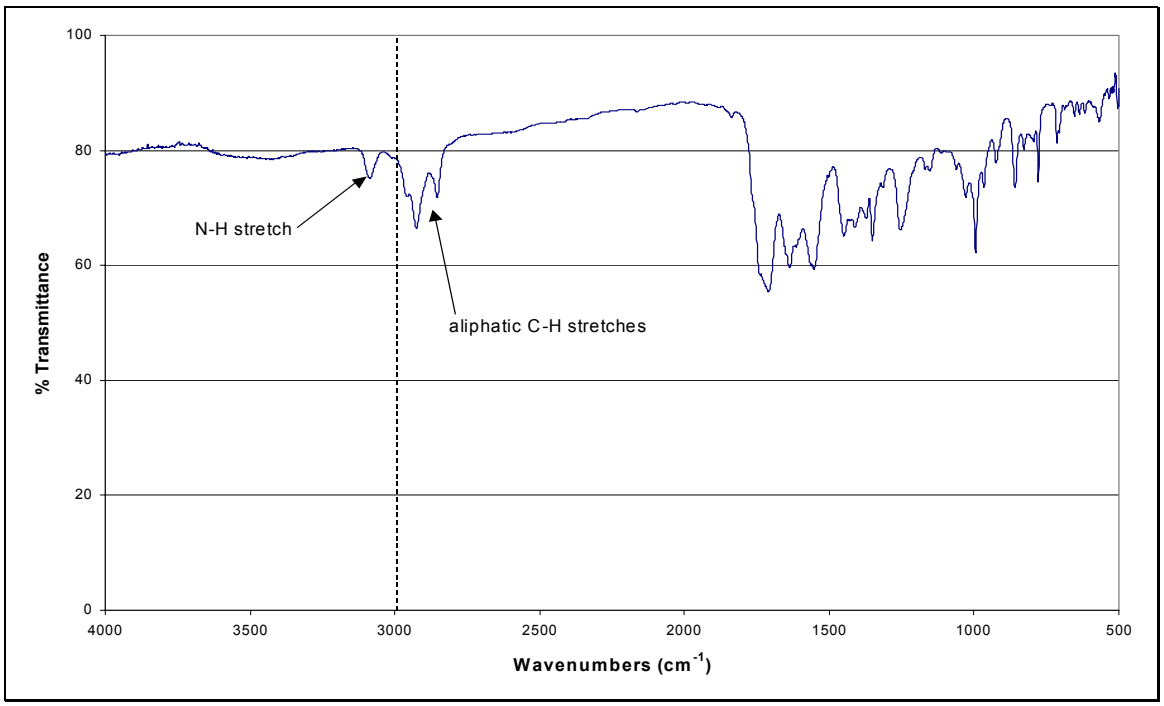

Figure 1.6: FTIR spectrum of silica column fraction one.

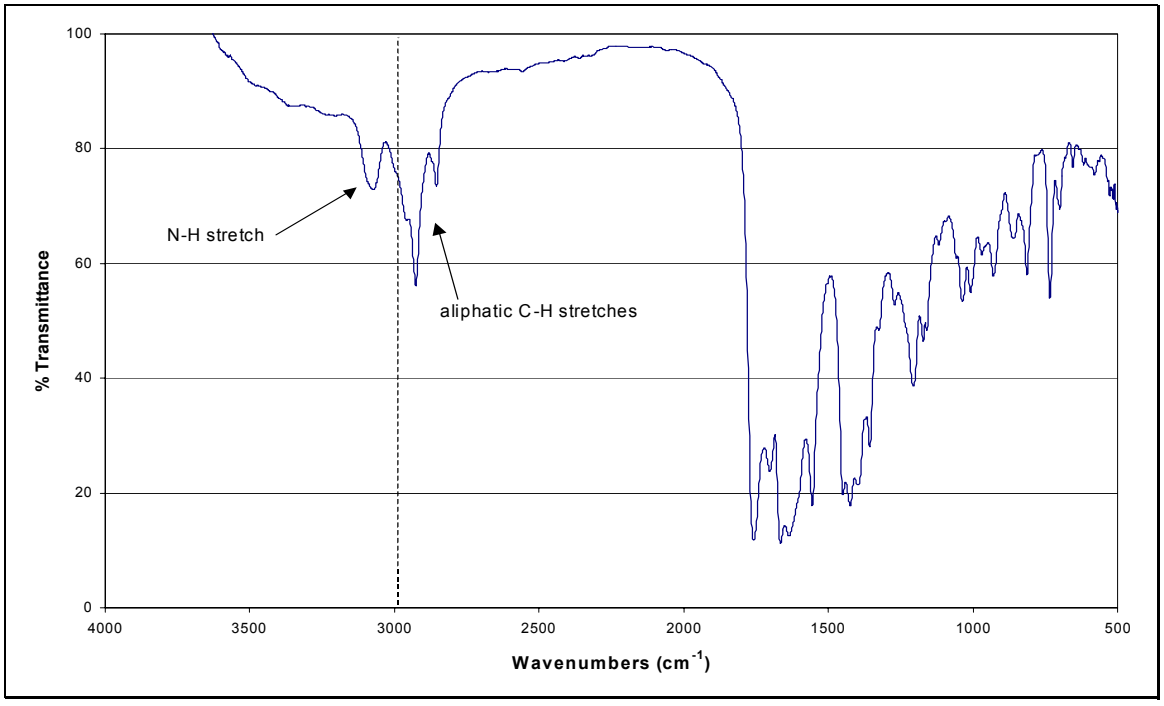

Figure 1.7: Improved FTIR spectrum of silica column fraction two.

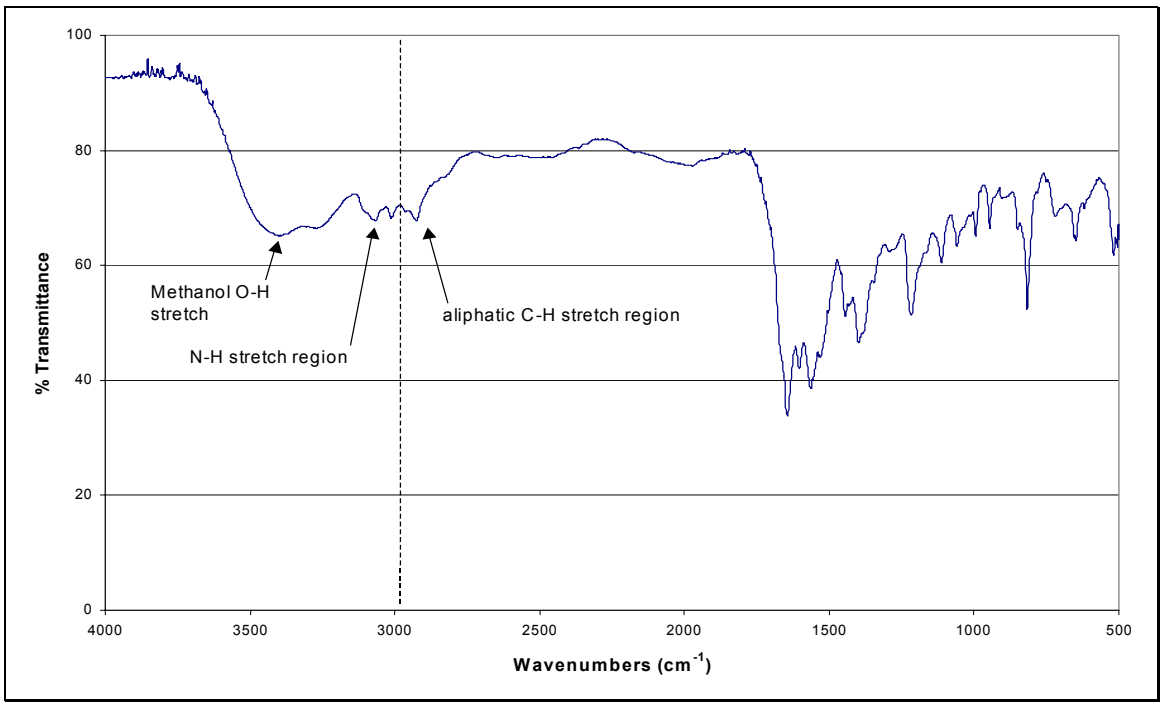

Figure 1.8: Improved FTIR spectrum of silica column fraction three.

starting material, these precautions might help drive the desired reaction. Further, experience gained during the previous two attempts would inevitably remove mistakes that were discovered in hindsight. As it would happen, this trial also failed, but it did bring this study another step closer to the final product.

To run the third reaction, methanol was removed from a slight excess of 1.0 mL PAMAM G0 20 wt % in methanol solution by rotary evaporation in a 5-dram vial and then by drying in an acetone-reflux drying pistol overnight. The starting material was weighed to be 268.6 mg (0.520 mmol). A 25-mL cone-bottom flask and stir bar was cleaned and flame dried, and the flask was allowed to cool to room temperature while capped to prevent moisture from condensing inside the flask. The dried PAMAM G0 was dissolved in about 4.5 mL of distilled pyridine, and the solution was transferred to

the cone-bottom flask along with about 100 mg of DMAP catalyst. The flask was placed into an ice bath, and the stir bar was activated to dissolve the DMAP. The flask was then filled with an argon atmosphere. After allowing a few minutes for the contents to thermally equilibrate, about 2.0 mL of acetic anhydride (10× excess) was added to the flask slowly. The first few drops created a vigorous reaction, leaving a white cloud in the solution, but successive drops were added without an event. Presumably, this reaction was caused by water and/or methanol impurities from the starting materials reacting to hydrate the acetic anhydride; once these impurities were consumed by the first few drops of anhydride, the remaining acetic anhydride dissolved neatly into the pyridine. The flask was returned to an argon atmosphere, and positive pressure was maintained with an argon-filled balloon. The stirring speed was increased, and the reaction was left to run. After about forty-eight hours, the solution had turned to a dark brown color, appearing almost orange or burnt orange when swirled. The reaction mixture was transferred to a larger round-bottom flask with methylene chloride, and the solvents were removed by rotary evaporation. The flask was then placed under a high vacuum pump to dry overnight. The dried product in the flask had a burnt appearance, being very dark brown and almost black in some areas. The product also had a shiny, "wet"-looking spot at the bottom, but it did not flow, as would a liquid. Also, this reaction did not appear to contain the white, flaky solids observed in previous reactions.

A review of the previous experiments seemed to indicate that the solubility properties of the starting materials and desired products were not well understood. It was evident that until appropriate solvents or solvent combinations were discovered, isolation of the desired product would not be achieved. Methylene chloride had performed

appropriately as it had been used for transferring products from flask to flask, for rinsing container walls, and also for loading liquid chromatography columns. However, as had been expected previously after the aqueous reaction work-up, the compounds of interest in this reaction appear to prefer polar solvents like methanol and water. Water and alcohols would both be inappropriate for this reaction due to their incompatibilities with acetic anhydride. The TLC experiments conducted thus far had been done in methanol, which had been chosen after attempts at using methylene chloride, isopropanol, and combinations of these in order to resolve product bands. A TLC experiment was run using ethyl acetate as the eluent in place of methanol, and the TLC plate resolved seven chromatographic bands where there had been only three previously. It had been suspected that the acetyl groups placed at the dendrimer periphery might show preference to ethyl acetate, but until this point it had seemed more practical to use the more common standbys for a TLC eluent. It was then hoped that if ethyl acetate could resolve seven bands on TLC, it might be able to resolve a silica column where the other solvents had failed.

A liquid chromatographic column was prepared with approximately 8 g of gravity silica (43 – 75 μm) in a slurry of methylene chloride. The crude reaction product was rinsed and vacuum filtered with methylene chloride to separate out any pyridinium salts, and then it was loaded on the top of the column in methylene chloride with three methylene chloride rinses. Methylene chloride was eluted into a large Erlenmeyer flask until the second band began to appear on a TLC analysis in ethyl acetate, and from then, the eluent was collected in test tube fractions of 5-mL to 10-mL quantities. Fifty milliliters of a 9:1 methylene chloride/ethyl acetate mixture was added to the top of the

column. The methylene chloride/ethyl acetate mixture was flashed through the column while continuing to collect 5-mL to 10-mL test tube fractions. This procedure was repeated as a gradient elution, increasing the methylene chloride/ethyl acetate ratio to 4:1, 3:2, and then 1:4. After collecting eighty test tube fractions, 100% ethyl acetate was run through the column into another large Erlenmeyer flask until spotting on a TLC plate indicated that the ethyl acetate was no longer eluting anything from the column. Using TLC in ethyl acetate, the test tube fractions were sorted and combined into seven round-bottom flasks as appropriate. Once completed, all seven flasks were run in comparison on a TLC plate; the first flask contained the first chromatographic band; the second flask had the second band; the third flask contained bands three, four, and five; the fourth and fifth flasks contained bands four and five; the sixth flask contained a smeared baseline spot, and the seventh flask contained only a baseline spot.

Once again, the challenge presented itself of determining in which chromatographic band the desired product had eluted. Because there existed seven bands in what was thought to be a relatively simple mixture, it was believed that some of the bands could be incompletely acylated byproducts; in particular, if the starting material was a baseline spot, perhaps the four closely eluted bands were tetra-, tri-, di-, and mono-acylated products, making band four the desired product. On the other hand, assuming that the tetra-acylated dendrimer had the most affinity for ethyl acetate, perhaps the first band was the desired product. ^{1}H NMR spectra were collected for fractions 1 and 5 in d-chloroform and calibrated to the d-chloroform singlet at 7.26 ppm (Gottlieb, Kotlyar et al. 1997) on a Bruker DPX-400 MHz NMR spectrometer, but both spectra had poor signal-to-noise ratios, indicating that dendrimer concentrations were too low for the

spectrometer. The concentration of the fraction one analyte was increased in the NMR sample tube, and the NMR experiment was repeated on fraction one. In addition, an NMR spectrum for fraction two was collected. None of these spectra displayed the peaks expected for the desired product. The seven fractions were transferred into seven 5-dram vials and the transfer solvents were removed by rotary evaporation. Fraction seven required several additional hours on a vacuum pump before it was completely dry, and when it had dried, it appeared to puff up into a foam – a characteristic of dendrimers – and it had a very sticky, waxy consistency. Upon weighing each fraction, it was noted that none of the fractions contained more than 30 mg of matter except for fraction seven, which weighed 216.4 mg. With an expected theoretical yield of about 355 mg, only fraction seven could contain any of the desired product with appreciable yield, dispensing with everything that had been assumed thus far about the chromatographic behavior of the dendrimers. A ^{1}H NMR spectrum was collected for fraction seven in d-chloroform (calibrated at 7.26 ppm (Gottlieb, Kotlyar et al. 1997)) on a Bruker DPX-400 MHz NMR spectrometer (Figure 1.9), and using integral analysis, chemical shift peaks of proportionate integral ratios were detected between 1.8 – 3.4 ppm. However, while the integral ratios seemed to provide evidence of the desired product, the spectrum also indicated that fraction seven was extremely polluted with byproduct compounds. Because fraction seven was not a chromatographic band and because the product was still largely impure in fraction seven, this brought into question the utility of using liquid chromatography at all during the work-up for this reaction. Hoping to identify any or all of the chromatographic bands, samples of all seven fractions were submitted for electrospray-ionization mass spectrometry (Kallos, Tomalia et al. 1991), and sodiated

mass peaks were compared to a list of suspected byproduct compounds, including the partially acylated dendrimer products. None of the expected masses appeared in any of the spectra, with the exception of mass 707 amu, the sodiated mass of the tetra-acylated target product, which appeared only in fractions one and seven. It is possible that some of the product eluted off of the front end when the silica became saturated with the product, and then the 100% ethyl acetate washed the bulk of the product off of the silica and into fraction seven.

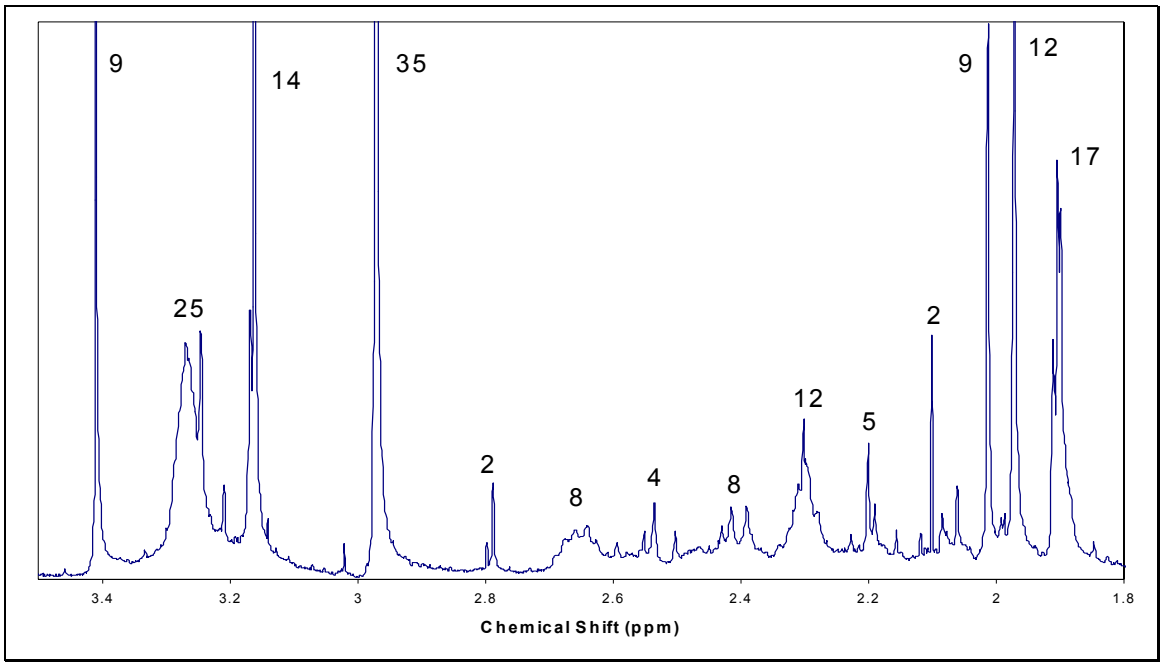

Figure 1.9: ^{1}H NMR spectrum of silica column fraction seven in d-chloroform.

Since liquid chromatography on a silica column had now been determined ineffective, a different separation method had to be found. An improved understanding of the AcPAMAM solubility properties led to the idea that the molecule may be a good

candidate for trituration, or precipitation out of a nonpolar solvent. Toluene was tested against a small portion of the matter from fraction seven in a test tube, and nothing appeared to dissolve. Methanol dissolves the product well, and methanol is miscible in toluene. Fraction seven was dissolved in 15 drops of methanol, and the solution was added drop-wise into a 50-mL centrifuge tube filled with toluene. Each drop dissipated into the toluene, while small particles of material were seen suspended in the solvent. The centrifuge tube was shaken vigorously and then centrifuged at 5000 rpm for ten minutes. The toluene took on a yellow/orange color, and a dark reddish-brown solid precipitated to the bottom of the tube. The toluene was decanted, and the precipitate was again dissolved in a minimal amount of methanol. The trituration process was repeated for a total of four precipitations, and then the residual toluene was removed from the final precipitate by drying on a high vacuum pump overnight. After drying, the product had puffed up as before, but it no longer had a waxy consistency. The product was now dry and crystalline, and it broke apart when struck with a spatula. A ^{1}H NMR spectrum was collected using a Bruker DPX-400 MHz NMR spectrometer (Figure 1.10), using d_4-methanol (CD_3OD) in the place of d-chloroform. In the process of unraveling the solubility attributes of the PAMAM dendrimers, it was realized that chloroform was likely to be causing the products to aggregate in the NMR tube, and hence, it could be degrading the quality of the NMR spectra. The d_4-methanol was the obvious choice for these dendrimers, and the resulting NMR spectrum, calibrated to the d_4-methanol quintuplet at 3.31 ppm (Gottlieb, Kotlyar et al. 1997), was moderately clean and indicated AcPAMAM. Although not 100% conclusive, the spectrum displayed large singlets at 1.96 and 3.27 ppm, representing the acetyl protons and the chemical shift

merger of the peripheral ethylenediamine protons, respectively. The integral ratios seemed to be of the right order of magnitude, but the resolution was poor, lacking definitive triplets. This NMR spectrum, along with the appearance of the correct sodiated molecular ion peak from an electrospray-ionized mass spectrum were enough evidence to indicate that the reaction had been successful to some degree and that it was time to attempt PAMAM G1. However, yet another product work-up would need to be devised to eliminate both the aqueous work-up and the silica column.

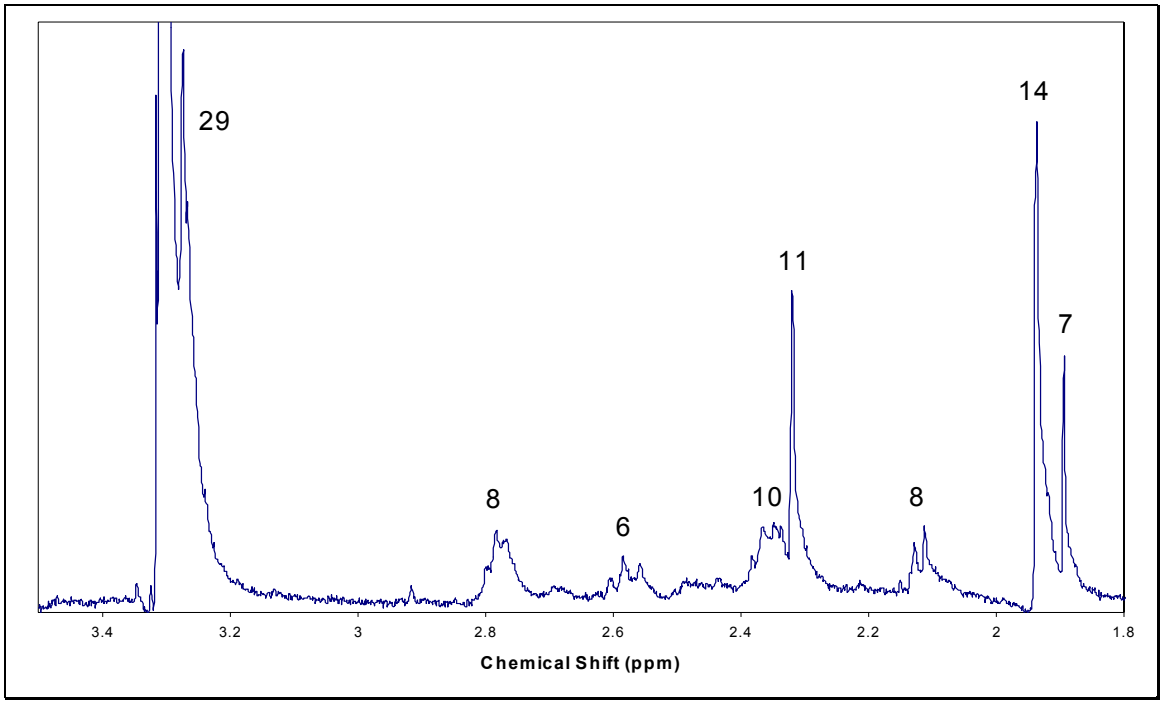

Figure 1.10: ^{1}H NMR spectrum of silica column fraction seven in d_4-methanol.

1.3: Working synthesis. It was becoming increasingly evident that these synthetic modification trials were right on the verge of successfully yielding the desired

AcPAMAM product. Aqueous washes and silica column chromatography were now out of the question, and trituration seemed to be promising. It was suggested that an ion exchange column could be used in the place of vacuum filtration to remove the pyridinium salts, and that the ion exchange eluent could then be taken directly into the trituration step.

About 1 mL each of PAMAM G0 and PAMAM G1 were placed into two separate 5-dram vials, and the methanol was removed from each by rotary evaporation and then by drying both overnight in an acetone-reflux drying pistol. Two 25-mL cone-bottom flasks were cleaned, flame dried with stir bars, purged with argon, capped, and allowed to cool to the touch. The dried dendrimers were transferred separately into the two cone-bottom flasks with three 2-mL portions of distilled pyridine each, for a total of 6 mL of solvent per flask. About 100 mg of DMAP catalyst was added to each flask and stirred to dissolve. The two flasks were then filled with argon, capped with a rubber septum, and placed into a large ice bath while stirring. Once the flasks had cooled in the ice bath, about 1.25 mL of distilled acetic anhydride was added to the G0 flask and about 1.0 mL was added to the G1 flask, to achieve a 10× excess of reactant in each. The argon pressure was returned and maintained in each flask by argon-filled balloons. After 24 hours, the G0 reaction had a faint yellow-orange color, while the G1 reaction was already a much darker, red-brown color. Both reaction vessels were swirled by hand when it was noticed that the G1 flask had a substantial amount of matter congealed at the bottom of the flask. About 4 mL of distilled 1,2-dichloroethane (CH_2ClCH_2Cl) was added to the flask, and the solids were broken up with a mini-spatula. The flask was swirled again, and the stir bar came free from the congealed mass. The reaction was allowed to

continue in the melted ice water bath. After 48 hours, both reactions appeared to be roughly the same dark, reddish-brown color, and both were still stirring. After 96 hours, both reactions appeared unchanged; the stirring was discontinued.

In an effort to reduce mechanical product losses incurred by vacuum filtration, an ion exchange resin column was employed to eliminate the pyridinium acetate salts from the reaction mixtures. Several grams of Amberlite IRA-410 ion exchange resin were exchanged from chloride (Cl^-) to hydroxide (OH^-) in a beaker of 3 M sodium hydroxide (NaOH) for one hour. The resin beads were then filtered from the caustic solution and rinsed with distilled water. A thin column was loaded with roughly six inches of resin using distilled water. The PAMAM G0 reaction mixture was transferred to a 250-mL round-bottom flask with methylene chloride, and the solvents were reduced by rotary evaporation until only a few milliliters of mixture remained. The concentrated mixture was loaded onto the ion exchange column with methanol, and methanol was run through the column into a 250-mL round-bottom flask until the eluent appeared to run clear. The methanol was then removed from the eluent by rotary evaporation to the maximum extent possible. This entire ion exchange process was repeated for the PAMAM G1 reaction mixture, after recharging the ion exchange resin with 3 M NaOH and rinsing with methanol.

A repeat of the trituration procedure from the previous experiment was conducted to purify the two reaction mixtures. Eighty drops of methanol were pipetted into each of the two round-bottom flasks containing the PAMAM G0 and G1 reaction products. Twenty drops of these two solutions were then precipitated into each of eight centrifuge tubes (four for G0 and four for G1) filled each with 50 mL of toluene. These tubes were

capped, shaken vigorously for one minute each, and then centrifuged for 10 minutes at 5000 rpm. Each tube had a varying quantity of dark material at its tip, and the toluene had taken on an orange, translucent hue. This process was repeated by adding additional methanol to the round-bottom flasks for rinsing, using the methanol rinses to dissolve the dark material in the centrifuge tubes, and then refilling the tubes with toluene to be centrifuged and decanted. With each successive round, the toluene turned less orange, then yellow, and then it appeared almost clear; this color change required a total of six precipitations. The residual material in the centrifuge tubes was consolidated into two tubes, one for G0 and one for G1, and these tubes were placed under a vacuum pump overnight to remove the residual toluene and methanol. The PAMAM G1 product appeared crystalline and flaky as expected, but the G0 product appeared as a crust in the bottom of the tube. The G0 product was broken up with methylene chloride and then re-dried, but this did not change the product appearance.

At this point, it seemed that toluene alone was not adequately purifying the desired AcPAMAM product. Both the PAMAM starting material and the AcPAMAM product dissolve in methanol, demonstrated by the ease with which methanol transfers and elutes the product mixture. However, methanol seemed to be too polar, as seen in the way that product fractions smeared together in both silica chromatography and TLC. Isopropanol was attempted as a TLC mobile phase with poor results. On the other end of the spectrum, toluene and benzene appeared completely immiscible with the products. Methylene chloride was also too nonpolar, as witnessed during attempts to use it for product transfers and during the unsuccessful aqueous washes in the first experiment. Chloroform demonstrated its incompatibility in the NMR tubes, prompting the switch to

d_4-methanol for NMR, and even pyridine appeared to be an insufficient solvent for the PAMAM G1 reaction, requiring the addition of 1,2-dichloroethane. By elimination, only one other readily accessible solvent remained that had provided some successes to these experiments in the past: ethyl acetate. Ethyl acetate had been the solvent that made the difference in the TLC experiments, but subsequently failed to elute the desired product from the silica column. To test solubility properties, both the PAMAM G0 and G1 products were run on a TLC plate in methanol, 1,2-dichloroethane, and ethyl acetate. Each plate was stained in potassium permanganate ($KMnO_4$) after being developed, and neither the 1,2-dichloroethane nor the ethyl acetate appeared to move the products from their baseline spots. The methanol plate did develop, resolving three spots from the PAMAM G0 products, and nothing resolved from the PAMAM G1 products, except for a long, faint smear along the length of the plate. These results, showing the G0 products to contain a mixture, were consistent with the product appearance as well; the G0 product mixture still had impurities and did not crystallize like the G1 products. Further, by the 1,2-dichloroethane and ethyl acetate evidence, it appeared that these solvents could be trituration candidates, and they are both more polar than toluene. In an effort to purify the PAMAM G0 product mixture, the mixture was dissolved in a few milliliters of methanol and loaded onto a fresh ion exchange resin column using the same procedure as before. However, to increase the time spent on the column, the product was eluted by gravity, rather than by flashing with air. The G0 products were collected in a 250-mL round-bottom flask and dried by rotary evaporation.

Meanwhile, the PAMAM G1 products were precipitated through ethyl acetate, following a similar procedure as that used with the toluene. The G1 products were

dissolved in a minimal amount of methanol and divided among four centrifuge tubes, each containing about 50 mL of ethyl acetate, by pipetting fractions of the solution to the centrifuge tubes drop by drop. The centrifuge tubes were capped, shaken vigorously for one minute each, and then centrifuged for ten minutes at 5000 rpm. A very dark precipitant was deposited at the tip of each tube, and the ethyl acetate took on an orangish color but appeared very cloudy, unlike the previous toluene waste. It was suspected that something different was taking place, so the ethyl acetate waste was retained and consolidated into a round-bottom flask. The solvent was then removed by rotary evaporation, and a ^{1}H NMR spectrum was collected using a Bruker DPX-400 MHz NMR spectrometer (Figure 1.11 and 1.12), using d_4-methanol (calibrated at 3.31 ppm (Gottlieb, Kotlyar et al. 1997)) as the solvent. For the first time, a clean NMR spectrum ensued; several distinct peaks appeared amongst a very small level of background impurities. Three of the NMR peaks displayed integral ratios much higher then the rest: a triplet at 1.26 ppm, a singlet at 2.03 ppm, and a quartet at 4.11 ppm. Considering only these three peaks, the integral ratios are 3 (triplet): 3 (singlet): 2 (quartet), and a comparison to a literature NMR spectrum (Pouchert 1983) clearly identified these peaks as residual ethyl acetate, as shown in figure 1.11. The triplet and quartet are coupled together and represent the ethyl group functionality, while the singlet near 2.0 ppm represents the methyl group functionality. Disregarding these solvent peaks, an examination of the remaining peaks (Figure 1.12) indicated that the integral ratios would match that which would be expected for the AcPAMAM G1. In addition, the spectrum seemed to be comprised of singlets and triplets, a trait also expected of the desired product but not previously elucidated. Further NMR analysis (explained in the next section) would show

that both the PAMAM G0 and G1 had been successfully modified to AcPAMAM G0 and G1 and had been moderately well purified.

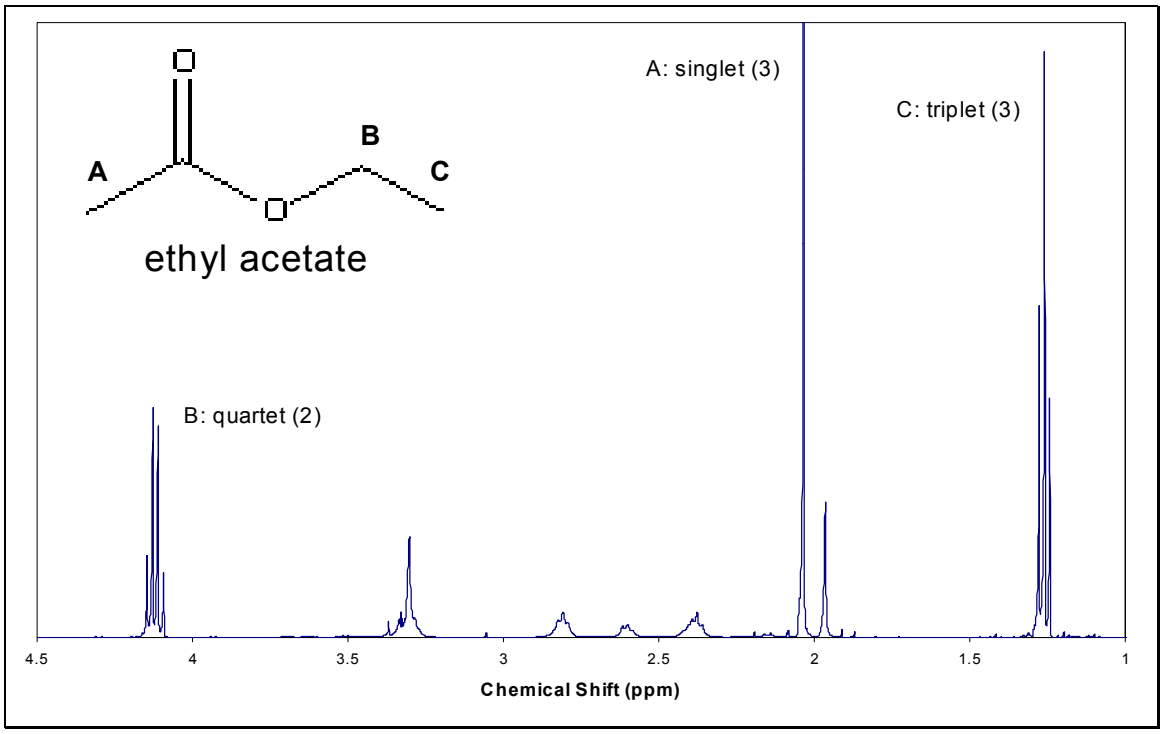

Figure 1.11: ^{1}H NMR spectrum of ethyl acetate with an unidentified extracted compound.

1.4: Improvements in synthesis. After finding a working synthesis, the research focus turned to the production of AcPAMAM for use in spectroscopic studies. It was accidentally observed that prolonged exposure to pyridine without acetic anhydride turned PAMAM G0 to the dark red-brown color observed in previous experiments. It had been hypothesized that this discoloration had been due to oxidation of the amine functionalities by exposure to air and/or light (Chen and Knochel 1988; DeJong, Davidson et al. 2001). Yet, amine-terminated PAMAM failed to turn this color under

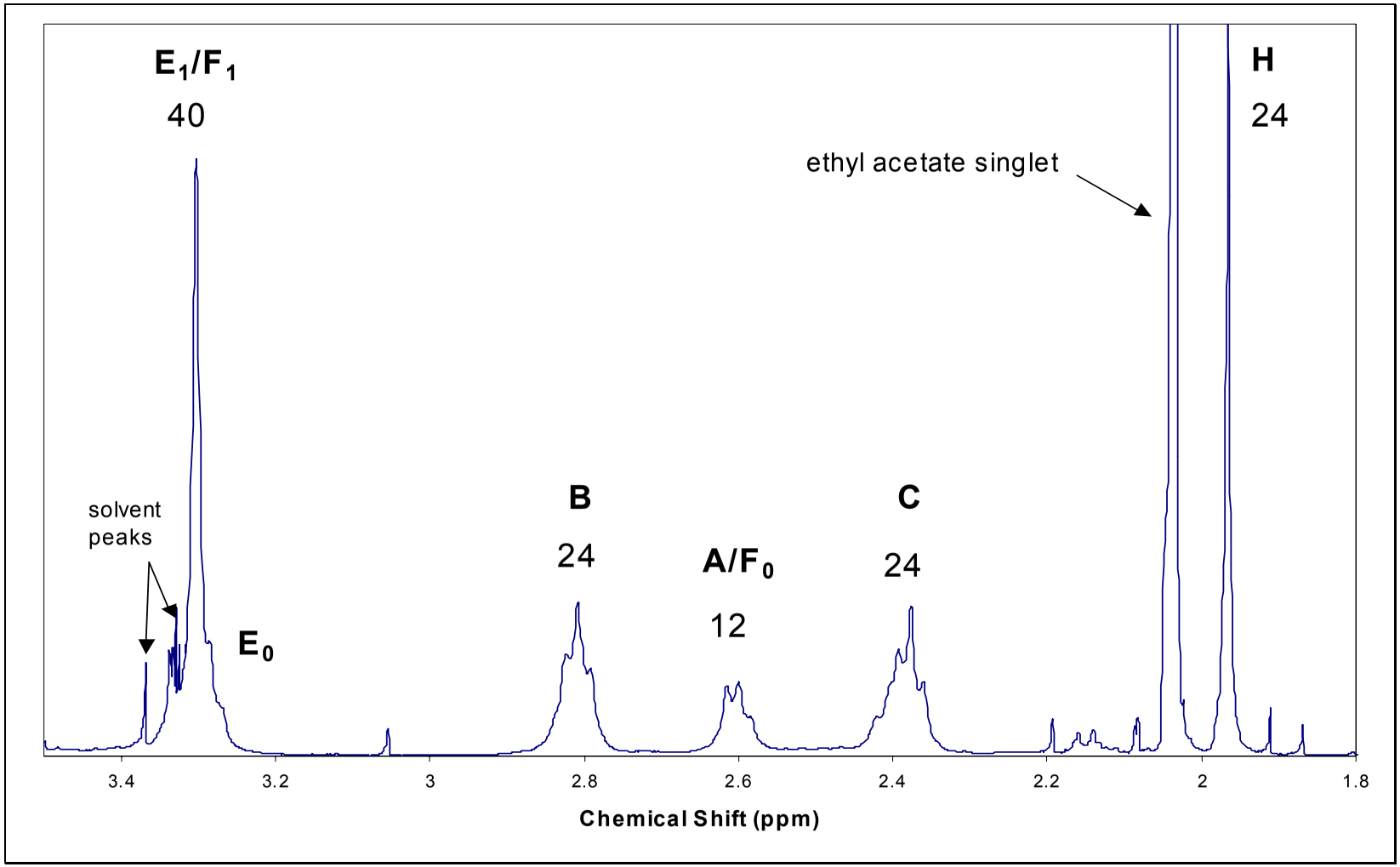

Figure 1.12: ^{1}H NMR spectrum of AcPAMAM G1 extracted with ethyl acetate (1.8 ppm – 3.5 ppm). ***(Annotations explained in chapter 2.)***

prolonged exposure to both air and light. This new observation with pyridine could explain the observed impurities, reduced yield, and the dark color change; the alkaline conditions created by the pyridine catalyzed a reverse Michael addition, slowly cleaving off the dendrimer branches into waste byproducts.

1.4.1: Use of a polar solvent in lieu of pyridine. In order to reduce the opportunity for pyridine to catalyze a reverse Michael addition while maintaining its ability to catalyze the acylation reaction, pyridine could no longer be used as both the catalyst and solvent. This was not a major inconvenience, because pyridine had already been observed to be a poor solvent for PAMAM – increasingly so with increasing generation. The difficulty in finding an appropriate solvent was in the affinity the dendrimers have for very polar solvents; the most polar solvents, water, methanol, and ethanol, would all react with the acetic anhydride before it could perform the acylation. Dimethylformamide (DMF) was selected for its high polarity and inertness toward the acylation reagents. The major drawback of using DMF is its high boiling point, 153 °C, which makes it more difficult to remove. By comparison, the boiling point of pyridine is 115.2 °C. In using a different solvent, the quantity of pyridine required would be reduced to a stoichiometric amount, matching the amount of acetic anhydride.

About 1.5 mL PAMAM G0 20 wt % in methanol was dried in a 5-dram vial by rotary evaporation and then by high vacuum overnight. The starting material PAMAM was weighed as 264.8 mg (0.5125 mmol). The PAMAM was dissolved in 3 mL DMF and transferred to a 25-mL cone-bottom flask, to which was added 1.7 mL of distilled pyridine and a small amount of DMAP catalyst. The flask was set to stir with a small magnetic stir bar, and then about 2.0 mL of acetic anhydride was added drop-wise. As

before, the solution bubbled vigorously during the first two to three drops, but the mixture immediately settled down to accept the remainder of the acetic anhydride. The flask was capped with a rubber septum, evacuated by vacuum, and backfilled with argon gas. The reaction mixture was a cloudy, milky-white color; the reaction was left to run at room temperature overnight.

After twenty-two hours, the solution had acquired a faint yellow color, and the reaction was halted. Most of the white color in the mixture appeared to be due to suspended solids, so these solids were removed by vacuum filtration and rinsed with ethyl acetate. The white solids were expected to be insoluble pyridinium acetate salts. The mother liquor from the vacuum filtration, which was faintly yellow, was collected in a 100-mL round-bottom flask and dried by rotary evaporation/high vacuum. The remaining residue was comprised of a small amount of an orangish-colored gel. The residue was dissolved in 15 drops of methanol and triturated one drop at a time through a 50-mL centrifuge tube filled with toluene. The tube was capped, shaken vigorously for one minute, and then centrifuged for 10 minutes at 5000 rpm. The toluene, which remained colorless, was decanted and retained, and the precipitation procedure was repeated once with toluene. After the second trituration with toluene, the same procedure was conducted six more times with ethyl acetate in place of toluene. The ethyl acetate was collected each time into a 250-mL round-bottom flask and removed by rotary evaporation in between extractions. Once all of the extractions were completed, the product was dried by rotary evaporation/high vacuum. The dried product was weighed and sampled for NMR analysis. The crude product mass indicated a 20.9% product yield, but a 400-MHz ^{1}H NMR spectrum (Figure 1.13) indicated with multiple peaks that

the reaction had not gone to completion. A fully reacted product would display only two triplets and a singlet between 2.1 – 2.8 ppm; the additional peaks observed in the spectrum could have been the result of a mixture of partially-acylated and fully-acylated dendrimers. The low product yield seemed to indicate that most of the dendrimer probably remained in the vacuum filtrate; in addition, partially-acylated products would manifest as a lower crude product mass.

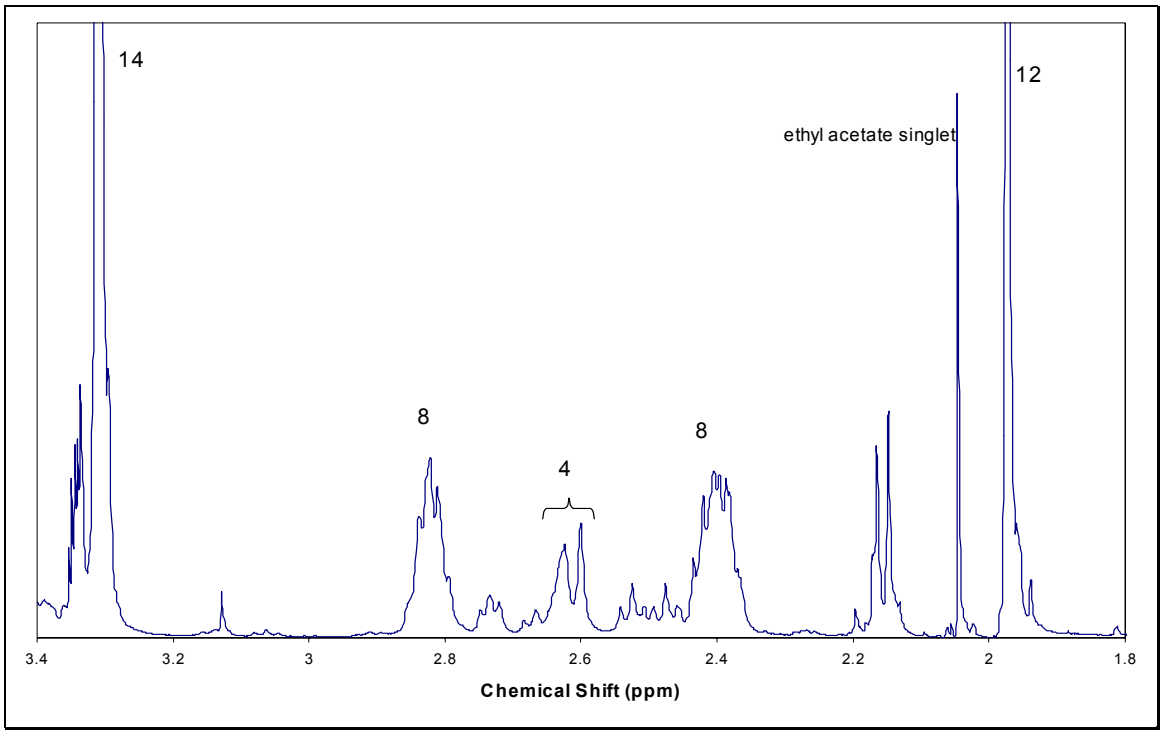

Figure 1.13: ^{1}H NMR spectrum of first attempt AcPAMAM G0 product using a polar solvent and stoichiometric amounts of pyridine.

In an attempt to complete the synthetic modification, the reaction was reinitiated and run for another day. The product fractions (the NMR tube, centrifuge tube, etc.) were returned to a round-bottom flask with methanol and dried by high vacuum

overnight. The vacuum filtrate solids were then placed back into the round-bottom flask, and then about 5 mL of DMF and 1.7 mL of pyridine were added to the flask. The flask was set to stir with a stir bar, and about 75 mg of DMAP was added to the solution. After stirring for a few minutes to mix, about 2 mL of acetic anhydride was added one drop at a time. The flask was capped and left to stir overnight. The solution was faintly yellow, and the white solids, presumed to be pyridinium acetate, failed to dissolve in the DMF. After about 20 hours, the solution had turned an orangish color.

Several attempts were made to purify the product from the continued reaction, but neither the yield nor the purity was significantly improved. An ion exchange column was loaded with Amberlite IRA-410 ion exchange resin charged with hydroxide ions (OH^-) from 3 M NaOH. The reaction mixture was run through the column twice by gravity in methanol, but a large amount of white solid was still visible in the effluent. The ion exchange resin was recharged in 3 M NaOH for one hour and reloaded into the column in methanol. The product effluent was reduced by rotary evaporation and re-run through the recharged column by gravity at an extremely slow flow rate. The effluent was now yellow in color, and the methanol was again reduced by rotary evaporation. This product was triturated with toluene three times, as before, and then extracted by ethyl acetate twice. The ethyl acetate was filtered to remove visible solids, the solvent was removed by rotary evaporation, and then the product was dried by high vacuum overnight. A 400-MHz ^{1}H NMR spectrum (Figure 1.14) again displayed too many peaks to indicate a successful synthesis. After sitting overnight, the toluene waste from the precipitations had produced a clearly visible amount of loosely aggregated solids at the bottom of the flask in which it was stored. Previous experience had shown that this solid was

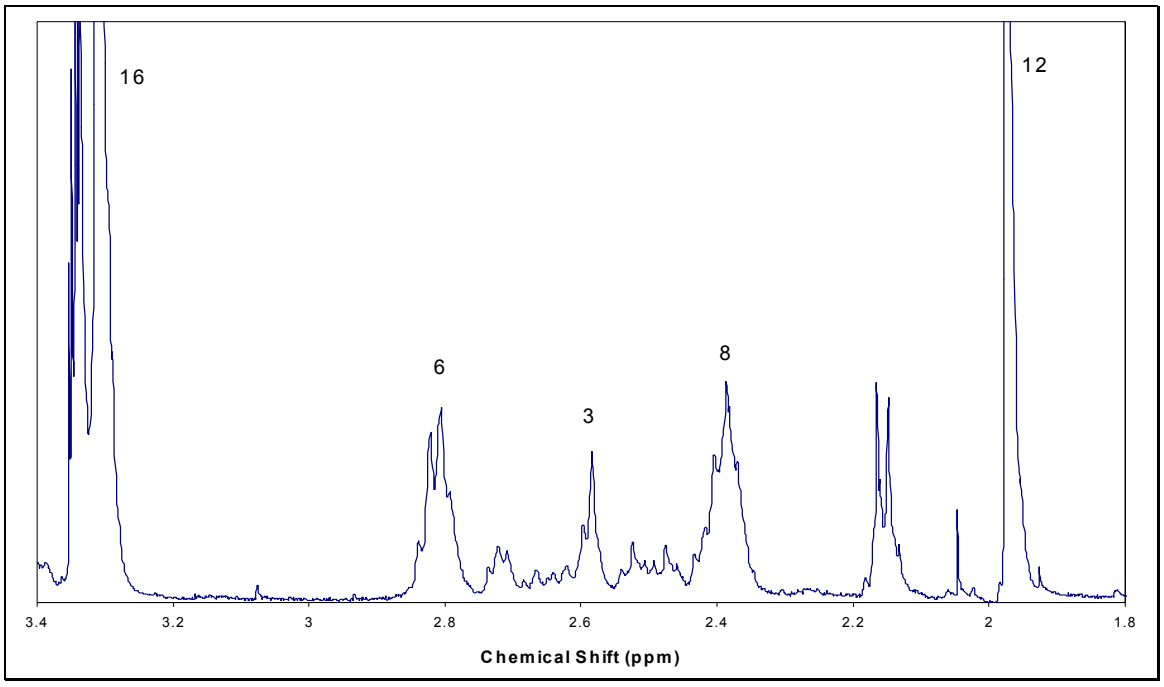

Figure 1.14: ^{1}H NMR spectrum of second attempt AcPAMAM G0 product using a polar solvent and stoichiometric amounts of pyridine.

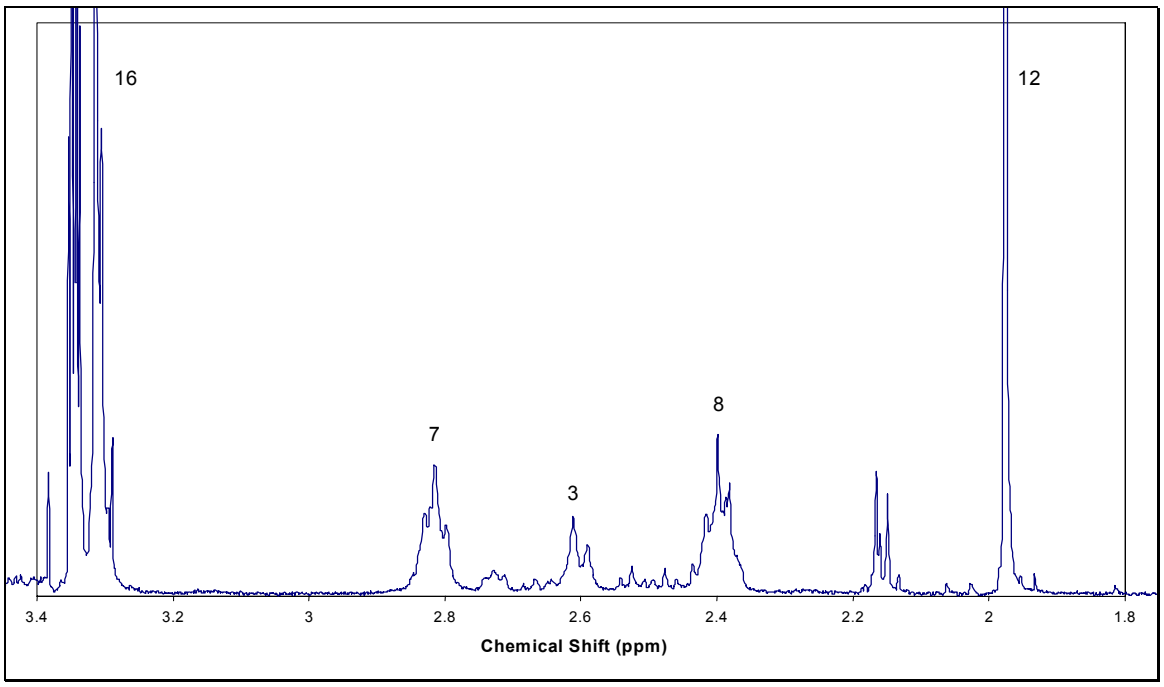

Figure 1.15: ^{1}H NMR spectrum of second attempt AcPAMAM G0 product using a polar solvent and stoichiometric amounts of pyridine after crystallizing in toluene.

AcPAMAM; to attempt a recovery, the toluene was removed from the flask by rotary evaporation. To that residue, small amounts of toluene, 2 mL at a time, were added and heated with a hot air gun. This was continued until most of the solid matter appeared to be dissolved, and then the flask was set on a cork ring on the bench to cool to room temperature. When the flask reached room temperature, it was placed in a refrigerator for one hour. Solid crystals were evident in the toluene; these crystals were collected by vacuum filtration and dried in an oven. The crystals were weighed to be 100 mg; however, 400-MHz ^{1}H NMR analysis (Figure 1.15) indicated that this product was of no better quality than the part extracted previously with ethyl acetate. Furthermore, the product extracted by ethyl acetate was only 29.4 mg – not even 30% of what was found in the toluene.

1.4.2: Use of poly(4-vinylpyridine) in lieu of pyridine. Reducing the amount of pyridine used in the reaction appeared to protect the dendrimers from reverse Michael addition in the time scale of previous reactions, but it seemed to slow the reaction so that it was also not complete in the time scale of previous reactions. This approach left unacceptable uncertainty in the modification process: not knowing how long the reaction needed for completion required prolonging the dendrimer exposure to pyridine; prolonging exposure to pyridine meant increasing opportunities for reverse Michael addition; increasing reverse Michael addition would result in lower product yield and higher impurity levels. By switching to a solid-support material in suspension, such as poly(4-vinylpyridine), the undissolved nucleophile could catalyze the acylation at the dendrimer periphery while leaving the reverse Michael addition kinetically unfavorable due to steric hindrance from the molecular interior. The only foreseen drawback would

be the dilution caused by the increase of solvent required to suspend a stoichiometric amount of the nucleophilic polymer. This would require longer reaction times, which should be safe if the polymer was inhibited from the reverse Michael addition. Poly(4-vinylpyridine) (PVP) was procured from Aldrich, Inc., in powder form with 2% cross-linking.

About 1.5 mL PAMAM G0 20 wt % in methanol was dried in a 5-dram vial by rotary evaporation and then by high vacuum overnight. The starting material PAMAM was weighed as 262.4 mg (0.5078 mmol). The PAMAM was dissolved in 6 mL DMF and transferred to a 100-mL round-bottom flask, to which was added 2.5 g of PVP and a small amount of DMAP catalyst. The solution/suspension was an opaque, off-white color. The flask was set to stir with a magnetic stir bar, and then about 2.0 mL (10× excess) of acetic anhydride was added drop-wise. The flask was capped with a rubber septum, evacuated by vacuum, and backfilled with argon gas. The reaction mixture was left to run at room temperature for three days.

After three days, the appearance of the reaction mixture had not changed noticeably. Under the previous procedure with pyridine, three days would have left the reaction mixture an extremely dark reddish-brown color. The contents of the reaction flask were vacuum filtered, removing the PVP solids, and the solids were flushed with generous amounts of methanol. The methanol was then removed by rotary evaporation, and the DMF was removed overnight with a vacuum distillation apparatus. The next morning, a small amount of a yellow oil remained in the flask, indicating the remaining presence of DMF. The oil was mixed with 2 mL of toluene, the toluene wash was decanted, and the flask was left under high vacuum for another twenty-four hours. After

the second day of vacuum, a solid, yellow-white residue remained in the flask. The solid was weighed as 448.9 mg; the theoretical yield for the reaction was 347.8 mg. Assuming that some PVP had slipped through the filter paper during the vacuum filtration, the product solids were dissolved in 50 mL of methanol in a centrifuge tube and centrifuged at 5000 rpm for 10 min. About 30 mg of a white solid collected at the tip of the centrifuge tube. The methanol was decanted into a 250-mL round-bottom flask and removed by rotary evaporation. The flask was then dried overnight under high vacuum.

Having removed any remaining suspended solids by centrifuge, the remainder of the excess mass was presumed to be DMAP by the process of elimination. Because DMAP dissolves well in most solvents, the flask contents were rinsed several times by swirling large amounts of toluene in the flask. However, repeated weighing indicated that this had little effect on the crude product mass. Observing that the product solids appeared to be somewhat layered, having a white deposit on the bottom, the rinsing procedure was repeated using methanol in place of toluene, in the hopes that the desired product would dissolve more readily than the DMAP. Using 15 mL of methanol, the product was swirled in the solvent quickly and immediately decanted. The large white deposit mostly remained in the flask as a solid. The methanol was then removed from the product by rotary evaporation and then vacuum, and the procedure was repeated two more times. Meanwhile, all of the white solids were retained in a separate flask. The product solids were dried overnight by high vacuum. The remaining solids were weighed as 197.5 mg, but a 400-MHz ^{1}H NMR spectrum (Figure 1.16) indicated that the product was still impure. The product peaks were present, but the integral ratios, especially for the singlets, were not correct. In addition, the presence of DMAP was observed as two

sets of doublets at 6.9 and 8.1 ppm and a singlet at 3.2 ppm, having integral ratios of 2:2:6, respectively. Also, a singlet at 3.2 ppm suggested either acetic acid or acetic anhydride impurities.

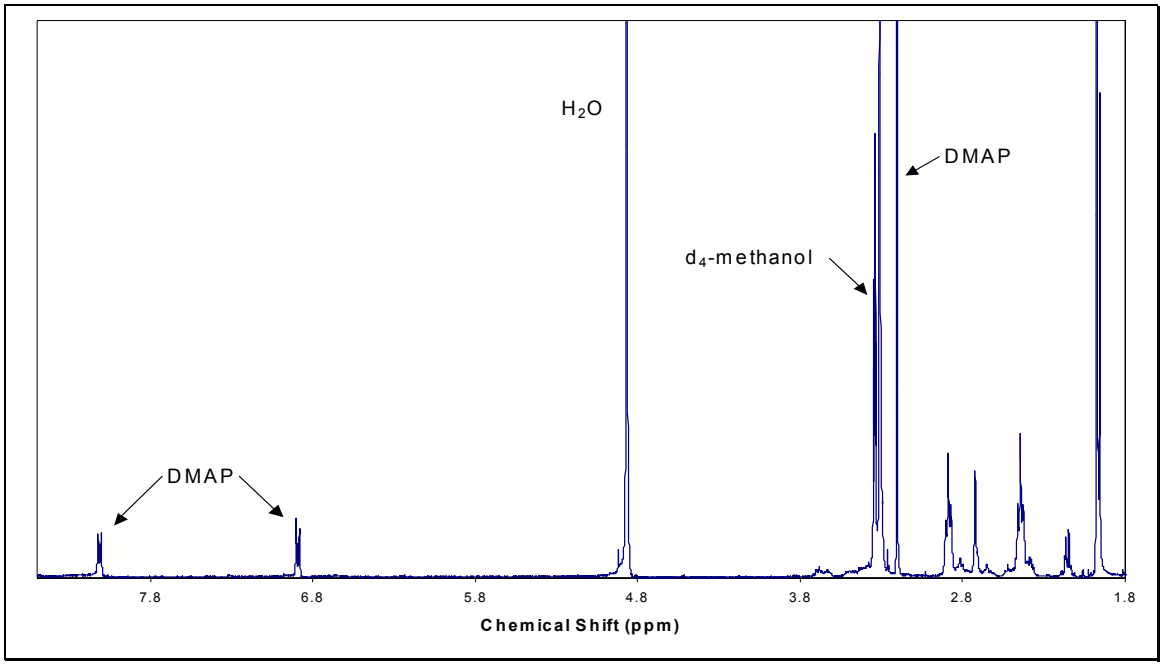

Figure 1.16: ^{1}H NMR spectrum of first attempt AcPAMAM G0 product using poly(4-vinylpyridine) in lieu of pyridine.

The desired product was finally purified by trituration with toluene. At this point, two conclusions became very clear: 1) too much DMAP had been used in this experiment, making removal difficult, and 2) DMAP was too soluble for any type of extraction method that might purify the AcPAMAM. Reverting back to the facts that DMAP is very soluble in toluene and that AcPAMAM has been observed to aggregate in toluene when left to sit overnight, the product solids were dissolved in a minimal amount

of methanol and poured into a beaker containing 200 mL of toluene. The white solids, which were retained out after the methanol rinses, were also dissolved in a minimal amount of methanol, and 200 mL of toluene were added to the flask in which it had been retained. Both the beaker and flask were stirred well and then left to sit. Solids were observed aggregating in both vessels in a manner similar to that observed previously with AcPAMAM in toluene. The two vessels were stored in a refrigerator overnight. In the morning, the aggregated solids were vacuum-filtered from the toluene together in one funnel. The solids were air-dried for several minutes on the vacuum filter, transferred to a watch glass, and then oven-dried for one hour. The product was scraped onto the watch glass from the filter paper and weighed as 145.4 mg, a 41.8% yield from theoretical. The product solids were then transferred to a 5-dram vial and dried in an acetone-reflux drying pistol overnight. The product appeared a dirty white color and clumped together in small pieces. A 400-MHz ^{1}H NMR spectrum (Figure 1.17) indicated the cleanest product yet obtained – the integral ratios were appropriate, and the only non-product peaks were those due to the NMR solvent. Electrospray ionization mass spectrometry (Kallos, Tomalia et al. 1991) verified the desired product mass.

1.5: Final Synthetic Procedure – Experimental Section. [Acetyl]$_4$-poly(amidoamine) G0 starburst dendrimer, (AcPAMAM G0). To a stirred solution of poly(amidoamine) G0 starburst dendrimer (PAMAM G0) (262.4 mg, 0.508 mmol), poly(4-vinylpyridine) (PVP), 2% cross-linked, (2.52 g, 24.2 mmol), and 4-(dimethylamino)pyridine (8.0 mg, 0.066 mmol) in 15 mL of dimethylformamide (DMF), acetic anhydride (1.35 g, 13.2 mmol) was added drop-wise via pipette over 2 min at 25 ºC. After the addition was complete, the flask was capped with a rubber septum, the

atmosphere in the flask was evacuated by vacuum, and the reaction was stirred for 3 days under argon gas maintained at 1 atm. PVP solids were removed by vacuum filtration and rinsed with methanol. The solution was centrifuged 10 min at 5000 rpm to remove residual solids and decanted. Methanol was removed by rotary evaporation, and DMF was removed into a Kugelrohr bulb under high vacuum at 50 ºC. Resultant residue was dried under high vacuum for 12 hours then dissolved in 10 mL methanol. The methanol solution was added drop-wise via pipette into 80 mL toluene, and then the toluene solution was reduced by 10 mL under rotary evaporation to remove methanol. The toluene solution was left to sit for 18 hours, and then the product solids were removed from the toluene by vacuum filtration and dried in an oven (> 70 ºC) for one hour, affording AcPAMAM G0 (145.4 mg, 0.212 mmol, 42%) as a white solid. ^{1}H NMR (400 MHz, CD_3OD) δ 1.98 (s, 12H), 2.40 (t, J = 6.7 Hz, 8H), 2.61 (s, 4H), 2.81 (t, J = 6.8 Hz, 8H), 3.31 (s, 16H) ppm; ^{13}C NMR (400 MHz, CD_3OD) 23.1, 34.9, 40.3, 40.5, 51.5, 52.5, 174.0, 175.6 ppm; ESI-MS for $C_{30}H_{56}N_{10}O_8Na$ (M^+): Calcd 707.417478; obsd 707.41947.

The final procedure has been summarized in step-by-step form in table 1.3. The same procedures were attempted twice with PAMAM G1, and each attempt failed to yield the product, appearing under- or overacylated in the ^{1}H NMR. The reactions time was varied, but none of the trials produced the desired product. The correct timeframe is estimated to be 24 - 48 hours. In addition, PAMAM G1 has slightly different solubility properties than PAMAM G0. As a result, AcPAMAM G1 does not precipitate out of toluene as cleanly as AcPAMAM G0; the G1 product collects as a gel at the flask bottom.

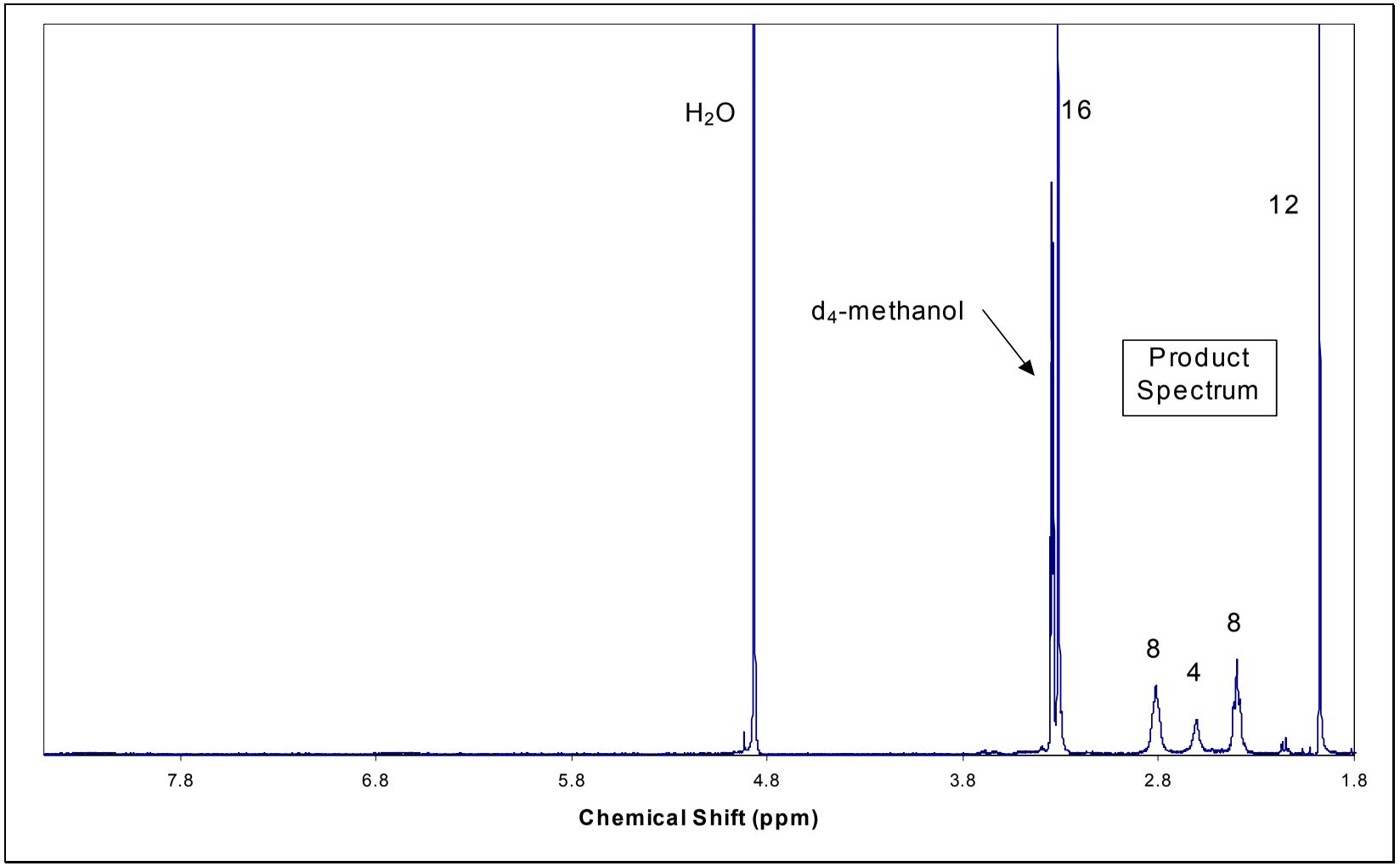

Figure 1.17: ^{1}H NMR spectrum of AcPAMAM G0 product using poly(4-vinylpyridine) in lieu of pyridine, after crystallization in toluene.

	Final Procedure for Best Yield of AcPAMAM G0
1	Place PAMAM G0 20 wt % in methanol into tared container. Remove methanol by rotary evaporation and dry under high vacuum overnight.
2	Weigh PAMAM G0. Dissolve in dimethylformamide (DMF). Transfer to reaction vessel and add stir bar.
3	Measure and add 10× excess (40 equivalents) of poly(4-vinylpyridine) (PVP) powder. Increase DMF as needed to facilitate stirring (5 mL DMF/1 g PVP); energize stir bar.
4	Add 1/20 equivalents of 4-dimethylaminopyridine (DMAP). This may be immeasurably small.
5	Slowly add 10× excess (40 equivalents) of acetic anhydride. One drop at a time is sufficient. Cap vessel with a rubber septum, vacuum out the air, and replace with an inert atmosphere. Maintain positive pressure with a balloon.
6	After six days, use vacuum filtration to remove solids from the reaction. Flush solids with methanol.
7	Reduce solvents by rotary evaporation, and transfer solvents to a centrifuge tube. Centrifuge remaining solids from solution. Decant solution.
8	Remove remaining methanol/DMF by evaporation. DMF evaporation requires the use of high vacuum, mild heat, and a Kugelrohr bulb.
9	Dissolve the remaining products in the minimum amount of methanol possible. Drip methanol solution into a flask containing 10× quantity toluene. Product will begin to aggregate in the toluene; leave flask uncapped overnight.
10	Use vacuum filtration to collect the product solids from the toluene. Dry solids on a watch glass in a drying oven.
11	Weigh solids; product yield should be near 60%.

Table 1.3: Final experimental procedure for the best yield of AcPAMAM G0.

1.6: Synthesis of d-AcPAMAM G0. Following the procedures outlined in table 1.3, d-AcPAMAM G0 was synthesized from PAMAM G0 by substituting d_6-acetic anhydride ($CD_3COOCOCD_3$) for acetic anhydride in step five. The d-AcPAMAM G0 product appeared as a white solid powder, and the reaction completed with a 57.3% product yield. Product composition and purity were verified by ^1H NMR (Figure 1.18). The NMR spectrum indicated that this product was the purest of any AcPAMAM product yet produced; only the predicted ^1H peaks appeared along with the solvent peaks. The methyl singlet near 2.0 ppm was absent, indicating appropriate deuteration.

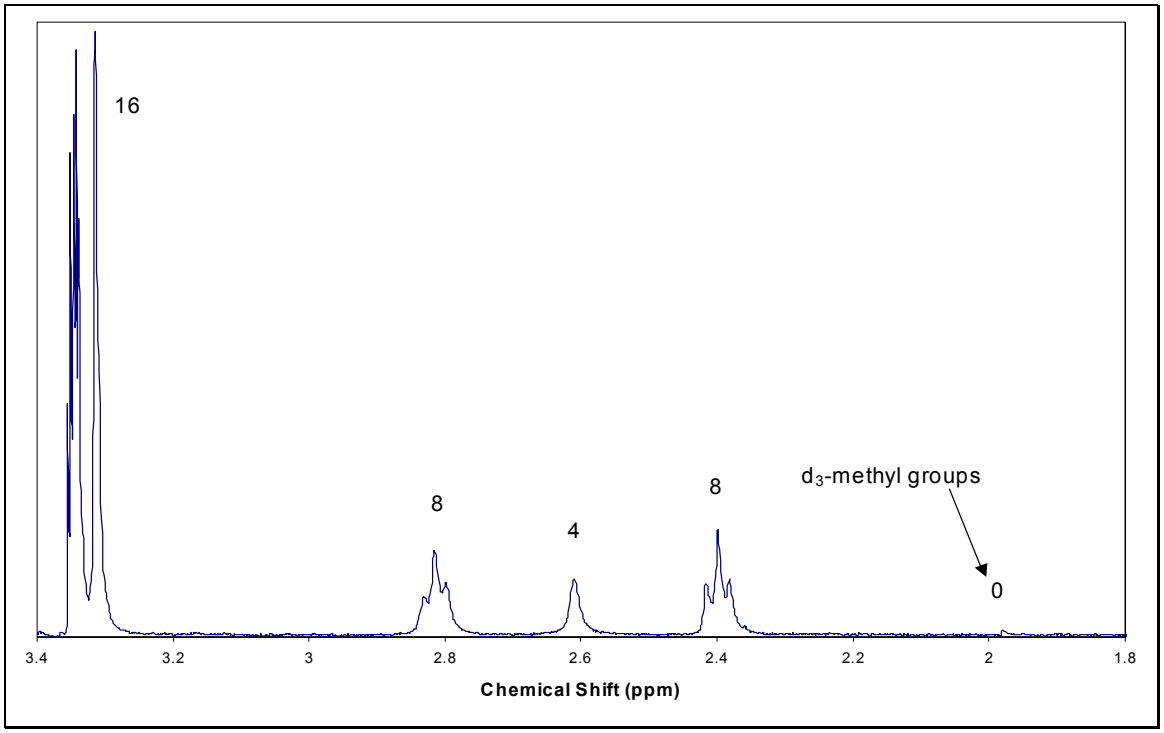

Figure 1.18: ^1H NMR spectrum of d-AcPAMAM G0.

CHAPTER 2

^{1}H AND ^{13}C NMR STUDY OF PAMAM AND ACYLATED PAMAM

2.1: Theory. Nuclear magnetic resonance (NMR) spectroscopy is arguably the single most useful analytical tool for the organic chemist. Atomic nuclei possess a value called the *spin quantum number* that can range from zero to 1 ½. That is not to say that the nuclei are physically spinning, as in classical mechanics, but to assume that nuclei do spin helps to explain the quantum mechanical properties of nuclei that give rise to NMR spectroscopy. All spinning objects have angular momentum, and because nuclei are charged particles, their act of "spinning" creates a magnetic moment, analogous to inductance. As in physics, these properties are vectors, having both a magnitude and direction. In a magnetic field, the spin vectors of all of the atomic nuclei with spin quantum numbers of 1/2 will line up with the field or against it, and there is a distinct energy difference between these two states. This energy difference is very small, and it is equivalent to the energies found in the radio region of the electromagnetic spectrum (Skoog and Leary 1992).

Provided that the magnetic field is strong enough, there will be a larger number of nuclei in the lower energy state. This small excess is enough to create a condition where a radio frequency absorbance experiment can be conducted to produce an analytical spectrum. While absolute field strengths cannot be measured, a scan along radio

frequencies can produce values of chemical shift in relation to a known standard. The magnitude of the chemical shift is dependent on the nuclear shielding effects caused by the magnetism of the surrounding electrons precessing in the magnetic field. Therefore, any quality of a nearby atom that reduces the electron density of the nuclei under study, such as electronegativity, will magnetically deshield the nucleus and increase its chemical shift. Chemical shifts, which are also dependent on the strength of the magnetic field, are generally converted from units of hertz to a dimensionless relative chemical shift, expressed in parts per million. In this way, standard chemical shifts of a compound can be recorded regardless of the strength of the magnet (Skoog and Leary 1992).

For the synthetic organic chemist, two types of NMR experiment are indispensable: ^{1}H and ^{13}C. Both ^{1}H and ^{13}C nuclei possess a spin quantum number of ½, and so they are both viable for NMR studies. Carbon and hydrogen are the most common atoms found in organic chemistry, underscoring the importance of NMR to organic chemistry. The near-100% natural abundance of ^{1}H makes ^{1}H NMR the simpler of the two experiments: Protons provide strong NMR signals, requiring fewer scans and providing more information. From a single spectrum, one can elucidate the number of chemically equivalent hydrogen atoms bonded to carbon, one can integrate the area under the peaks to determine ratios of abundance between the different hydrogen atoms, one can speculate as to the functionalities of the atom based on chemical shift, and one can observe coupling between neighboring atoms to determine how many atoms are bonded to each carbon and which atoms are coupling with which. NMR software will display and integrate the spectra, as well as assist with coupling constants, and for simple spectra, the "N + 1" rule for the number of peaks in a multiplet indicates the number of hydrogens

bonded to each carbon, where N is the number of neighboring atoms. In contrast, ^{13}C is 1.1% abundant in nature, making ^{13}C NMR much more challenging. By conducting numerous scans and by decoupling, signal averaging will produce a spectrum of singlets that will both indicate the number of chemically equivalent carbon atoms in a molecule and also hint at functionality based on chemical shift (Wade 1999). The advantages of ^{13}C NMR over ^{1}H NMR are that carbon comprises the backbone of an organic molecule and that the chemical shift for ^{13}C is in the range of 200 ppm, reducing signal overlap (Skoog and Leary 1992). Other techniques exist for obtaining more information from ^{13}C NMR, but they are beyond the scope of this thesis.

In order to understand the chemical shifts observed from AcPAMAM dendrimers enough to use NMR to identify completed products, it was necessary to first examine the starting material PAMAM dendrimers, G0 and G1. This task was accomplished first by consulting a commercial software application, ChemDraw, which is capable of empirically predicting both ^{1}H and ^{13}C NMR chemical shifts. Then, by comparing the empirical predictions with observed spectra, reasonable conclusions could be made as to chemical shift peak assignments. Because of the molecule size limits in the ChemDraw software NMR scripts, PAMAM G1 was evaluated as a half molecule.

2.2: NMR Study. All of the spectra utilized in this study were taken with a Bruker DPX-400 MHz NMR spectrometer using a 30º tip angle and a one-second recycle time. Proton NMR spectra were acquired in 16 scans; ^{13}C NMR spectra were acquired in 1024 scans. Both of the PAMAM dendrimers used for this study were obtained from Aldrich, Inc., dried of methanol, and sampled for NMR study. The AcPAMAM dendrimers used for this study were those prepared by the methods described in section 1.3 of this thesis.

2.2.1: PAMAM G0. Due to the radial symmetry of the PAMAM G0 molecule, chemical equivalence can be observed amongst all atoms found equidistant from the center of the molecular core. Judging by visual inspection, PAMAM G0 has six chemically unique carbon atoms, labeled as A – F in figure 2.1. All of these carbon atoms are covalently bonded to two chemically equivalent hydrogen atoms, with the exception of carbon atom D, the amide carbonyl.

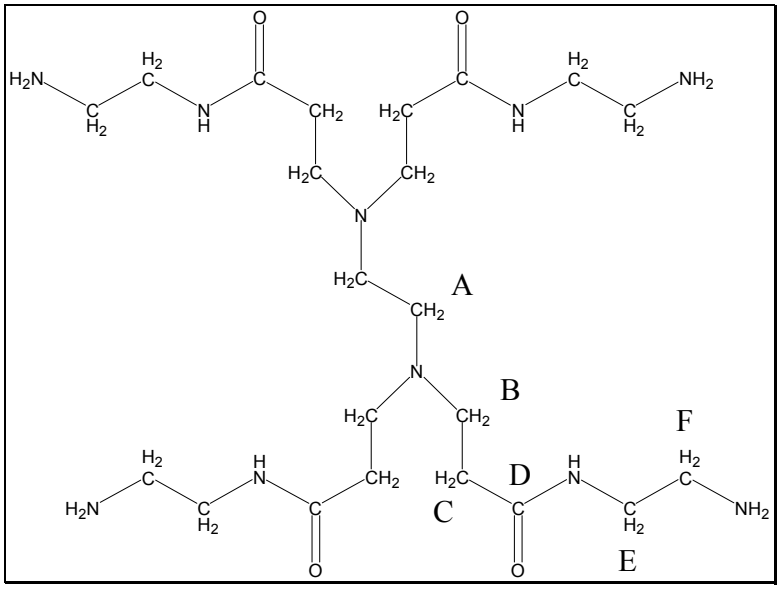

Figure 2.1: Starburst PAMAM Dendrimer, Generation 0, with chemically unique carbon atoms labeled A – F.

Considering first the ^{1}H NMR spectrum, it was predicted that the spectrum would consist largely of triplets; the ChemDraw software predicted that the chemical shifts for these protons would range from 2.28 – 3.46 ppm. The observed spectrum (Figure 2.2), calibrated to the d_4-methanol quintet at 3.31 ppm (Gottlieb, Kotlyar et al. 1997), largely correlated with these predictions. The carbon A protons are only capable of coupling

with each other, being the only protons at the ethylenediamine core; therefore, they are represented as a singlet observed at 2.54 ppm. The next two carbon atoms, B and C, have protons which couple with each other, and they are both represented as triplets bearing coupling constants near 6.8 Hz. Matching these peaks to the empirical predictions indicated that the carbon B protons are centered at 2.77 ppm, while the carbon C protons are centered at 2.36 ppm. Carbon atoms E and F are very similar to carbon atoms B and C; they are represented by triplets centered at 3.25 and 2.72 ppm and bearing coupling constants near 6.3 Hz.

The ^{13}C spectrum (Figure 2.3) is not as complicated. Calibrating with the d_4-methanol septuplet at 49.05 ppm (Gottlieb, Kotlyar et al. 1997), the ^{13}C NMR spectrum of PAMAM G0 displayed six peaks for the six unique carbon atoms. For peak assignments, the observed peaks were labeled in the same relative order in which they were empirically predicted (Table 2.1). For the purposes of this experiment, it was sufficient to note that the experimental spectrum resembled that which was expected, in order to validate the results of the ^{1}H NMR spectrum and the mass spectrum results.

C Atom	^{1}H Chemical Shift (ppm)	Multiplet	Integral	Coupling (Hz)	^{13}C Chemical Shift (ppm)
A	2.54	1	4	---	52.8
B	2.77	3	8	6.9	51.7
C	2.36	3	8	6.8	35.1
D	---	---	---	---	175.7
E	3.25	3	8	6.3	43.4
F	2.72	3	8	6.3	42.4

Table 2.1: NMR data for Starburst PAMAM G0 dendrimer.

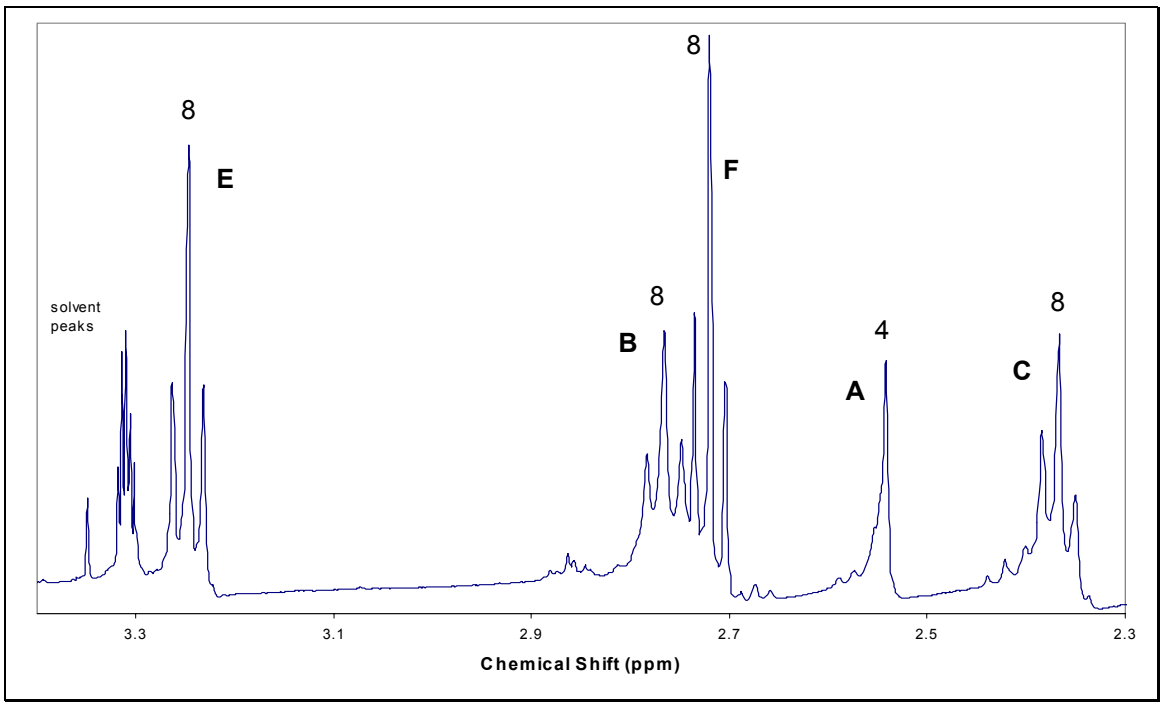

Figure 2.2: ^{1}H NMR spectrum of Starburst PAMAM G0 dendrimer.

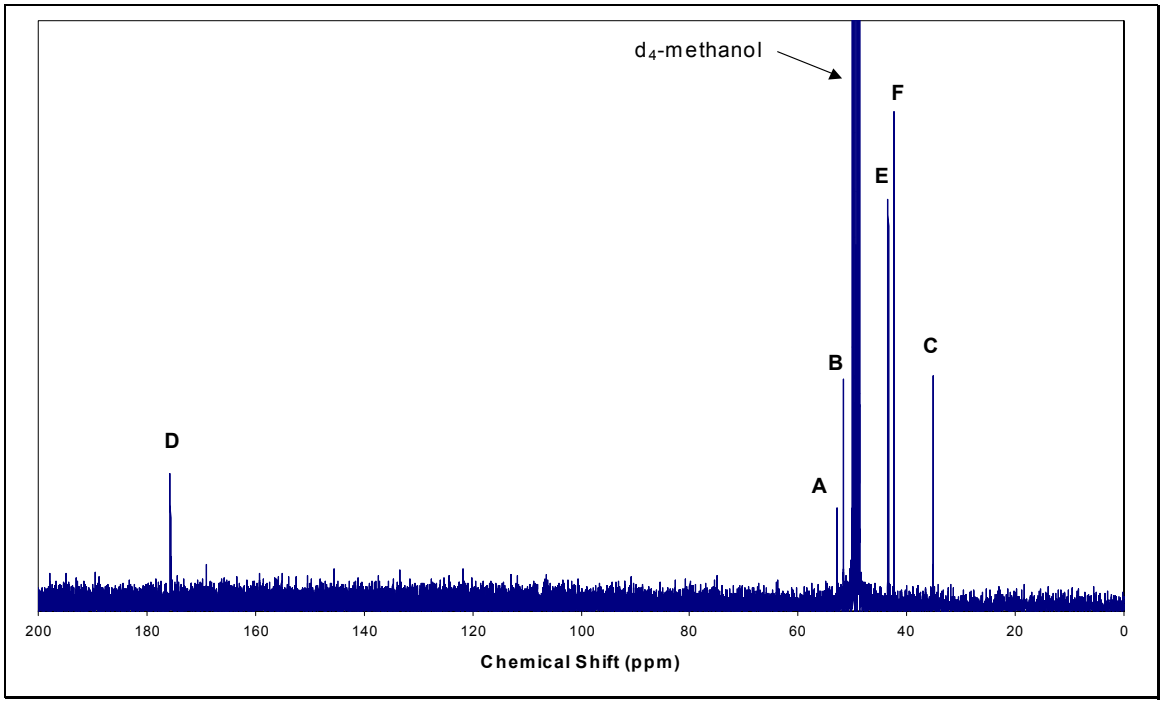

Figure 2.3: ^{13}C NMR spectrum of Starburst PAMAM G0 dendrimer.

2.2.2: PAMAM G1. Like the PAMAM G0 molecule, chemical equivalence can be observed in the G1 molecule amongst all atoms found equidistant from the center of the core. Counting from the center, PAMAM G1 has eleven chemically unique carbon atoms, labeled A, $B_0 - F_0$, and $B_1 - F_1$ in figure 2.4. The subscript numbers 0 and 1 denote the generation to which a carbon atom belongs; there is a noticeable structural similarity amongst carbon atoms labeled with the same letter in each generation. All of these carbon atoms are covalently bonded to two chemically equivalent hydrogen atoms, with the exception of carbon atoms D_0 and D_1, the amide carbonyls.

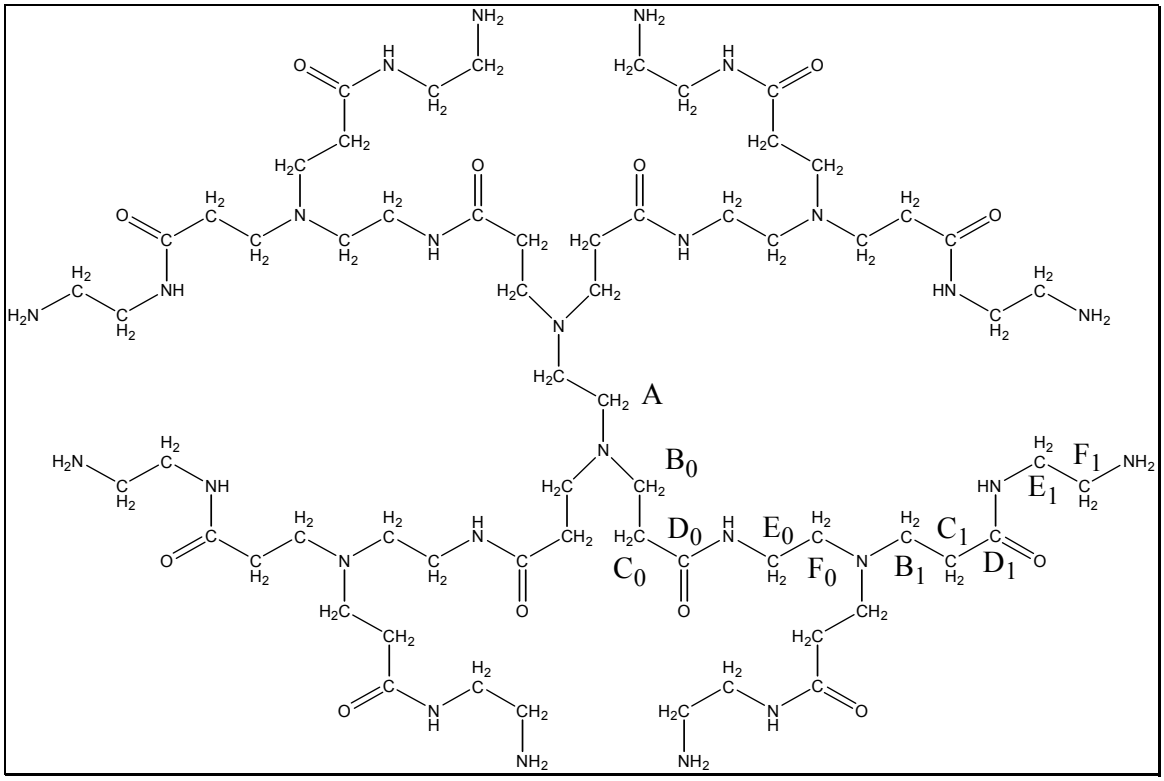

Figure 2.4: Starburst PAMAM Dendrimer, Generation 1, with chemically unique carbon atoms labeled A, $B_0 - F_0$, and $B_1 - F_1$.

Due to the structural similarities between PAMAM G0 and G1, the ^{1}H NMR spectrum of PAMAM G1 was predicted to be essentially the same as that of PAMAM G0, with one notable exception. Carbon atom F_0, bonded to a primary amine in PAMAM G0, is now bonded to a tertiary amine, due to the creation of generation 1, while their counterparts at F_1 are still bonded to a primary amine. In this respect, the carbon F_0 protons are more similar to the core protons, and the F_1 protons are more similar to the F protons of PAMAM G0. The observed spectrum (Figure 2.5), calibrated to the d_4-methanol quintet at 3.31 ppm (Gottlieb, Kotlyar et al. 1997), also largely correlated with these predictions. The carbon A protons are represented as a singlet observed at 2.58 ppm, and it is superimposed by a triplet at 2.59 ppm, representing the F_0 protons coupling with E_0. Carbon atoms, B_{0-1}, C_{0-1}, E_{0-1}, and F_1 are all represented as triplets in the same relative positions as the corresponding protons in the spectrum of PAMAM G0. Although the triplets for each corresponding set of methylene protons overlap, it was observed that they do not overlap so perfectly as to be indistinguishable. The G1 proton triplets are offset from the proton triplets from the inner generation, and they are the taller of the two due to having twice as many protons as the lower generation.

The ^{13}C spectrum of PAMAM G1 was calibrated with the d_4-methanol septuplet at 49.05 ppm (Gottlieb, Kotlyar et al. 1997). ChemDraw predicted eight peaks for the ^{13}C spectrum, with carbons B – D being equivalent in the two generational levels. The ^{13}C NMR spectrum of PAMAM G0 displayed six peaks for the six unique carbon atoms. For peak assignments, the observed peaks were labeled in the same relative order in which they were empirically predicted (Table 2.2).

C Atom	^{1}H Chemical Shift (ppm)	Multiplet	Integral	Coupling (Hz)	^{13}C Chemical Shift (ppm)
A	2.59	1	4	---	51.6
B_0	2.80	3	8	6.9	50.2
C_0	2.37	3	8	6.8	35.0
D_0	---	---	---	---	175.2
E_0	3.26	3	8	6.3	39.1
F_0	2.58	3	8	6.3	53.9
B_1	2.79	3	16	6.9	50.2
C_1	2.37	3	16	6.8	35.2
D_1	---	---	---	---	175.6
E_1	3.25	3	16	6.3	43.4
F_1	2.73	3	16	6.3	42.4

Table 2.2: NMR data for Starburst PAMAM G1 dendrimer.

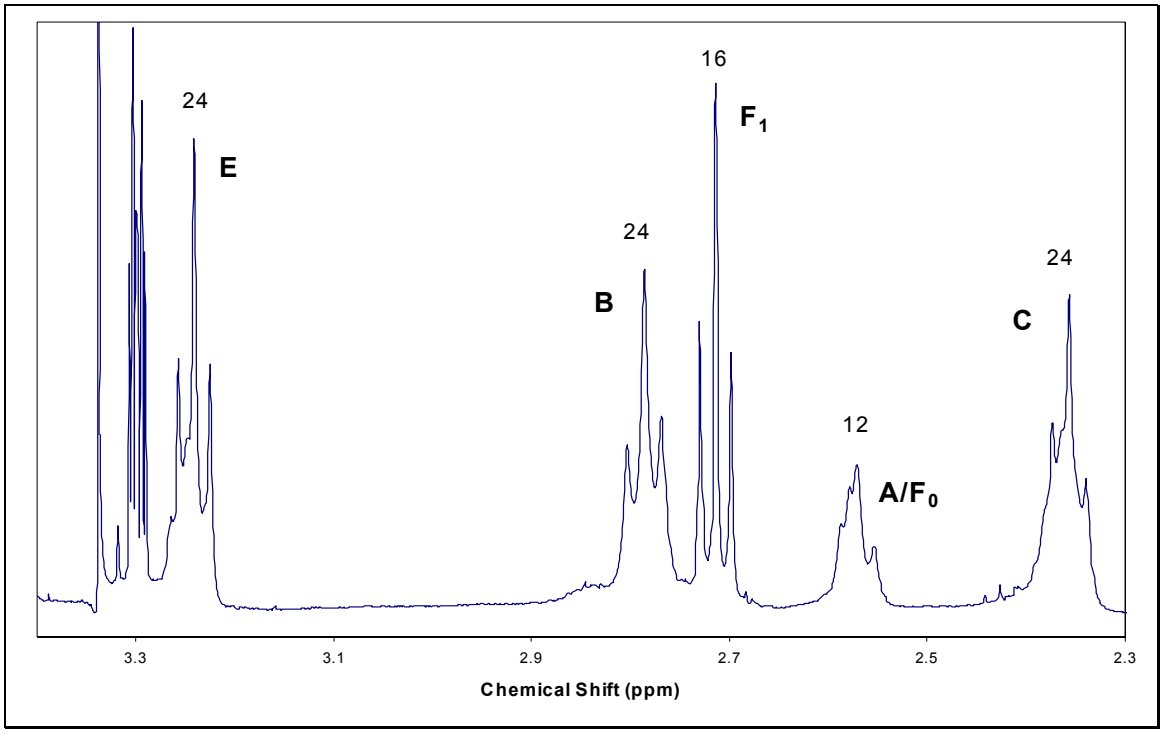

Figure 2.5: ^{1}H NMR spectrum of Starburst PAMAM G1 dendrimer.

2.2.3: AcPAMAM G0. AcPAMAM G0 has eight chemically unique carbon atoms, labeled as A – H in figure 2.6. All of these carbon atoms are covalently bonded to two chemically equivalent hydrogen atoms, with the exception of carbon atoms D and G, the amide carbonyls, and carbon atom H, the methyl group. As similar as this molecule is to the non-acylated PAMAM G0, so are the NMR spectra of AcPAMAM G0 to PAMAM G0. The change between PAMAM G0 and AcPAMAM G0 causes only three structurally significant differences: 1) the addition of a carbonyl, 2) the addition of a methyl functionality, and 3) carbon F changes from a primary amine carbon to an amide carbon.

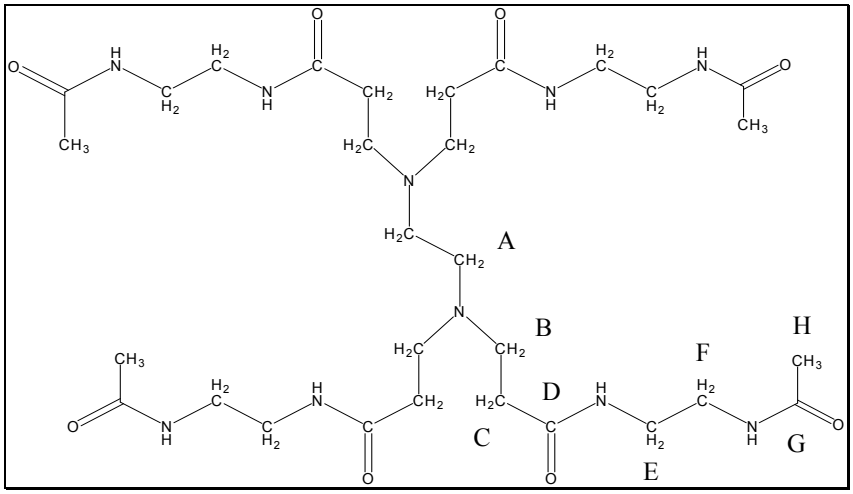

Figure 2.6: Starburst AcPAMAM Dendrimer, Generation 0, with chemically unique carbon atoms labeled A – H.

The ^{1}H NMR spectrum should only reflect the second and third changes. The methyl functionality was predicted to produce a new singlet near 2.0 ppm, and it was predicted that carbon F protons would become equivalent to the carbon E protons,

merging as a singlet at the chemical shift of the carbon E protons. The observed spectrum (Figure 2.7), calibrated to the d_4-methanol quintet at 3.31 ppm (Gottlieb, Kotlyar et al. 1997), correlated with these predictions. The spectrum was unchanged with respect to carbon atoms A – D, and the above-mentioned changes were observed. It can be shown that the protons on carbon atoms E and F have become chemically equivalent by tracing the molecule as far as four bonds from each proton. NMR deshielding effects are generally only significant as far as two bonds from a particular atom; a four-bond similarity is more than adequate enough to demonstrate equivalence.

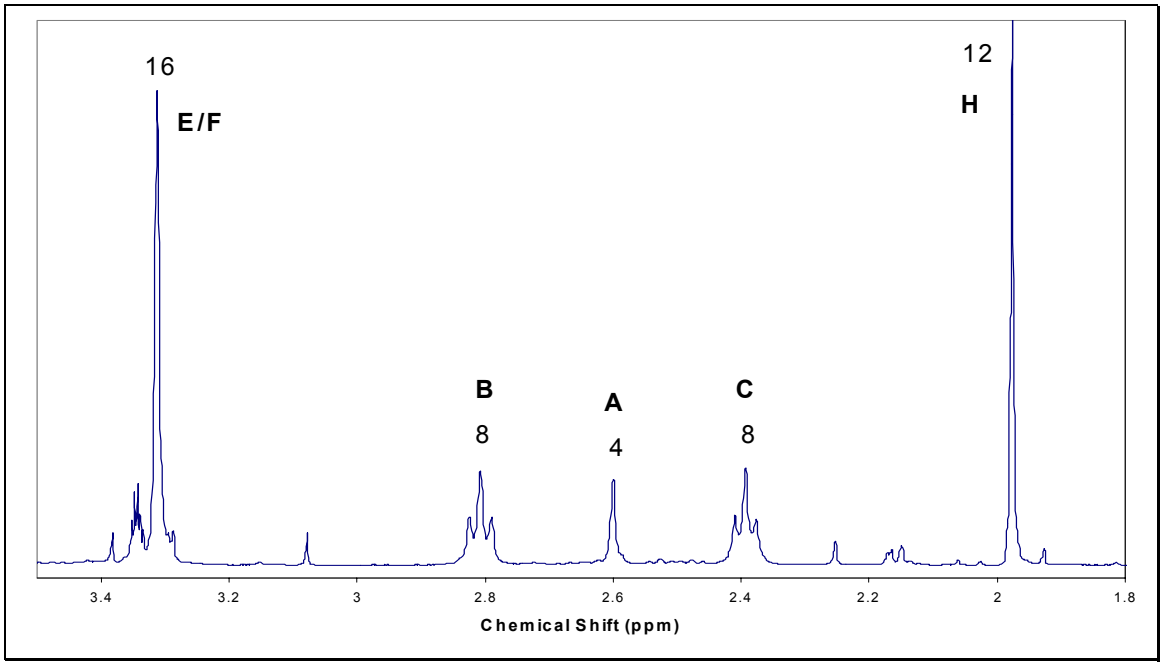

Figure 2.7: ^{1}H NMR spectrum of Starburst AcPAMAM G0 dendrimer.

The ^{13}C NMR spectrum of AcPAMAM G0 (Figure 2.8) was predicted to display all three structural changes in contrast to the spectrum of PAMAM G0. Calibrating with

the d_4-methanol septuplet at 49.05 ppm (Gottlieb, Kotlyar et al. 1997), the ^{13}C NMR spectrum of AcPAMAM G0 displayed eight peaks for the eight carbon atoms. First, assignments were made based on the PAMAM G0 spectrum. Remaining peak assignments were made considering the structural changes made by acylation: 1) a second carbonyl peak was observed at 173.97 ppm, 2) a methyl peak was observed at 23.09 ppm, and 3) the carbon F peak, observed at 40.34 ppm, had shifted to within 0.3 ppm of the carbon E peak.

C Atom	^{1}H Chemical Shift (ppm)	Multiplet	Integral	Coupling (Hz)	^{13}C Chemical Shift (ppm)
A	2.57	1	4	---	52.5
B	2.77	3	8	6.8	51.5
C	2.36	3	8	6.7	34.9
D	---	---	---	---	175.6
E	3.28	1	8	---	40.5
F	3.28	1	8	---	40.3
G	---	---	---	---	174.0
H	1.94	1	12	---	23.1

Table 2.3: NMR data for Starburst AcPAMAM G0 dendrimer.

2.2.4: AcPAMAM G1. Like the AcPAMAM G0 molecule, AcPAMAM G1 differs only slightly from its PAMAM G1 counterpart. AcPAMAM G1 has thirteen chemically unique carbon atoms, labeled A, B_0 – F_0, and B_1 – F_1, G, and H in figure 2.8. The subscript numbers 0 and 1 denote the generation to which a carbon atom belongs; again, there is a noticeable structural similarity amongst carbon atoms labeled with the

same letter in each generation. All of these carbon atoms are covalently bonded to two chemically equivalent hydrogen atoms, with the exception of carbon atoms D_0, D_1, and G, the amide carbonyls, and carbon atom H, the methyl group.

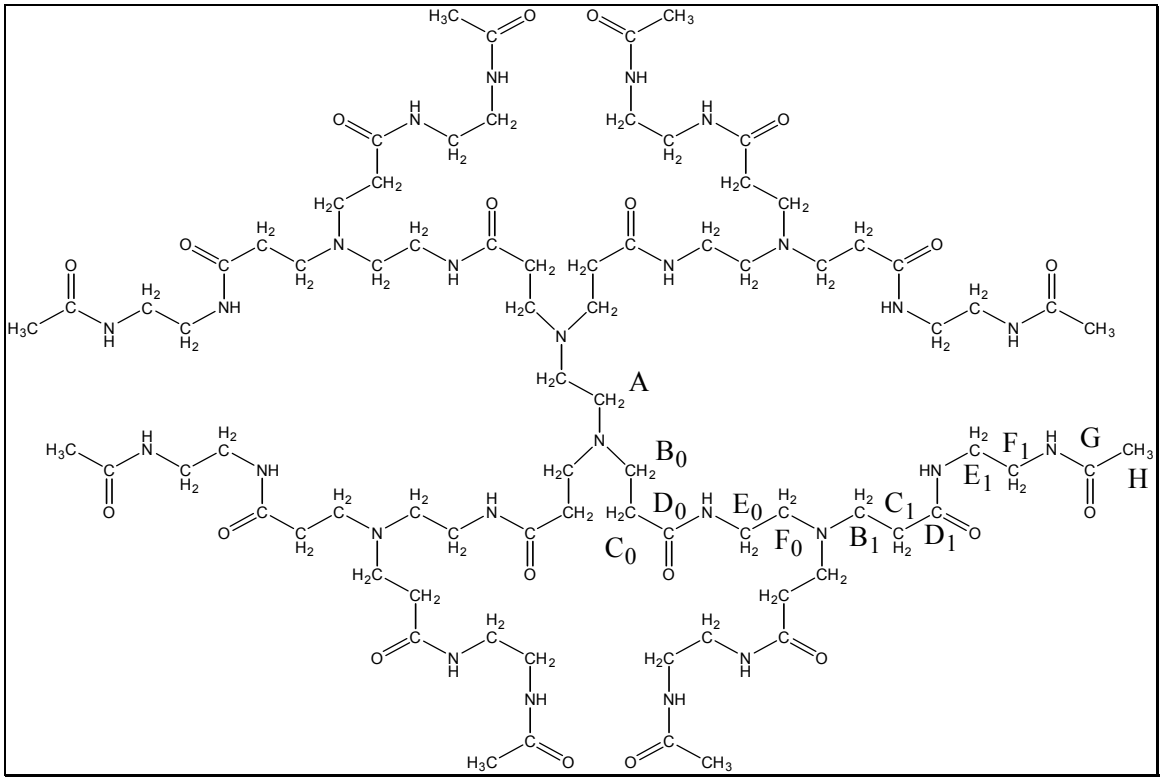

Figure 2.8: Starburst AcPAMAM Dendrimer, Generation 1, with chemically unique carbon atoms labeled A, $B_0 - F_0$, $B_1 - F_1$, G, and H.

The ^{1}H NMR spectrum of AcPAMAM G1 differs from the ^{1}H NMR spectrum of PAMAM G1 in a nearly identical fashion as AcPAMAM G0 differs from PAMAM G0. Again, a singlet arises near 2.0 ppm to signify the addition of eight methyl groups to the periphery of the molecule, and the protons on carbon F_1 become chemically equivalent to the amide protons on carbon atom E_1, merging into a singlet near 3.3 ppm. Also, like the

C Atom	^{1}H Chemical Shift (ppm)	Multiplet	Integral	Coupling (Hz)
A	2.59	1	4	---
B_0	2.80	3	8	6.7
C_0	2.38	3	8	6.7
D_0	---	---	---	---
E_0	3.26	3	8	6.5
F_0	2.58	3	8	6.5
B_1	2.79	3	16	6.6
C_1	2.35	3	16	6.6
D_1	---	---	---	---
E_1	3.28	1	16	---
F_1	3.28	1	16	---
G	---	---	---	---
H	1.94	1	24	

Table 2.4: NMR data for Starburst AcPAMAM G1 dendrimer.

spectrum for PAMAM G0, the triplets for the two generations of carbons atoms B and C do not overlap perfectly, causing the peaks to appear broader or less resolved. Because there is no structural change to the carbon F_0 protons, they remain as a triplet overlapping the core proton singlet, as in the PAMAM G1 spectrum.

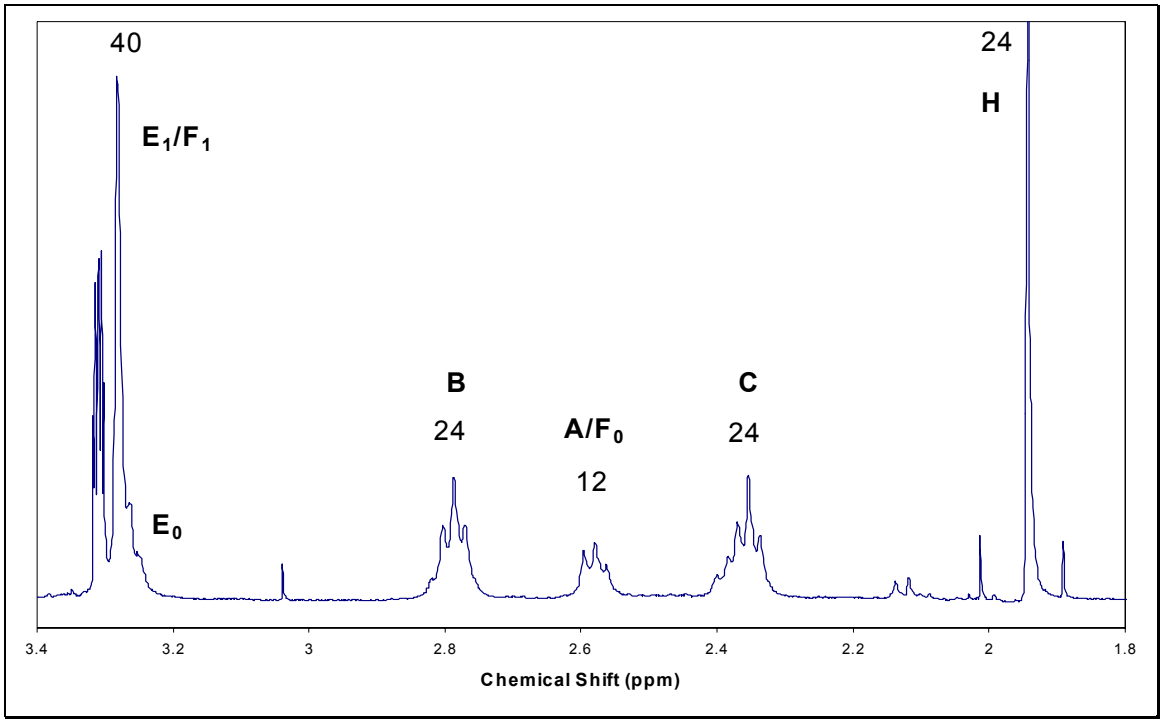

Figure 2.9: ^{1}H NMR spectrum of Starburst AcPAMAM G1 dendrimer.

CHAPTER 3

VIBRATIONAL STUDY OF PAMAM, AcPAMAM, AND d-AcPAMAM

3.1: Background. Since relatively few vibrational studies have been completed on PAMAM dendrimers (Dillon and Shriver 2001; Manna, Imae et al. 2001; Kovalenko, Furer et al. 2002) or their acylated products, little was known about the vibrational characteristics of these molecules prior to this study. A request made to the manufacturer, Aldrich, Inc., for any available spectra resulted in an FTIR spectrum of the 20 wt % methanol solution and an HPLC chromatogram demonstrating the product purity. After an extensive literature search, one article was found discussing vibrational mode assignments for PAMAM G4 dendrimers (Manna, Imae et al. 2001).

This began a two-pronged approach to interpreting the vibrational spectra collected from these compounds. First, the dendrimers were broken down into smaller molecules that may have been studied previously. Second, the dendrimers, in whole and as their "decomposed" counterparts, would be subjected to *in silico* studies using Gaussian software. Two issues had to be overcome: the software learning curve and the lack of computer resources available to conduct the study. The locally available computers equipped with Gaussian were not powerful enough to complete calculations on a molecule as large as PAMAM in a reasonable timeframe. Ethylenediamine was chosen as a model study both for learning procedure and for learning how to conduct a

comparison between calculated and experimental studies. A grant of computer resource credit was obtained from the Ohio Supercomputer Center in order to access enough computational power to analyze a molecule as large as AcPAMAM G0; even on the most powerful computer available, the geometric optimization of the AcPAMAM G0 molecule required approximately one and a half weeks.

3.2: Computational predictions of vibrational spectra.

3.2.1: HyperChem 6.0. To prepare a molecule for analysis under the Gaussian software program, it must first be constructed in either a Cartesian coordinate format or in a format called z-matrix. The use of HyperChem, a 3-D graphical interface application, greatly facilitated this task. In addition, a low-level geometric optimization calculation can be performed by HyperChem in a short amount of time, providing a first iteration for Gaussian, thereby reducing the amount of computational time consumed during the optimization by Gaussian. HyperChem version 6.0 was used for this study.

The following procedure was used to build the ethylenediamine molecule for study. The N-C-C-N backbone was assembled roughly on the HyperChem worksheet, and the backbone was given the ethylenediamine shape using the "Add H's and Model Build" command. This command uses a valence bond theory approach to add an appropriate number of hydrogen atoms to each backbone atom and then shapes the molecule by rearranging the atoms into empirical bond lengths and angles. The s-*trans*-conformer of ethylenediamine appeared as a result. A molecular mechanics geometric optimization was then performed on the empirical molecule; the settings were set to AMBER2, distance dependent dielectric, scale factor 1, electrostatic/Van der Waals 0.5, and no cutoffs. The geometry optimization was calculated using Polak-Ribiere with an

RMS gradient of 0.1. After the molecule converges with a gradient of 0.1, the gradient can be decreased by factors of 10 for successive runs until HyperChem will no longer converge. Smaller molecules can converge at much smaller gradients than larger molecules. Finally, for the transfer to Gaussian, the molecule was saved to disk in the Brookhaven *.ent format.

3.2.2: Gaussian 98.A.9. The Brookhaven file created by HyperChem was transferred to the Ohio State Supercomputer Center and accessed by a secure shell client. The file was opened by a text editor, and two carriage returns were appended to the end of the file. Next, at the command line, a z-matrix file was created using the command, "newzmat -ient <filename>.ent <filename>.com." Without the extra spaces added at the end of the Brookhaven file, the "newzmat" command will not properly recognize the file.

Using a text editor, the newly created z-matrix *.com file was edited into a Gaussian job file (Figure 3.1). The command "%mem=24Mw" was added to the top of the file to allocate 24 Mw of memory from the Supercomputer Center. Next, the file's command line was altered to read, "# HF/6-31G* OPT FREQ," indicating a geometry optimization and vibrational frequency calculation using a Hartree-Fock approximation and a 6-31G* basis set. Finally, a title line was added, and the job was saved at the Supercomputer Center. The job was run using Gaussian 98 version A.9; Gaussian calculations create a *.log file that contains predicted vibrational frequencies and relative intensities for both infrared and Raman spectra.

```
%mem=24Mw

# HF/6-31G* OPT FREQ

Optimization and vibrational frequencies for ethylenediamine

 0 1
 C
 C,1,R2
 N,1,R3,2,A3
 H,1,R4,2,A4,3,D4,0
 H,1,R5,2,A5,3,D5,0
 N,2,R6,1,A6,3,D6,0
 H,2,R7,1,A7,6,D7,0
 H,2,R8,1,A8,6,D8,0
 H,3,R9,1,A9,2,D9,0
 H,3,R10,1,A10,9,D10,0
 H,6,R11,2,A11,1,D11,0
 H,6,R12,2,A12,11,D12,0
      Variables:
 R2=1.52900523
 R3=1.47442328
 R4=1.07865147
 R5=1.09160158
 R6=1.47347922
 R7=1.07910796
 R8=1.09213964
 R9=1.00645218
 R10=1.00449042
 R11=1.00645218
 R12=1.00449042
 A3=109.0958493
 A4=107.32905317
 A5=109.73126078
 A6=109.10866628
 A7=107.32163614
 A8=109.72128241
 A9=114.50286622
 A10=112.73003463
 A11=114.51514031
 A12=112.72522546
 D4=118.16056501
 D5=-125.10346087
 D6=-179.34179749
 D7=118.20921132
 D8=-125.1494745
 D9=162.23818913
 D10=128.79566256
 D11=162.23642605
 D12=128.80232565
```

Figure 3.1: Z-matrix format Gaussian job file for calculating a geometric optimization and vibrational frequencies for s-*trans*-ethylenediamine.

3.2.3: VibSpec 1.1. Gaussian predictions are very difficult to compare to an experimentally acquired spectrum. Apart from not being able to visualize the data as a spectrum, Gaussian provides "3N - 6" vibrational modes; it is very rare to resolve a vibrational spectrum into "3N - 6" peaks. To generate predicted spectra, a computer program was written in C and compiled to accept a data file of frequencies and intensities, transform them into Lorentzian line shapes, and then arrange them into a spectrum, adding the absorptions where there is overlap. Initially, the program was written with a built-in broadening factor of 50 cm^{-1} and no scaling; an upgrade was written to allow the user to specify both the scaling factor and broadening factor. The upgrade program was named VibSpec 1.1, and its code and programming details are contained in Appendix A.

3.2.4: Ethylenediamine model study. Ethylenediamine seemed like a logical choice for a model study to determine how much credence could be placed on the results of such a study. It is a relatively small molecule, requiring much less computer resource time, yet it is large enough to have thirty vibrational modes. It is also a major component of PAMAM dendrimers, being both the initiator core and the outer "half" of each branch, and ethylenediamine is extremely common, making literature searches fairly abundant. Following the procedures described above, ethylenediamine ($NH_2CH_2CH_2NH_2$) was modeled for computational study. The s-*trans*- conformer was chosen as the global minimum, but as it will be shown, the s-*cis*- conformer has some effect on the experimental vibrational spectrum. The s-*trans*- and s-*cis*- prefixes denote the rotating single-bond analogues of the commonly-known *trans*- and *cis*- isomerism (Wade 1999). Using the job file used as an example in figure 3.1, thirty vibrational modes were

calculated for s-*trans*-ethylenediamine, along with relative intensities for both infrared and Raman spectra. These modes were compiled into data files and plotted as spectra using VibSpec 1.1 with a scaling factor of 0.9 (Scott and Radom 1996) and a broadening factor of 50 cm^{-1} (Figures 3.2 and 3.4).

For comparison, IR and Raman frequencies and mode assignments for ethylenediamine were acquired from literature (Giorgini, Pelletti et al. 1983). The literature spectra shown here (Figures 3.3 and 3.5) were approximated from the literature data using VibSpec 1.1 (Appendix A). Table 3.1 summarily compares the calculated frequency values to the reported values. The frequencies listed in the calculated column were taken from the VibSpec plots of the calculated data to accurately compare the spectra, since no spectrometer can resolve individual vibrational modes from a liquid sample. The calculated spectra, after scaling, provided approximate vibrational frequencies. More importantly, the mode assignments were predicted in the correct relative order.

Lit IR	**Lit Raman**		**Calc/Scaled**
3349	3355	NH_2, as	3432
3279	3290	NH_2, ss	3359
3189	3185	NH_2, ss	
2922	2925	CH_2, ss	2944
	2904	CH_2, as	
2853	2852	CH_2, ss	2817

Table 3.1: A comparison of ethylenediamine vibrational frequency (cm^{-1}) literature values with calculated values for s-*trans*-ethylenediamine.

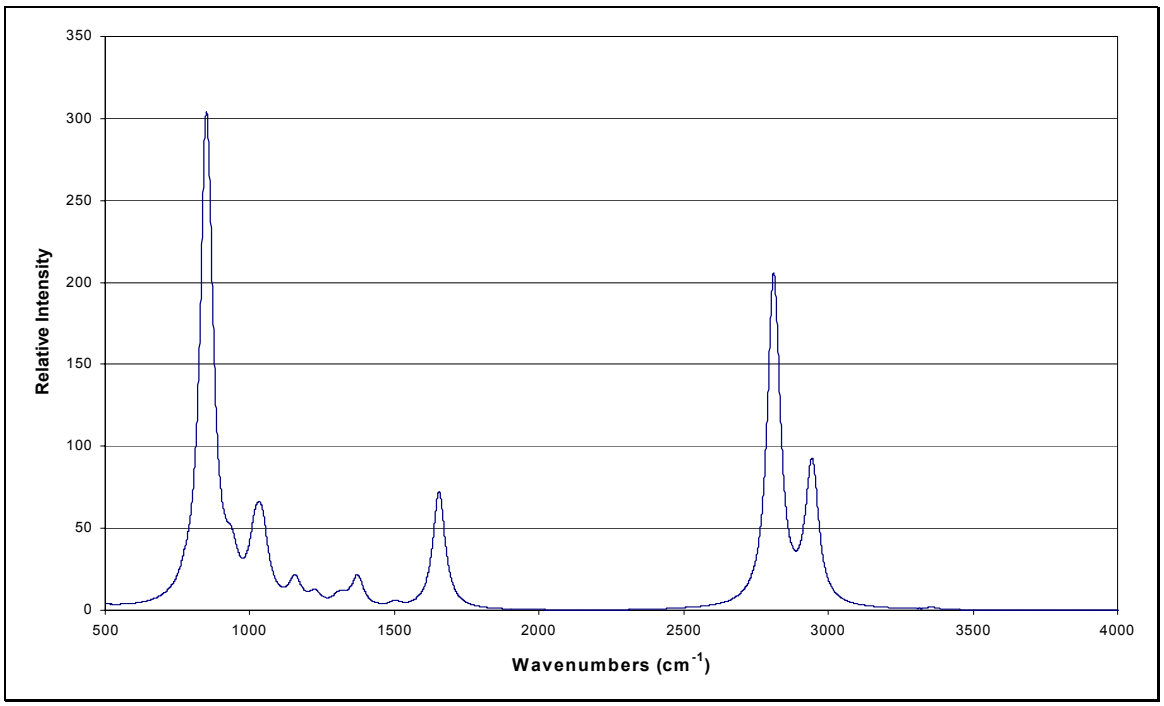

Figure 3.2: Calculated IR spectrum of s-*trans*-ethylenediamine from Gaussian 98.A.9.

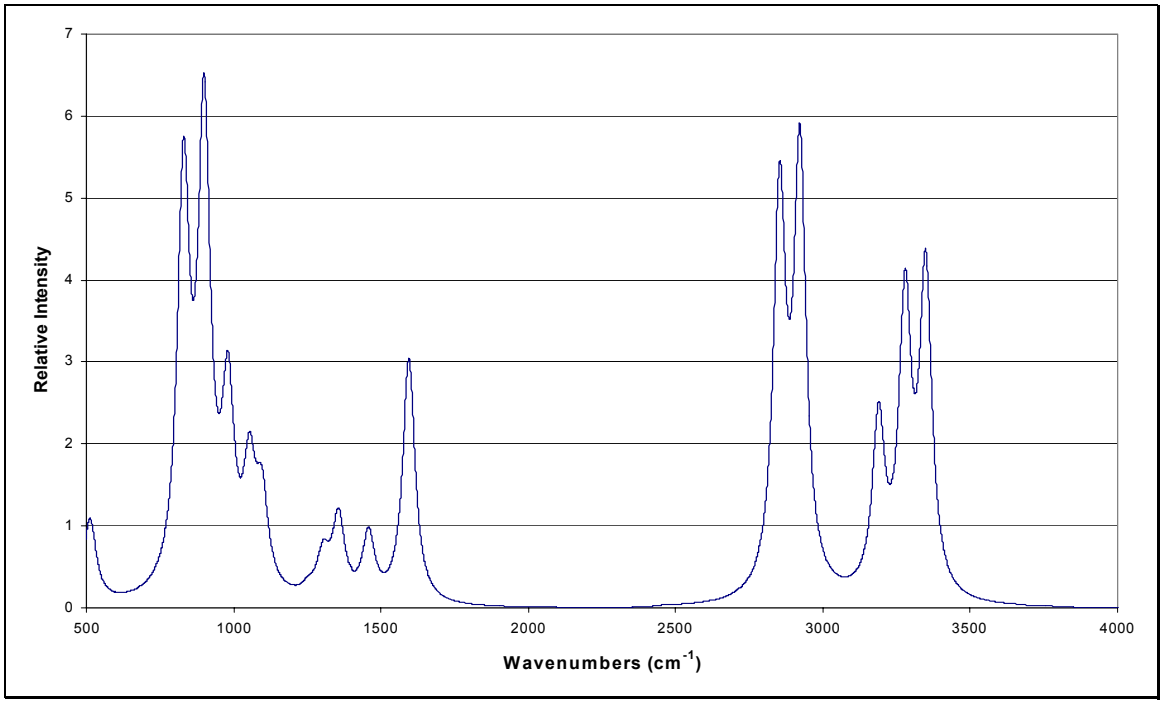

Figure 3.3: Literature IR spectrum of ethylenediamine (Giorgini, Pelletti et al. 1983).

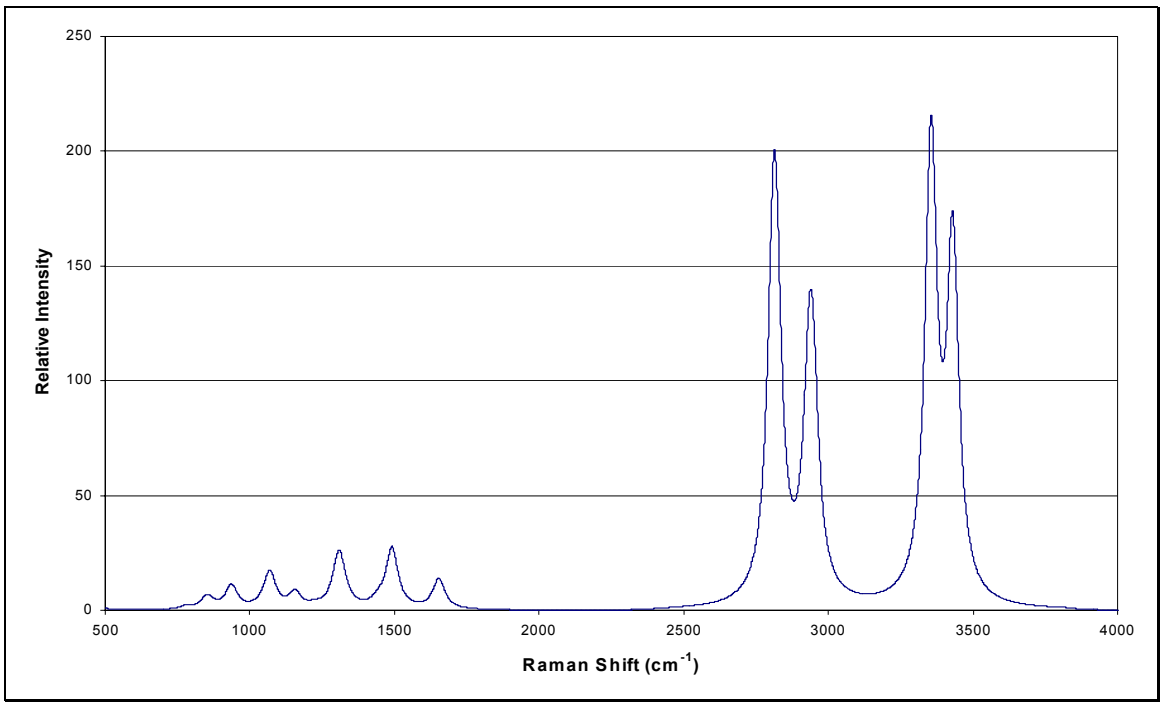

Figure 3.4: Calculated Raman spectrum of s-*trans*-ethylenediamine from Gaussian 98.A.9.

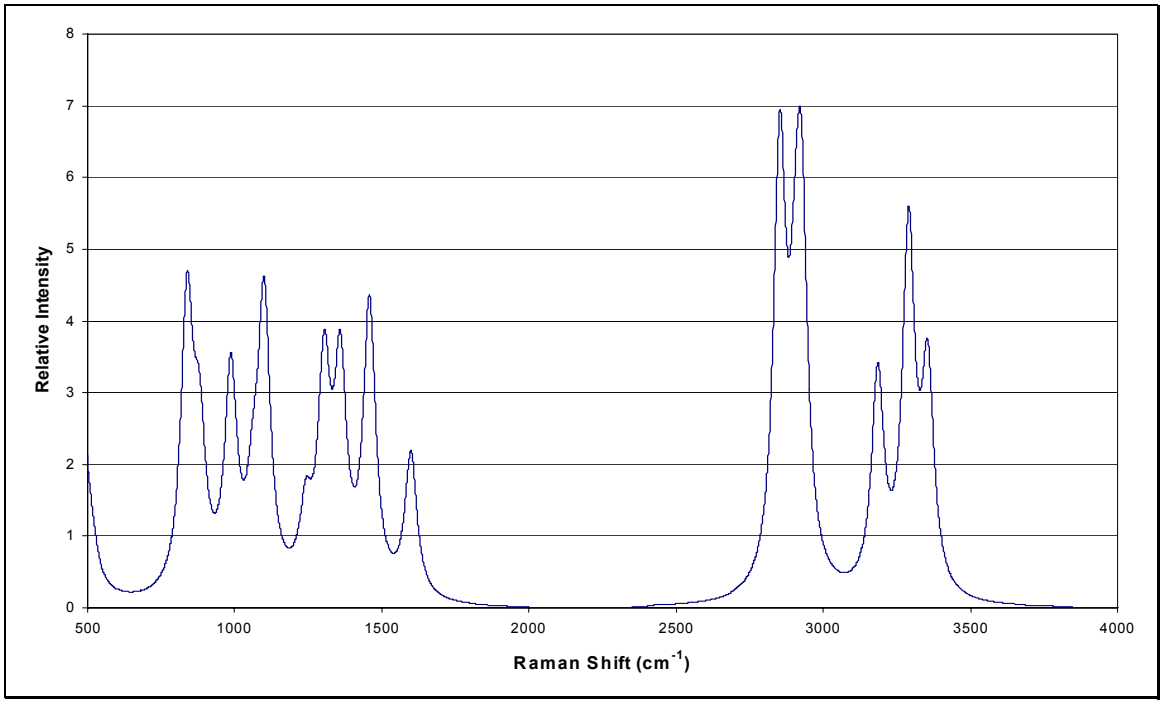

Figure 3.5: Literature Raman spectrum of ethylenediamine (Giorgini, Pelletti et al. 1983).

A visual comparison between the calculated and literature spectra demonstrates the qualitative value of the calculated data. The same inspection also glaringly points out the shortcomings of relying solely on computational modeling. The largest computational oversight would be the complete omission of the N-H stretch vibrations in the calculated IR spectrum. A review of the Gaussian *.log file revealed that the frequencies were calculated - they are present in the Raman spectrum - but Gaussian concluded that the spectral intensity would be nearly zero in relation to the other vibrational modes. This is obviously wrong, judging by the literature spectrum, but more than likely, this is a result of using only the s-*trans*-ethylenediamine model and neglecting s-*cis*-ethylenediamine (Omura and Shimanouchi 1975). Ethylenediamine is free to spin about its C-C bond ensuring that at any given moment a significant population of s-*cis*-ethylenediamine is present, not to mention any number of skewed conformations in between s-*cis*- and s-*trans*-. It is thought that Gaussian determined that the s-*trans*- conformer, being of C_{2h} symmetry, would not satisfy the IR selection rule that states that the vibration must alter the dipole moment of the molecule. The s-*cis*-conformer, being C_{2v}, would experience a much stronger dipole change from N-H stretches, supplying an intense IR absorption signal. A second major drawback to the predicted spectrum would be the absence of a third resolved peak in the N-H stretch region of the calculated Raman spectrum. Minor weaknesses include a weak correlation to the literature spectra peaks in the fingerprint region and the shortcomings in the relative intensities of the fingerprint region peaks in the calculated Raman spectrum. Having pointed out these weaknesses, the calculated spectra do provide a first iteration-type prediction of the true spectra. Also, buried within the calculated peaks are enough

unresolved vibrational modes to make up for the missing peaks. To demonstrate this, table 3.2 is a list of the scaled vibrational frequencies calculated by Gaussian in the C-H and N-H stretch regions, showing that the four large peaks plotted by VibSpec are actually eight unresolved vibrational modes. The vibrational mode assignments were interpreted from the Gaussian *.log file by animation created by a computer program called Molden.

Frequency (cm^{-1})	Mode Assignment
2807.93	CH_2, a-as
2817.51	CH_2, a-ss
2933.18	CH_2, a-as
2947.00	CH_2, a-ss
3354.79	NH_2, s-as
3355.31	NH_2, s-ss
3430.30	$NH_2(1)$, as
3430.66	$NH_2(2)$, as

Table 3.2: Calculated vibrational frequencies with vibrational mode assignments for s-*trans*-ethylenediamine.

3.2.5: PAMAM G0 calculations. In order to simplify the vibrational spectra of the large PAMAM molecules, additional calculations were run on model branch segments of the dendrimer molecules. Each of the calculations on the complete PAMAM G0 molecule, both the optimization and the frequency jobs, lasted on the order of weeks at the Ohio Supercomputer Center; numerous attempts to runs these jobs on smaller computers resulted in failures and system crashes. The first model molecule studied was a hypothetical one, named "PAMAM Arm," and it was comprised of one amidoamine

branch, terminated at the core nitrogen ($NH_2CH_2CH_2CONHCH_2CH_2NH_2$). The second model molecule was the closest "real" molecule to the PAMAM Arm that could be found in literature, N-acetylethylenediamine ($CH_3CONHCH_2CH_2NH_2$). All three molecules, PAMAM G0, PAMAM Arm, and N-acetylethylenediamine, were modeled on HyperChem and then run on Gaussian for both geometric optimization and vibrational frequency calculations. The resulting IR and Raman spectra were plotted for the C-H and N-H stretch regions using VibSpec 1.1 (Figures 3.6, 3.7, and 3.8). Generally, the Raman spectra were predicted to be more intense and to contain more spectroscopically active modes. In particular, the Raman spectra of all three predict three distinct resolvable vibrational peaks in the N-H stretch region, while the IR spectra only predict absorptions for the amide N-H stretch, neglecting the two modes resulting from the terminating amines. Superimposed on the predicted spectra are sharp peaks representing the individual vibrational modes that comprise the larger peaks, as if they could be resolved with minimal line shape broadening (1 cm^{-1}). These mode peaks were plotted using the calculated Raman intensities for display purposes.

Table 3.3 is a summary of the frequencies and assignments provided from Gaussian and Molden; the frequencies that were calculated as the result of features not found in PAMAM G0 were omitted from the table (*e.g.*: the methyl group in N-acetylethylenediamine). The letters in the vibrational mode assignments refer to the same lettering scheme used for the carbon atoms in the NMR studies found in chapter 2 (refer to figure 2.1). The abbreviations "ss" and "as" refer to "symmetric" and "asymmetric" stretches, and a hyphenated prefix refers to symmetric or asymmetric coordination between two different carbon atoms. For example, "A as" would indicate that one carbon

atom designated as "A" is experiencing vibrational excitation with its two hydrogen atoms stretching away from it asymmetrically, or alternately from each other. A mode assignment designated "A s-as" would refer to two "A" carbon atoms both having the same asymmetric stretch, but the hydrogen atoms on different carbon atoms would be operating symmetrically, or in synch. These designations become more arbitrary as the molecules increase in complexity, and so the reader is encouraged to rely more heavily on the primary "ss" or "as" designations. Assignments in parentheses are additional vibrations observed in the animations that were considered secondary in importance to the first assignment. Additional assignments not in parentheses appeared to be as large in magnitude as the primary assignment. This convention is applied throughout this thesis.

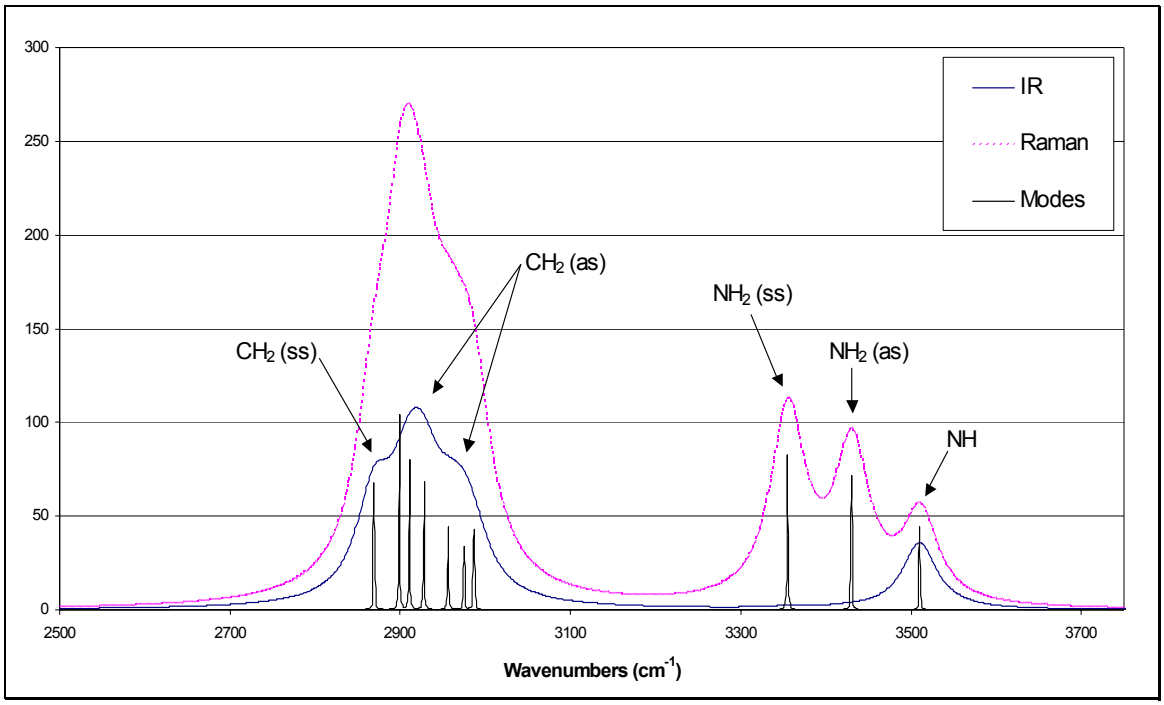

Figure 3.6: Calculated vibrational modes and spectra for N-acetylethylenediamine.

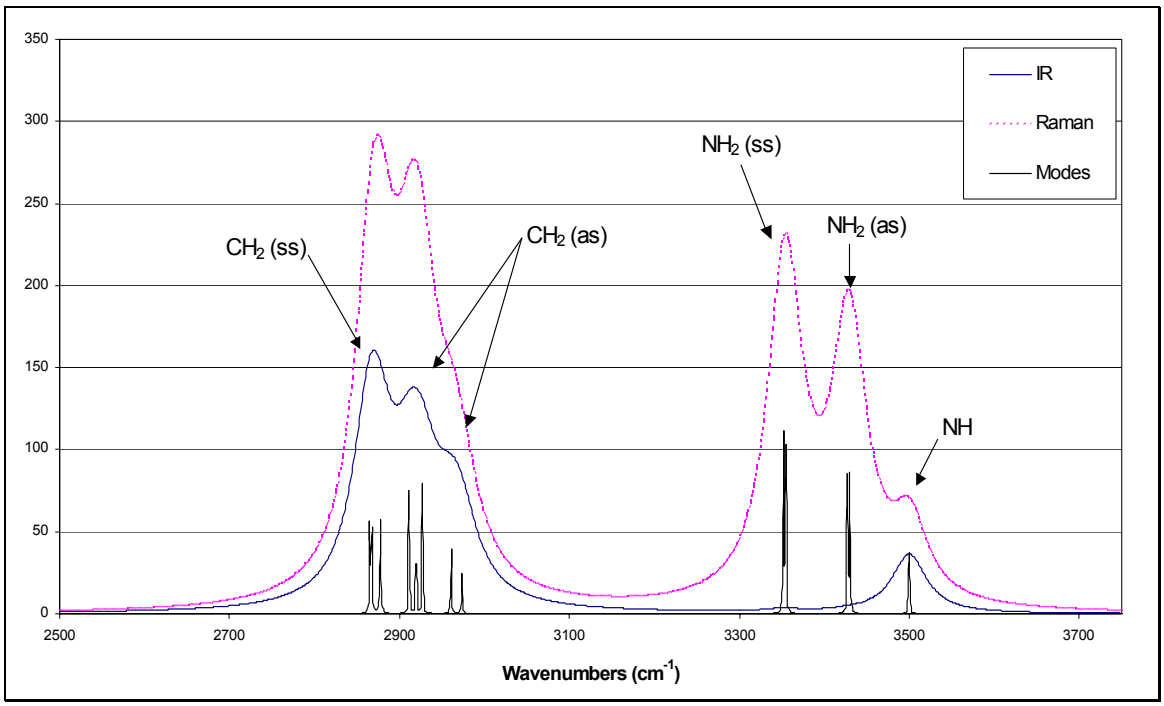

Figure 3.7: Calculated vibrational modes and spectra for PAMAM Arm.

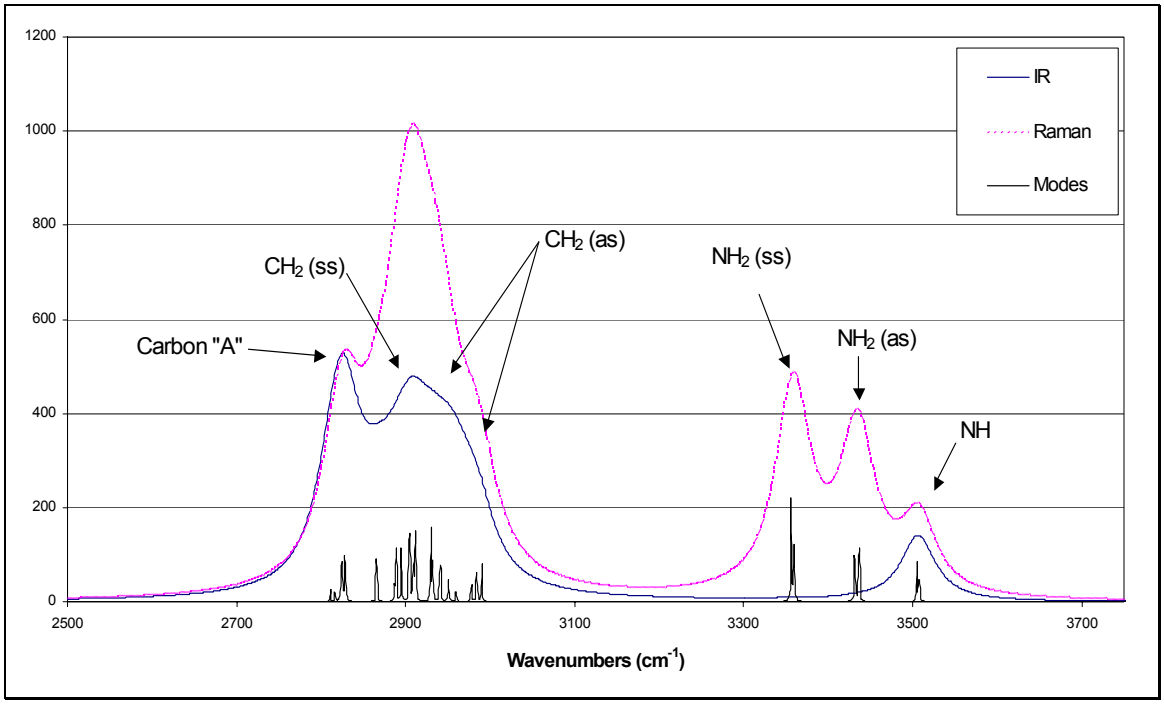

Figure 3.8: Calculated vibrational modes and spectra for PAMAM G0.

Ac-En		PAMAM "arm"		PAMAM G0	
				2811.064	A s-as
				2816.469	A s-ss
		2865.265	B ss (C/E)	2823.203	Bss/Aas
2869.200	F ss	2867.563	F ss (B/C)	2865.404	F s-as
		2877.397	C ss	2895.023	C s-as
2911.067	F as (E)	2911.129	F as (E)	2911.859	F a-as
		2919.506	C as (B ss)	2911.862	F a-ss
2927.799	E ss	2927.053	E ss (F as)	2929.899	E s-as
				2939.642	A as (B/C/E)
				2951.189	A a-ss (B/C)
		2960.771	B as (C)	2959.539	B/C s-as
2975.079	E as (F)	2973.677	E as (F)	2977.556	E a-as
3354.759	NH2 ss	3354.910	NH2 ss	3356.007	NH2 ss
3429.810	NH2 as	3429.991	NH2 as	3431.456	NH2 as
3509.863	NH	3499.766	NH	3504.999	NH

Table 3.3: Summary of vibrational mode calculations for PAMAM G0. (Complete listing can be found in Appendix B.)

In general, the calculated vibrational data were fairly consistent between the full PAMAM G0 molecule and the two PAMAM branch models. The data in table 3.3 are arranged for easy comparison between models, and a quick inspection across the rows highlights the close correlation between molecules in both frequency and assignment. Comparing the three calculated spectra (figures 3.6, 3.7, and 3.8), the two model branch molecules appear to show three CH_2 absorptions, one symmetric and two asymmetric, and the PAMAM G0 calculation displays an additional absorption peak near 2827 cm^{-1} from the core methylene groups, which are nonexistent in the two branch models. All three spectra have nearly identical results for the N-H stretch region: an NH_2-ss at 3354 cm^{-1}, NH_2-as at 3430 cm^{-1}, and the amide N-H stretch at 3500 cm^{-1}.

3.2.6: AcPAMAM G0 calculations. For consistency, AcPAMAM G0 was modeled in exactly the same manner as PAMAM G0. Three molecular models were assembled with HyperChem and then their geometries were optimized and their vibrational frequencies were calculated with Gaussian 98: AcPAMAM G0, AcPAMAM Arm ($NH_2CH_2CH_2CONHCH_2CH_2NHCOCH_3$), and N,N'-diacetylethylenediamine ($CH_3CONHCH_2CH_2NHCOCH_3$), each model being the acylated version of the three PAMAM models. The results were similar to those calculated for the three PAMAM models (Figures 3.9, 3.10, and 3.11 and Table 3.4).

The calculated results from the acylated model studies did not correlate between models as closely as the PAMAM model studies. There is a general trend in the order of the vibrational mode assignments, but the calculated frequencies differ between models by 10 cm^{-1} to 30 cm^{-1}. In addition, there was a disparity between the three spectra in

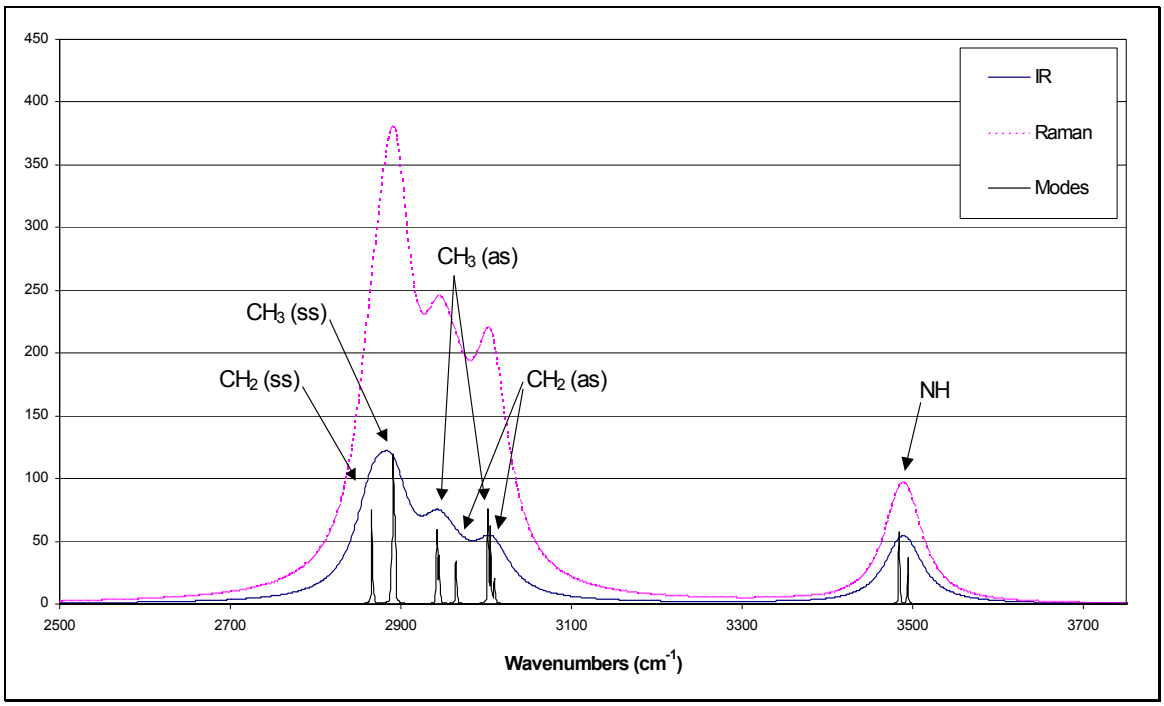

Figure 3.9: Calculated vibrational modes and spectra of N,N'-diacetylethylenediamine.

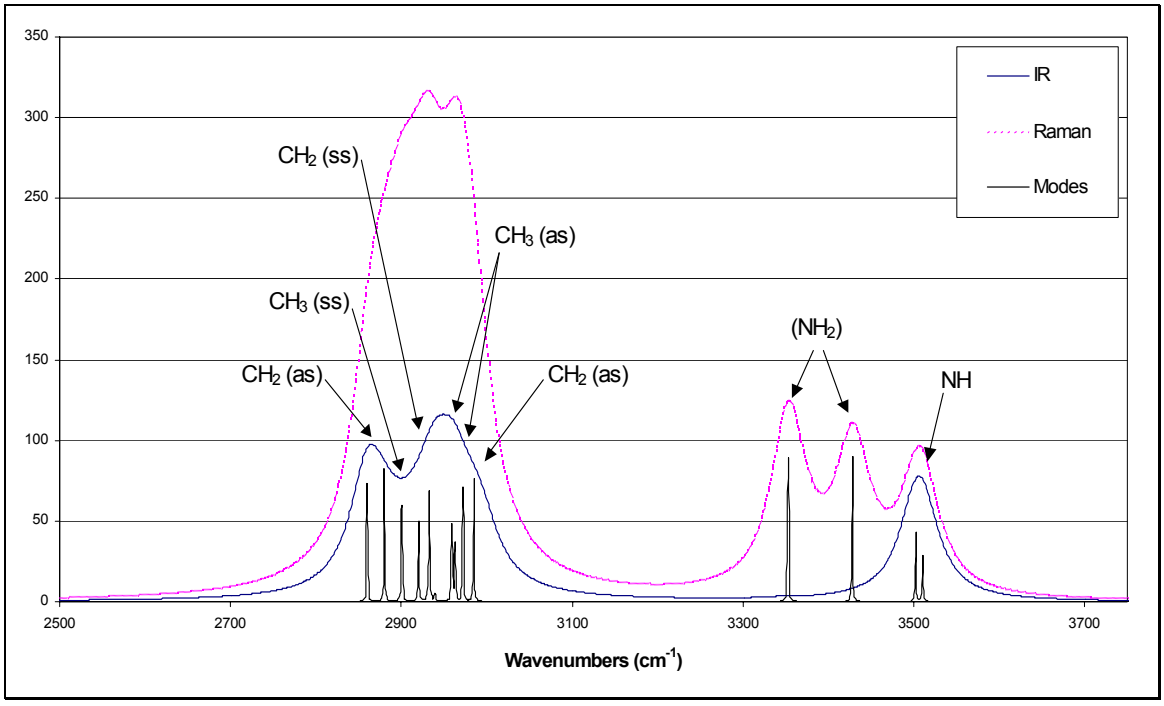

Figure 3.10: Calculated vibrational modes and spectra of AcPAMAM Arm.

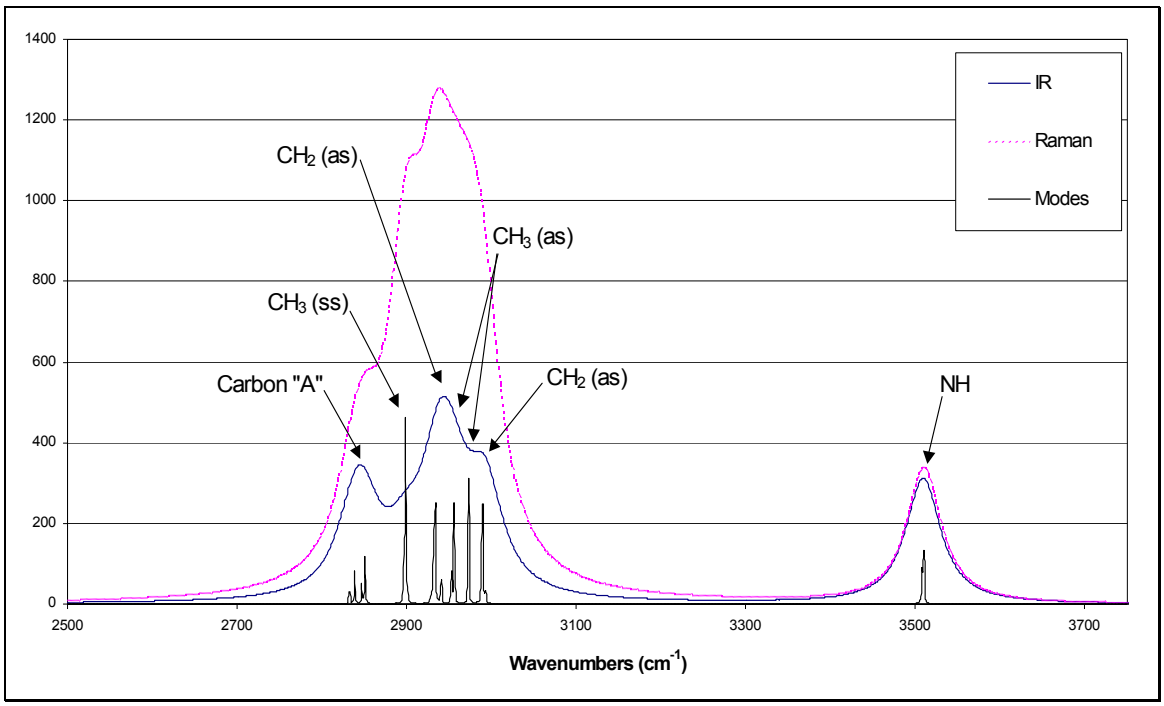

Figure 3.11: Calculated vibrational modes and spectra of AcPAMAM G0.

terms of which CH_2 peaks were considered symmetric or asymmetric: In N,N'-diacetylethylenediamine, the CH_2-ss peak is at the lowest energy of the three. In the AcPAMAM Arm, the CH_2-ss peak is in between the two CH_2-as peaks. In the AcPAMAM G0 model, none of the peaks stood out as being predominantly symmetric. The three calculations predicted the amide N-H stretch to reside between 3480 cm^{-1} and 3510 cm^{-1}. The NH_2 stretches in figure 3.10 are an artifact of terminating the AcPAMAM Arm at the core nitrogen as an amine, and they should be ignored. There are no 1º amine functionalities in the AcPAMAM G0 molecule.

diAc-En		AcPAMAM "arm"		AcPAMAM G0	
		2860.18	B as	2832.424	B as
				2846.846	A a-as
				2850.698	A a-ss
2866.310	E ss				
		2879.92	C ss	2897.016	C s-as
2889.540	E as				
2891.070	H ss	2900.55	H ss	2898.966	H ss
		2920.22	C as	2927.506	Cas/Aas
		2932.60	E/F s-ss	2933.446	E/F s-as
		2939.43	E/F s-as	2939.65	E/F s-as
				2941.083	A a-as(Cas)
				2952.969	A a-ss
2942.11	H as	2959.25	H as	2955.929	H as
		2962.71	B as		
2964.58	F ss	2972.21	E/F a-as	2973.091	E/F a-as
3002.03	H as	2984.96	H as	2989.015	H as
				2992.727	B as
3009.69	F as	2993.36	E/F a-ss	2994.06	E/F a-ss
3483.84	NH	3502.03	NH	3507.517	NH as
3494.08	NH	3510.37	NH	3510.308	NH as

Table 3.4: Summary of vibrational mode calculations for AcPAMAM G0. (Complete listing can be found in Appendix B.)

3.2.7: d-AcPAMAM G0 calculations. To estimate the red shift caused by deuteration of the acetyl group, calculations were run for deuterated versions of AcPAMAM Arm ($NH_2CH_2CH_2CONHCH_2CH_2NHCOCD_3$), and N,N'-diacetyl-ethylenediamine ($CH_3CONHCH_2CH_2NHCOCD_3$). The Gaussian job files were modified to read a list of isotope values appended to the end of the file, rather than to assume standard atomic mass values for each atom. A d-AcPAMAM G0 model was not calculated in an effort to save time and resources; previous calculations for PAMAM G0 and AcPAMAM G0 indicated that the model calculations were sufficient for the scope of this study. Notice also that N,N'-diacetylethylenediamine was deuterated at only one acetyl group to simulate a branch of the d-AcPAMAM molecule. Both spectra displayed vibrational peaks between 2000 cm^{-1} to 2300 cm^{-1} where there were none before; the other frequencies and assignments remained the same as the non-deuterated forms.

d-diAc-En		**d-AcPAMAM Arm**	
2081.60	CD_3 ss	2087.10	CD_3 ss
2179.17	CD_3 as	2193.19	CD_3 as
2225.69	CD_3 as	2213.41	CD_3 as

Table 3.5: Calculated frequencies for deuterated methyl groups.

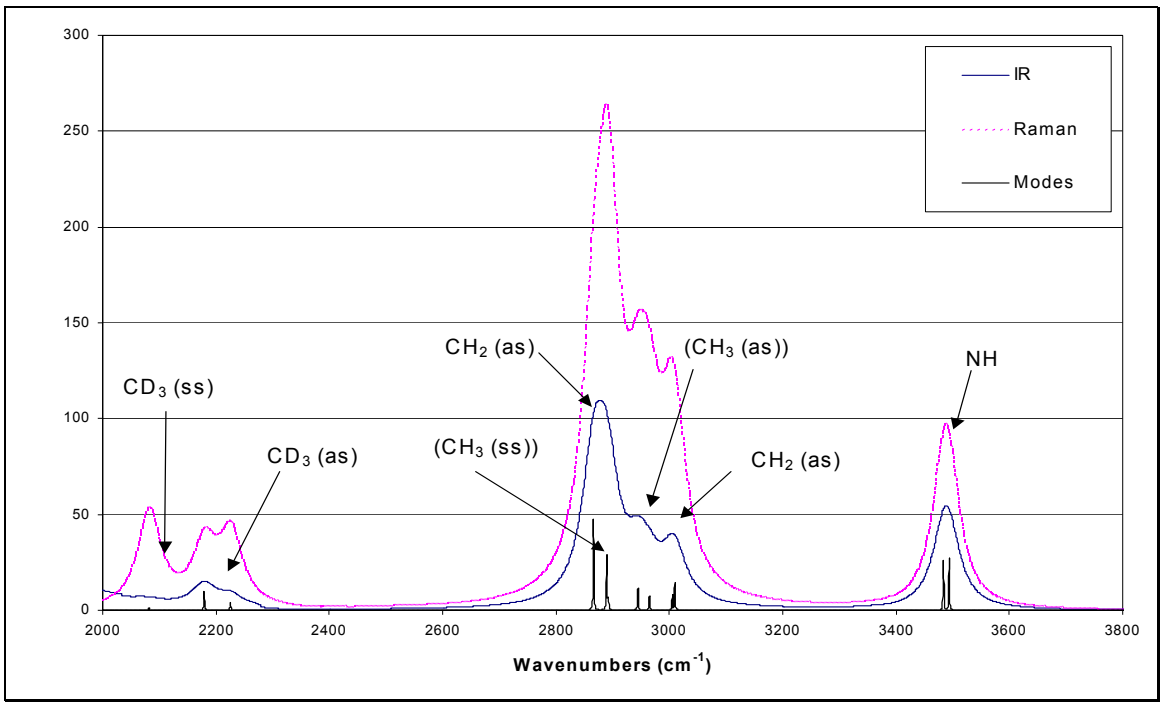

Figure 3.12: Calculated vibrational modes and spectra of N-d_3-acetyl-N'-acetylethylenediamine.

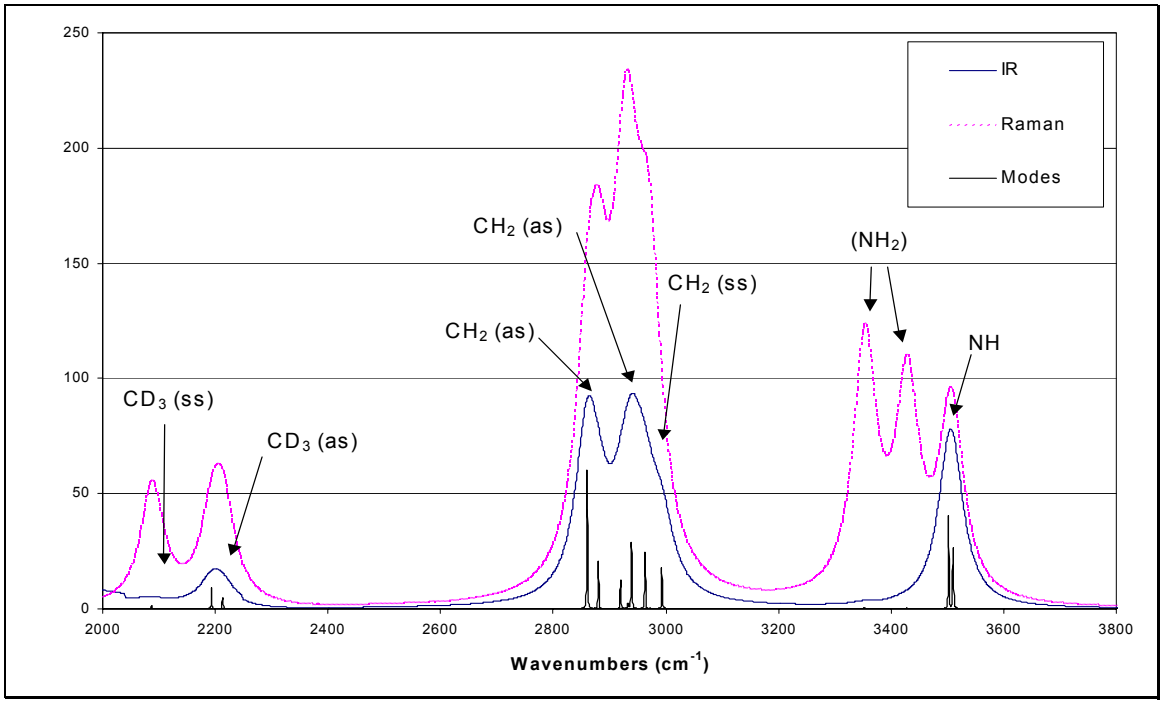

Figure 3.13: Calculated vibrational modes and spectra of d_3-AcPAMAM Arm.

3.3: Infrared absorption spectroscopy.

3.3.1: Theory. The energy levels that correspond to molecular vibrations are equivalent to those found in the IR region of the electromagnetic radiation spectrum (770 nm to 1000 μm). IR absorption spectroscopy is a method of measuring which IR frequencies are absorbed by an analytical sample. Certain molecular functionalities absorb IR in certain frequency ranges, making it possible to detect the presence of those functionalities, and no two compounds absorb IR in exactly the same way, so an IR spectrum can also be used as a molecular "fingerprint" (Skoog and Leary 1992). All molecules vibrate, but not every molecule will absorb IR radiation; the phenomenon is dependent on the selection rules derived from the dipole moment term in the transition moment equation. If a vibration fails to create a differential in the dipole moment, the term cancels the entire transition moment equation (Ingle and Crouch 1988).

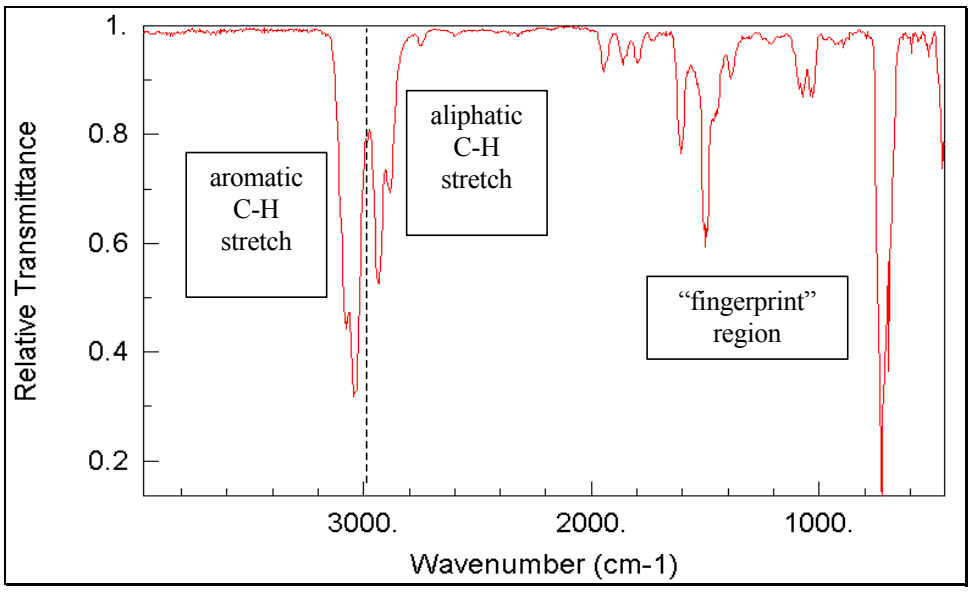

Figure 3.14: Infrared spectrum of toluene. (From *http://webbook.nist.gov/chemistry*)

3.3.2: Matson Cygnus 100 FTIR spectrophotometer. The Matson Cygnus 100 FTIR spectrophotometer is powered by a Globar IR source and operates with a Michelson interferometer. The apparatus is purged with an inert atmosphere by maintaining a positive pressure of IR-inactive nitrogen gas. All spectra acquired on this instrument for this study were taken from 500 cm^{-1} to 4000 cm^{-1} in 16 scans at 4 cm^{-1} resolution.

The ethylenediamine sample was prepared by placing a drop of analyte directly from a reagent bottle between two NaCl plates without a spacer. The PAMAM G0 and G1 samples were prepared by smearing a small quantity of the solvent-free gels onto one NaCl plate and then smearing the sample into a film with the second NaCl plate. If a saturated spectrum would result, the NaCl plates were separated, one plate was cleaned with methanol and acetone, and the plates were reassembled for another experiment. The AcPAMAM G0 and d-AcPAMAM G0 samples were prepared by encapsulating the powdered compounds in potassium bromide (KBr) pellets. To fabricate the pellets, 500 mg of IR-grade KBr was mixed loosely in a 5-dram vial with 4 mg of analyte and then dried in an oven overnight. The next morning, the vials were allowed to cool to the touch and then capped. Each sample was mixed in a mechanical shaker for 2 minutes, and then the samples were pressed into pellets in a vacuum-sealed 13-mm pellet die, held at 10 tons of pressure for 3 minutes each. A magnetic pellet holder then held the resulting pellet in the spectrometer for analysis. A background spectrum was taken for the liquids/gels using clean NaCl plates; a background spectrum was taken for the solids using a pure KBr pellet. The ethylenediamine spectrum (Figure 3.15) was taken as a standard spectrum, and it compared very favorably to the literature spectrum (Figure 3.3).

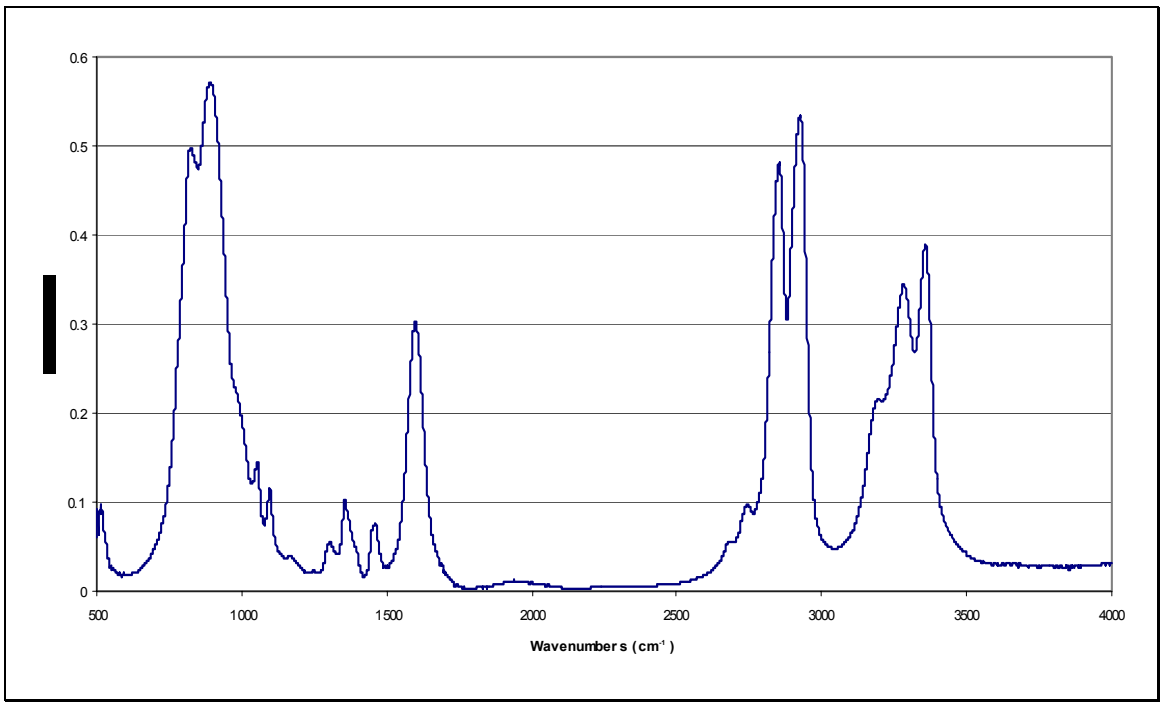

Figure 3.15: Experimental FTIR spectrum of ethylenediamine. (4 cm^{-1} resolution)

3.3.3: Experimental spectra.

3.3.3.1: PAMAM G0/G1. The two FTIR spectra acquired for the PAMAM G0 and G1 gels were remarkably similar. The two spectra are presented in figure 3.16, but the PAMAM G1 spectrum was scaled up and offset on the y-axis for comparison because the quantity of dendrimer used in each sample was very difficult to control. The area of the fingerprint region from 500 cm^{-1} to 1200 cm^{-1} is not identical between the two molecules, but the two spectra are nearly indistinguishable in the C-H/ N-H stretch region. Figure 3.17 shows the spectrum of PAMAM G0 in that region with estimates of the vibrational mode assignments based on the Gaussian calculations; disparities can be expected due to increased broadening in the liquid/gel phase, conformational differences, and the presence of combination modes.

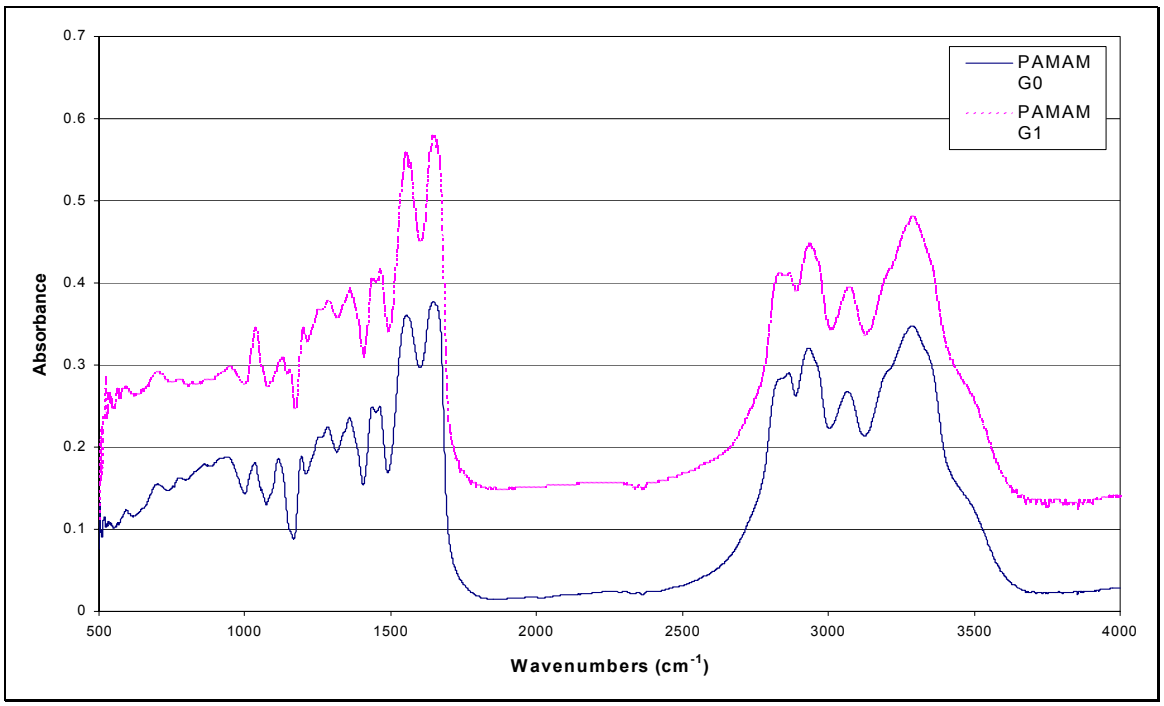

Figure 3.16: FTIR spectra of PAMAM G0 and G1.

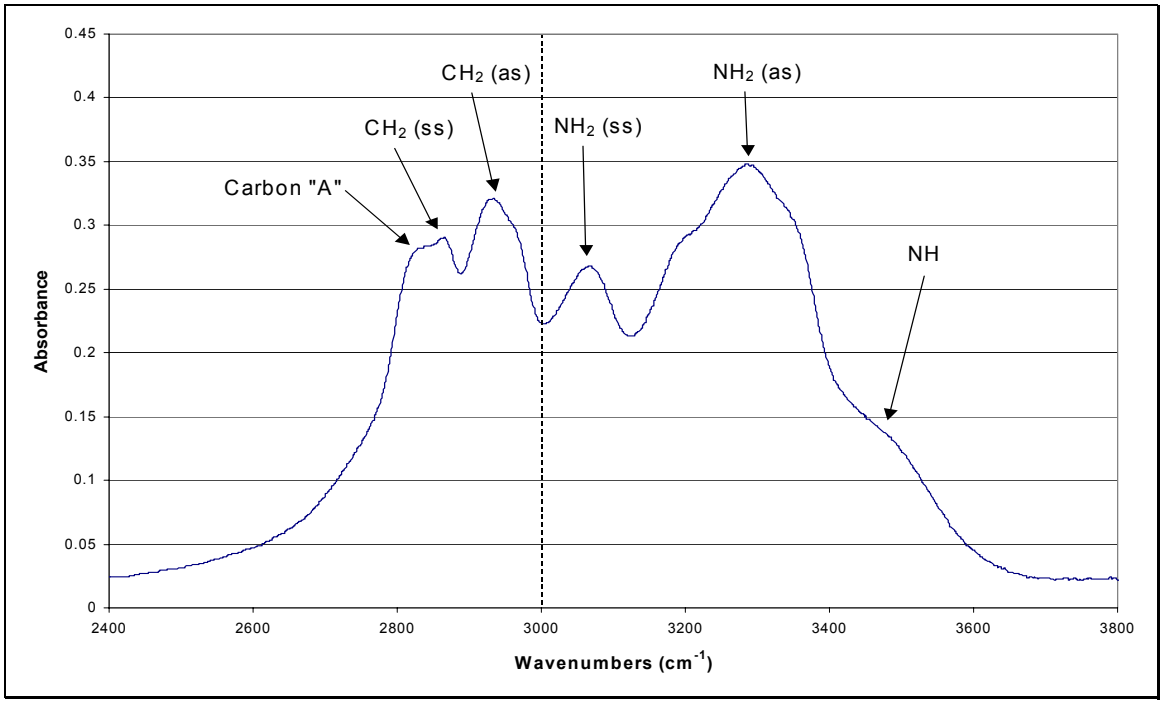

Figure 3.17: FTIR spectrum of PAMAM G0 from 2400 cm^{-1} to 3800 cm^{-1}.

3.3.3.2: AcPAMAM G0. The spectrum of AcPAMAM G0 (Figure 3.18) was taken using the purest product produced from the syntheses of chapter 1. Being a solid, the IR absorption peaks are sharper than those of the dendrimer gels. Solids undergo fewer conformational changes, and so less natural line broadening is observed. The C-H stretch region is extremely similar to the calculated IR spectrum (Figure 3.11). As a result, peak assignments were made for the CH_2 stretching modes directly from the Gaussian estimates in figure 3.11. At least four absorption peaks are visible in the N-H stretch region where Gaussian only predicted one resolvable peak. However, that single N-H peak is comprised of eight separate vibrational modes (Appendix B); perhaps various conformations in the solid phase separate the irresolvable frequencies over a wider range, with a predominant conformation creating the largest absorption.

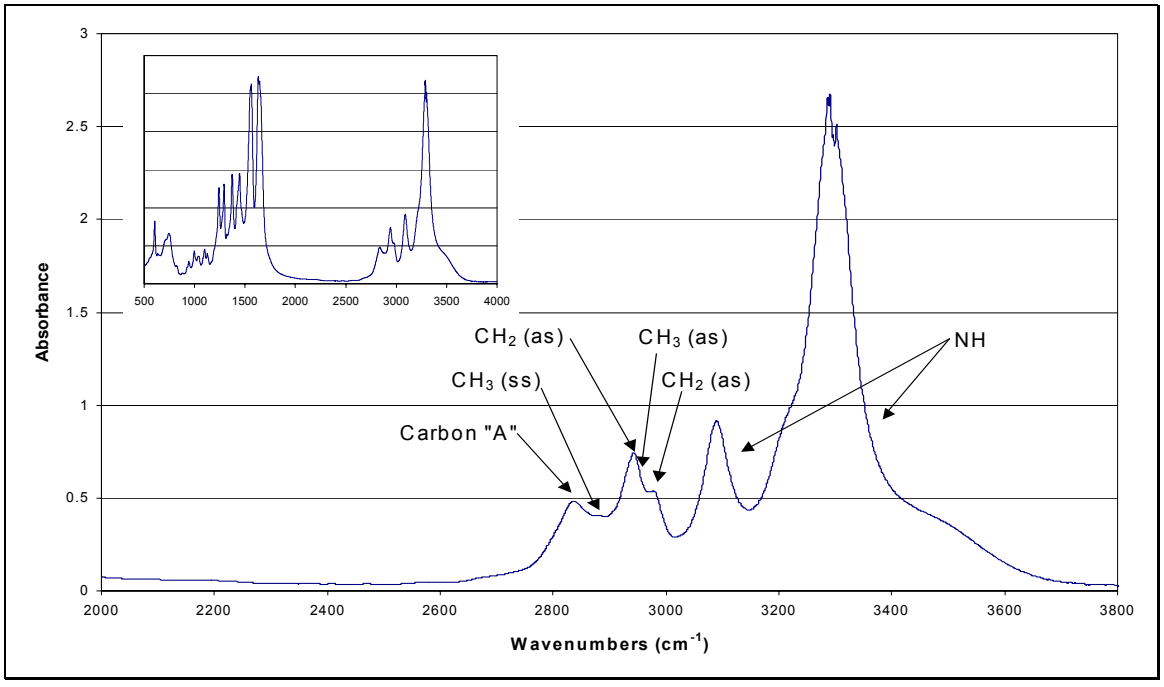

Figure 3.18: FTIR spectrum of AcPAMAM G0 from 2000 cm^{-1} to 3800 cm^{-1}. Inset: Full spectrum.

3.3.3.3: d-AcPAMAM G0. The spectrum of d-AcPAMAM G0 (Figure 3.19) was taken using the purest product produced from the syntheses of chapter 1. The C-H stretch region was not as similar to the calculated IR spectrum (Figure 3.13) as was observed for AcPAMAM G0, but the peak assignments made from the Gaussian estimates were able to fit the observed CH_2 stretching modes. The N-H stretch region was essentially identical to that observed in AcPAMAM G0, but since deuteration does not affect the N-H stretch vibrations, this result was expected.

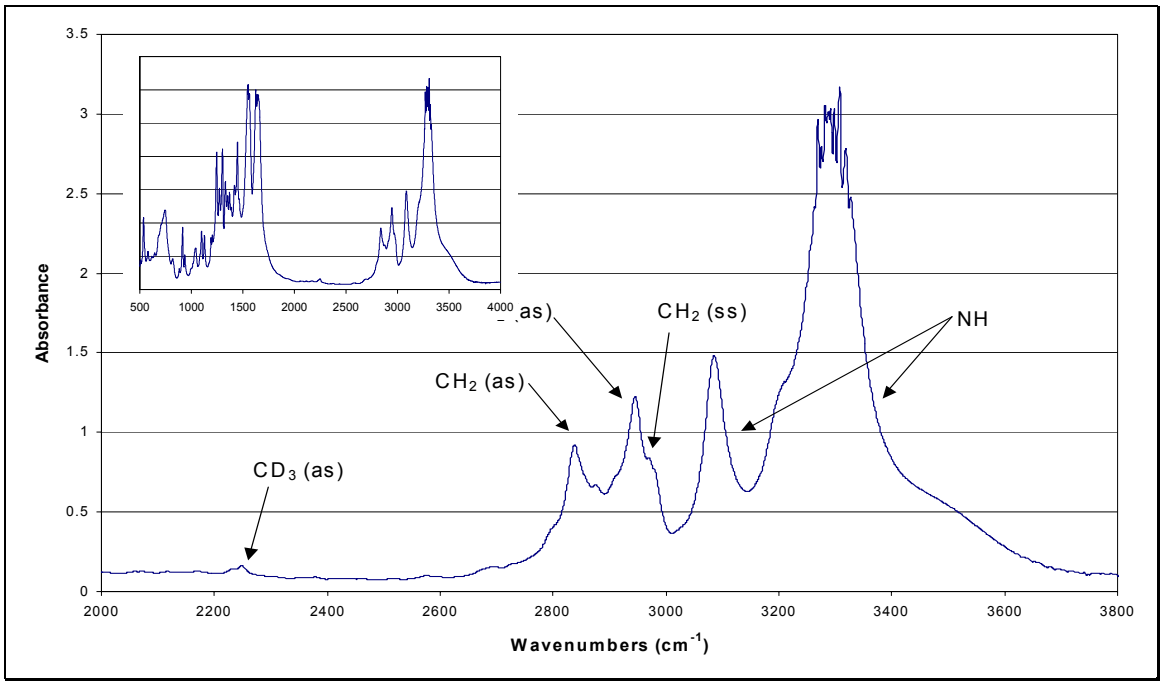

Figure 3.19: FTIR spectrum of d-AcPAMAM G0 from 2000 cm^{-1} to 3800 cm^{-1}. Inset: Full spectrum.

3.4: Raman spectroscopy.

3.4.1: Theory. Raman spectroscopy also records a vibrational spectrum for a chosen compound, but it relies upon a completely different phenomenon. Likewise,

Raman spectroscopy carries several advantages and disadvantages over infrared absorption spectroscopy. In 1928, Chandrasekhara Venkata Raman, a professor at the University of Calcutta, published his finding that a weak radiation secondary to Rayleigh scattering was emanating from the different liquids he was studying while investigating the light-scattering properties of water. This secondary radiation was always of a longer wavelength, and it was characteristic of the material from which it came. As it would happen, the molecules in his study were reducing the energy of the scattered light by the amount required to excite molecular vibrations. The discovery of this effect, named the Raman effect, earned Professor Raman the Nobel Prize in Physics in 1930 (Noggle 1996).

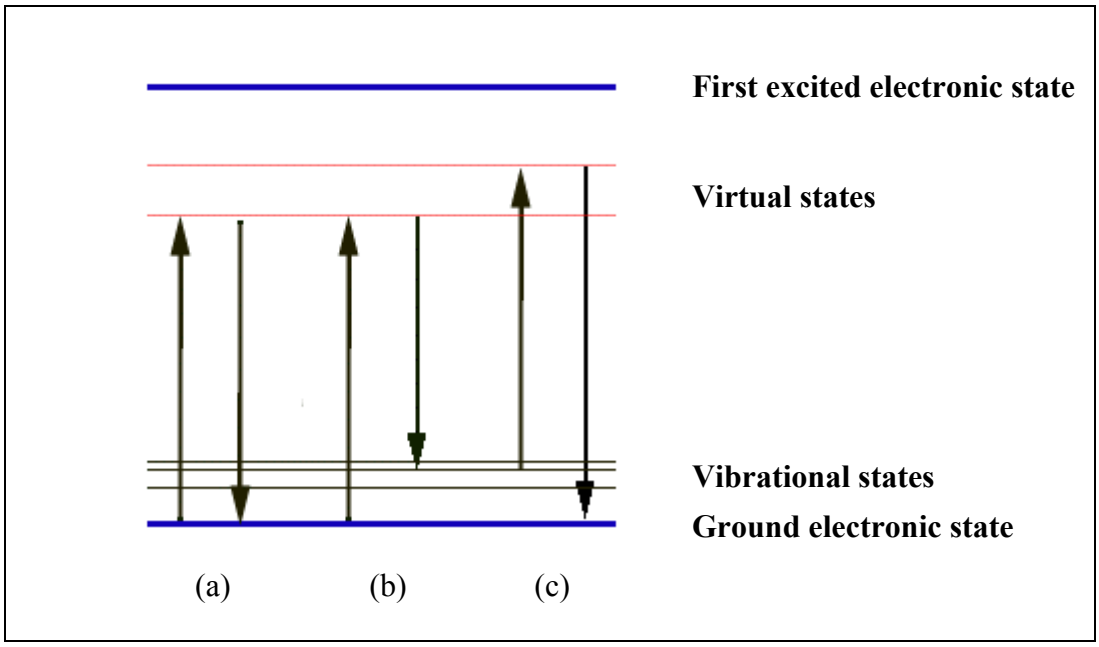

Figure 3.20: A comparison of Rayleigh and Raman scattering. (a) Rayleigh scattering. (b) Stokes Raman scattering. (c) Anti-Stokes Raman scattering. (Adapted from *Principles of Instrumental Analysis, 4th ed.*, Skoog and Leary 1992)

Although Professor Raman discovered this effect in 1928, the technology did not exist to exploit it for spectroscopy until the 1960's. The Raman effect is very weak, and though it had been both observed and explained with quantum mechanics, it was the invention of the laser that propelled Raman spectroscopy to everyday analytical chemistry. The Raman effect is independent of the wavelength of light used, but the intensity of scattered light is inversely proportional to the fourth power of the wavelength (Ingle and Crouch 1988). Any light source powerful enough to produce the effect in detectable quantities may be used. A laser source focused onto a sample will scatter back photons with energy differences corresponding to energies of vibrational excitation, to produce a vibrational spectrum that will both resemble and complement the IR spectrum.

3.4.2: InPhotonics Raman probe. The Raman probe manufactured by InPhotonics (Figure 3.21) is an all-in-one optical device for collecting Raman spectra. The probe is compact, no more than ½" in diameter, and it is affixed to the end of a double-fiber optic cable. The intake fiber optic has a diameter of 90 μm, and it is designed to couple into a standard attachment to receive the source light. The intake delivers the excitation beam into the probe, where it is collimated, purified by a band-pass filter, and refocused 5 mm in front of the probe. Backscattered light returns through the same focusing lens, where it is reflected to another chamber by a dichroic mirror/mirror periscope. In the receiving chamber, Rayleigh and anti-Stokes light is reduced by a long-pass filter, and the Stokes Raman signals are focused into a 200-mm diameter fiber optic. This collection fiber is split away from the excitation fiber at the opposite end from the Raman probe, and it is terminated in a standardized fitting. The probes are available for different excitation wavelengths, including 532 nm and 785 nm.

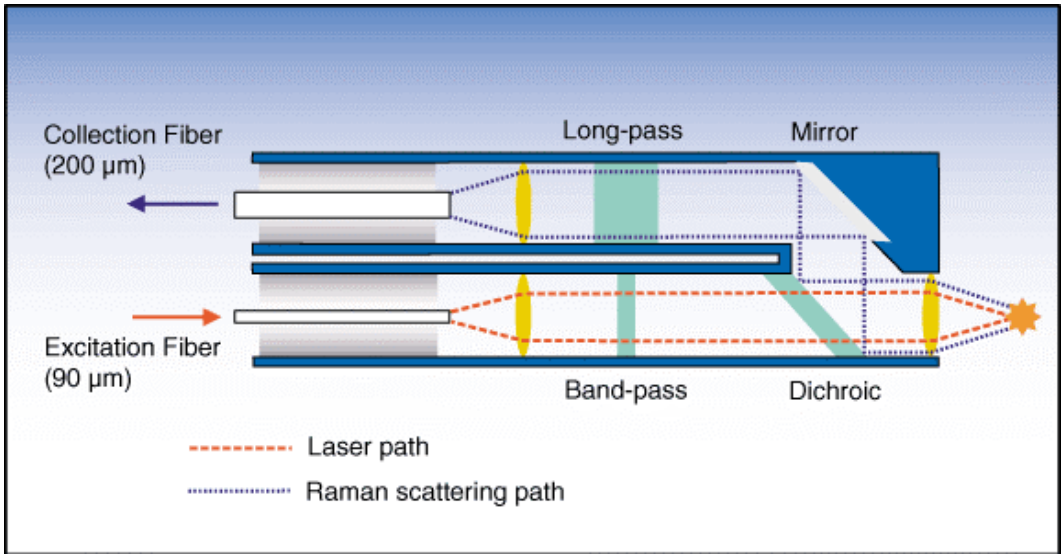

Figure 3.21: A schematic diagram of the InPhotonics Raman probe. (From *www.inphotonics.com*)

For this study, a simple setup (Figure 3.22) was used for the Raman probe. A 200-mW, 532-nm, collimated CW laser beam was directed into the excitation fiber of the probe. The end of the probe was secured into an aluminum block designed to hold a test tube in proximity to the tip of the probe. Power measurements at the end of the probe indicated that the sample received 75 mW of laser light. The collection fiber was then coupled into a 500-mm monochromator-CCD system (Acton Research SpectraPro SP-500; 1340 x 400 pixel array, Roper Scientific LN400EB back-illuminated CCD) with a 1200 g/mm grating blazed at 750 nm. The spectrum of ethylenediamine (Figure 3.23) was acquired by means of this setup. PAMAM G0 and G1 fluoresced under 532-nm excitation, a common source of interference in Raman spectroscopy. For the PAMAM spectra (Figures 3.24 and 3.25), the laser was replaced by a 200-mW, 785-nm, CW diode laser, and a probe optimized for 785-nm excitation was substituted for the 532-nm probe.

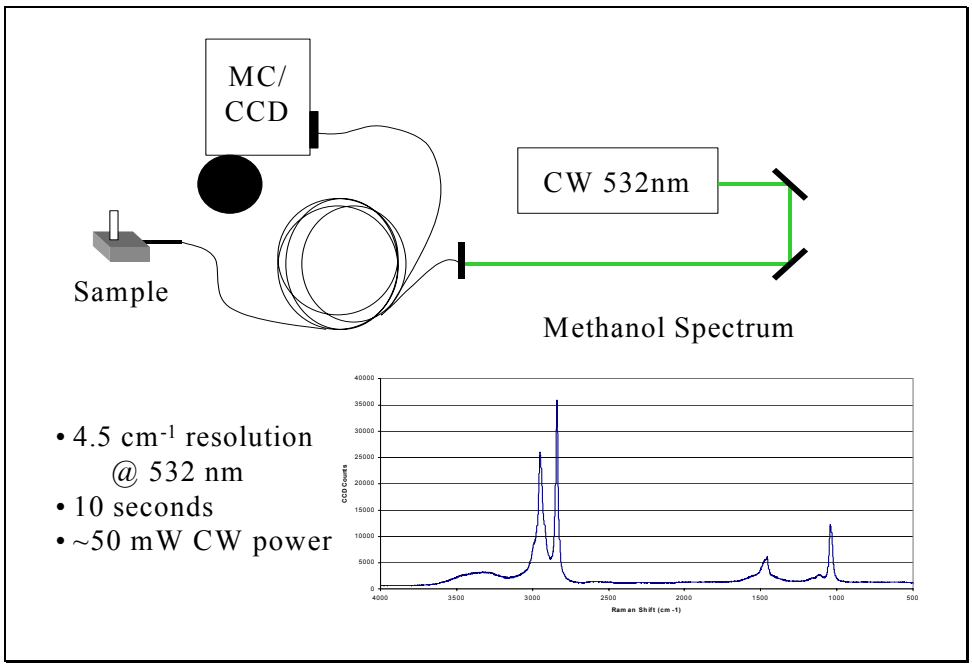

Figure 3.22: Diagram of experimental setup for InPhotonics Raman probe.

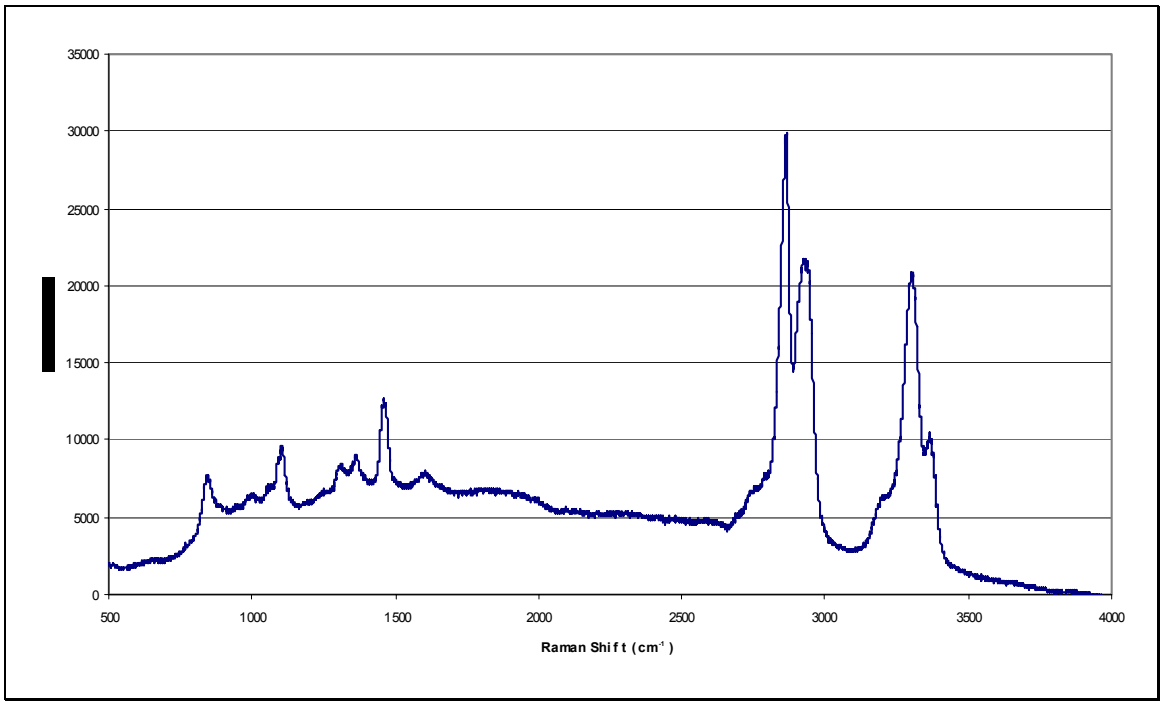

Figure 3.23: Raman spectrum of ethylenediamine taken with InPhotonics Raman probe. (532 nm excitation)

3.4.3: Experimental spectra of PAMAM G0/G1. Like the FTIR spectra of PAMAM G0 and G1, the Raman spectra of PAMAM G0 and G1 are remarkably similar (Figure 3.24). Although the baselines of the two spectra are not exactly the same, the relative intensities of the peaks at 1020 cm^{-1} and at 1445 cm^{-1} seem to be much higher in the PAMAM G1 spectrum. It is possible that these absorptions are in regions of the molecule that are the same between generations, meaning that each molecule of PAMAM G1 had three times the number of structures in that region for each similar structure in a molecule of PAMAM G0. Otherwise, the similarities of the IR and Raman spectra would seem to indicate that any spectra taken of higher-generation PAMAM dendrimers would be very similar as well, unless steric effects began to limit the number of structural conformations. Peak assignments (Figure 3.25) were made using calculated predictions from figure 3.8.

Prior to obtaining these Raman spectra, several unsuccessful attempts at acquiring the spectra were made. For reasons currently under investigation (Larson and Tucker 2001), PAMAM dendrimers possess an intrinsic fluorescence that precludes short wavelength Raman spectroscopy. The use of 532-nm lasers as an excitation source produced an overwhelming amount of fluorescence even at the shortest exposure times. Attempts using a 785-nm Raman spectrometer also failed; the fluorescence produced required exposure times so short that the Raman signals were undetectable. In addition, using 785 nm or 1064 nm renders detection of the C-H and N-H stretch regions nearly impossible without the use of Fourier transforms. This experiment was a success mainly due to the quality of the CCD camera. Even so, background fluorescence is apparent below 2000 cm^{-1}, and the N-H stretch region was nearly undetectable (Figure 3.24).

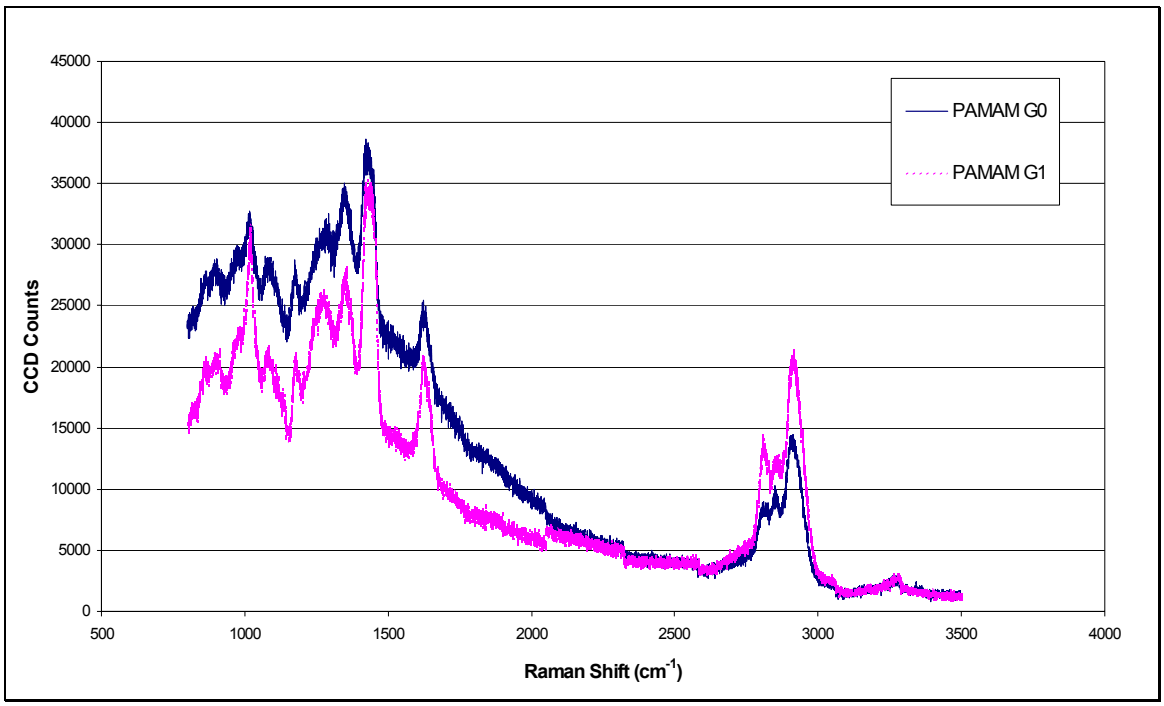

Figure 3.24: Raman spectrum of PAMAM G0 and PAMAM G1. (785nm excitation source)

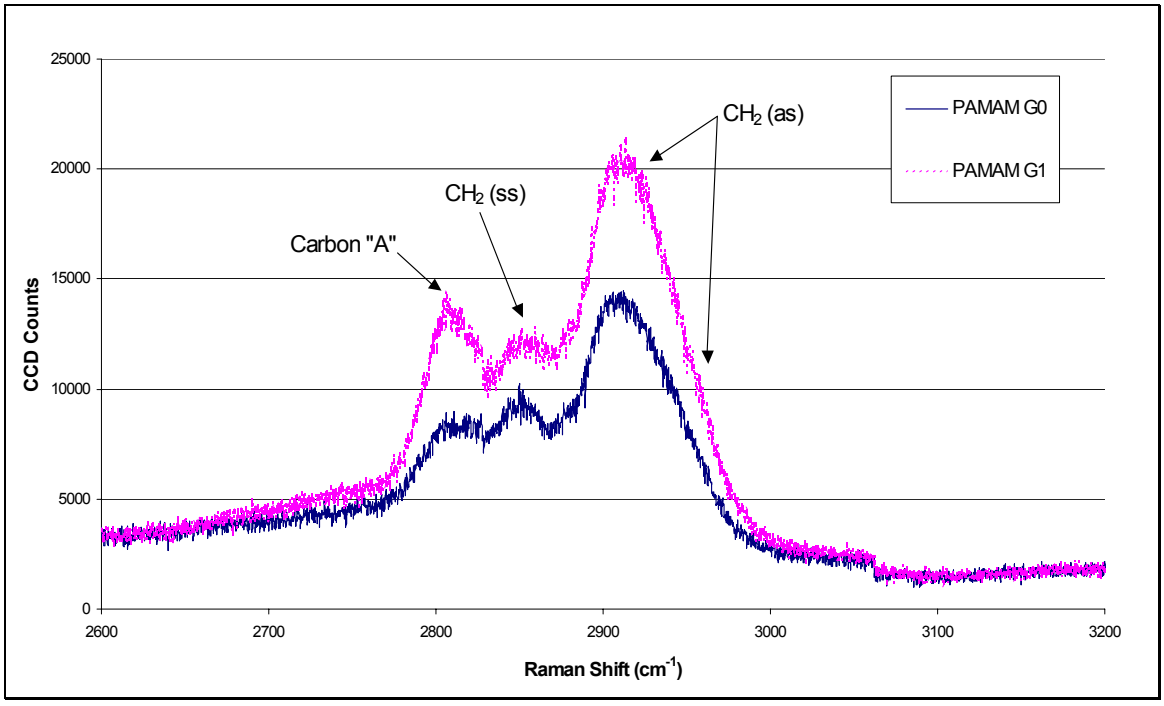

Figure 3.25: Raman spectra of PAMAM G0 and G1 from 2600 cm^{-1} to 3200 cm^{-1}.

3.5: Sum frequency generation spectroscopy.

3.5.1: Theory. Sum frequency generation (SFG), along with second harmonic (SHG) and difference frequency generation (DFG), falls into the category of spectroscopy referred to as second-order nonlinear spectroscopy. When radiation passes through a dielectric substance, the valence electrons are polarized by the electric field produced by the radiation. This polarization is directly proportional to the electric field, and under normal circumstances, this proportionality is linear. If the irradiance is high enough, but not so high as to break down the material, the proportionality must be described by a Taylor series expansion, and higher-order terms cannot be neglected. These processes are given the "nonlinear" moniker to emphasize this fact. Second-order nonlinear spectroscopy is the term given to any of these processes that exploit the relationships derived from the second-order term in the expanded polarization equation to elucidate chemical information from an analytical sample.

Not unlike Raman scattering, it was the development of lasers that made second-order nonlinear spectroscopy more easily attainable. Second-order nonlinear properties have always existed in matter, but only with the high photon intensity of a laser can one observe these minute contributors to the overall spectral intensity of a sample. Even still, most materials are either isotropic, like glass, or centrally symmetrical, like calcite. These arrangements preclude significant even-ordered nonlinear signals, including SHG, SFG, and DFG, from being evidenced (Franken and Ward 1963). One might believe that this consideration would limit second-order nonlinear spectroscopies to only the most specialized circumstances, but a surface chemist would quickly point out that while the bulk of a material may be centrosymmetric, by definition every surface and interface

possesses a lack of symmetry from one material to the other. In this way, second-order nonlinear spectroscopies can be used to probe surfaces, while competing signals from the bulk will be eliminated by the symmetry selection rule (Bloembergen 1999).

In sum frequency generation, two laser pulses are combined to produce a third signal with a frequency that is the sum total of the two laser beam frequencies. For example, if a visible laser of 532 nm (5.86×10^8 MHz) were combined with an IR laser of 2500 nm (1.20×10^8 MHz), the resultant SFG signal would be at 425 nm (7.06×10^8 MHz). Conveniently, if the IR laser is resonant with the frequency of a molecular vibration in the sample that is both IR and Raman active, the SFG signal can be made to address specific chemical functionalities in the sample, in the manner of an IR spectrum. If that same IR laser were tunable from 2500 nm to 4000 nm, the tunable laser could scan that region against a 532-nm laser, covering the IR spectral region from 4000 cm^{-1} to 2500 cm^{-1}, the region most responsible for the detection of organic functionalities, e.g.: aliphatic stretch, aromatic stretch, hydroxyl stretch, etc. Further, the SFG signal would range in the easily detectable visible region from 425 nm to 454 nm. A surface-specific infrared analysis can be conducted this way (Flörsheimer, Brillert et al. 1999). The intention of this study is to examine the surface activity of dendrimers in solution and on a solid surface. The signals generated by the dendritic methylene groups will give clues as to the orientation of the molecular branches, while the periphery of the dendrimer molecules could be distinguished from the center of the molecules by a red shift caused by deuterated methyl groups added to the terminal ends.

3.5.2: Experimental setup. While the author cannot assume any of the credit for this experimental setup, a brief description will be provided here. The BBSFG system

consisted of two regenerative amplifiers (Spectra-Physics Spitfire, fs and ps versions), both of which were seeded by a sub-50-fs, 800-nm pulse from a Ti:Sapphire oscillator (Spectra-Physics Tsunami). The oscillator was pumped by 4.7 W from a Nd:YVO_4 CW laser (Spectra-Physics Millennia Vs). The regenerative amplifiers are pumped by an all solid-state Nd:YLF laser (Spectra-Physics Evolution 30, 527 nm); 8 watts and 12 watts are used in the fs and ps regenerative amplifiers, respectively. The output of the 1-kHz repetition rate regenerative amplifiers provides 85-fs pulses at 800 nm (22-nm bandwidth) and 2-ps pulses at 800 nm (17 cm^{-1} bandwidth). The fs broad bandwidth pulses were then used to generate broad bandwidth infrared (~600 cm^{-1} bandwidth) light via an optical parametric amplifier (Spectra-Physics OPA-800CF).

The SFG experiment was performed in reflection geometry using the narrow bandwidth ps 800-nm beam and the broadband infrared beam. The two input beams, fs and ps, were overlapped at the sample surface spatially and temporally to produce a vibrationally resonant sum frequency generation spectrum. The infrared and 800-nm beams were incident on the sample at 66° and 58° from the surface normal, respectively. The SFG photons were emitted at 59.3° from the surface normal and were detected using a 500-mm monochromator-CCD system (Acton Research SpectraPro SP-500; 1340 x 400 pixel array, Roper Scientific LN400EB back-illuminated CCD) with a 1200 g/mm grating blazed at 750 nm. The narrow bandwidth ps pulses limit the BBSFG spectral resolution. The polarization combination for the studies presented here were SSP (S: SFG, S: 800 nm, P: infrared). The input energies of the 800-nm and infrared beams were 50 μJ and 10 μJ, respectively. The nonresonant SFG spectrum of a GaAs crystal surface was obtained both with and without a polystyrene film covering the OPA output port. The resulting

SFG spectra were used for normalization purposes and as a reference to calibrate the peak positions of the BBSFG spectra.

Glass slides were purchased from Fisher Scientific and were cleaned with an oxidizing agent in sulfuric acid, thoroughly rinsed with Nanopure water (18 MΩ resistivity), and then dried in an oven (> 70° C) for several hours before use in the SFG experiments. Dendrimer deposition was performed by placing one drop (0.02 mL) of the PAMAM G0 and G1 20 wt % in methanol onto a glass slide, and one hour was allowed for methanol evaporation. For dendrimer deposition of the modified PAMAM dendrimer, one drop (0.02 mL) of AcPAMAM G0 1.4 wt % in methanol was deposited onto a glass slide, and one hour was allowed for methanol evaporation. The surface coverage of the PAMAM G0, G1, and AcPAMAM G0 dendrimers were calculated to be 9×10^{17} cm^{-2}, 2×10^{17} cm^{-2}, and 2×10^{16} cm^{-2}, respectively. This indicated that multiple layers of dendrimer were deposited on the glass surface.

The bare gold surface film was purchased from Edmund Scientific and cleaned with spectrophotometric grade methanol prior to PAMAM dendrimer deposition. One drop (0.02 mL) of the PAMAM G0 dendrimer 20 wt % in methanol solution was deposited on the gold surface, and the methanol was allowed to evaporate. After 1 hour, the BBSFG spectrum was recorded. The multi-layer surface coverage was estimated to be 2×10^{17} cm^{-2}.

3.5.3: SFG spectra of PAMAM G0, G1, and AcPAMAM G0. Figures 3.26 and 3.27 show the surface vibrational BBSFG spectra of PAMAM G0 and G1 dendrimers obtained after deposition of the dendrimer on the glass slide. The methanol was allowed to evaporate for 1 hour, and then the spectra were obtained. The inset of figures 3.26 and

3.27 show the BBSFG spectra from the same samples, G0 and G1, respectively, obtained 36 hours after the initial methanol evaporation. In the four spectra shown in figures 3.26, 3.27, and their insets, two SF peaks are observed at 2802 cm^{-1} and 2920 cm^{-1}. Based on the Raman assignments discussed above, the peak at 2802 cm^{-1} is assigned to CH_2-ss modes, and the peak at 2920 cm^{-1} is assigned to CH_2-as modes, although there may also be an irresolvable contribution from the CH_2-fr on the high-energy side of the 2802 cm^{-1} band.

The ratio of the relative intensity of the CH_2-as peak (2920 cm^{-1}) versus the CH_2-ss peak (2802 cm^{-1}) and the sharpening of the CH_2-as peak in the insets of figures 3.26 and 3.27 reveal that the CH_2 groups on the dendron arms of the PAMAM G0 and G1 dendrimers have slightly changed in their relative surface conformation over the 36-hour period. The ratio of the relative intensity of these two peaks (as:ss) within each spectrum has increased from 0.14 to 0.22 for the PAMAM G0 and from 0.08 to 0.17 for the PAMAM G1. A likely explanation is that the dendrimers had not reached their stable conformation at the time that the initial spectra were recorded. After 36 hours, the SFG spectra reveal a larger and slightly narrower CH_2-as peak, which infers that there is a concerted orientation of the dendron arms of the dendrimer. Using the SSP polarization combination, if the CH_2 groups are situated relatively normal to the surface plane, a large symmetric stretch relative to the size of the asymmetric stretch would be observed. This is what was observed from figures 3.26 and 3.27. However, after 36 hours, the CH_2-as has changed, inferring a more ordered but less upright configuration of the CH_2 groups.

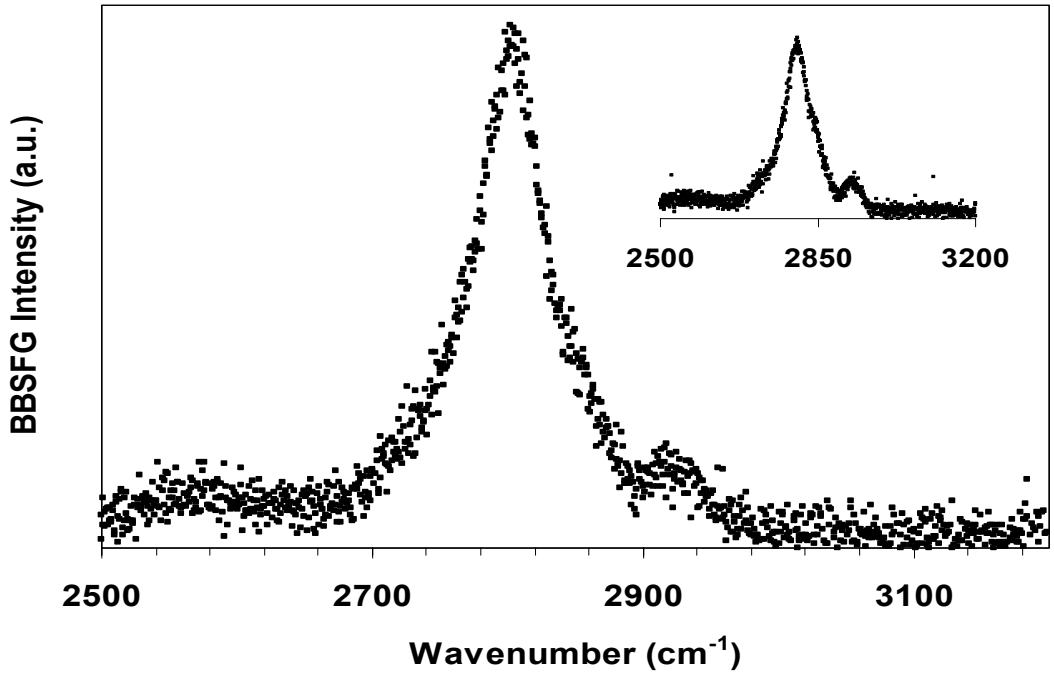

Figure 3.26: BBSFG spectrum (SSP polarization) of PAMAM G0 after deposition on a glass slide using a 5-minute acquisition time. Inset: 36 hours after deposition. ***(G. Ma)***

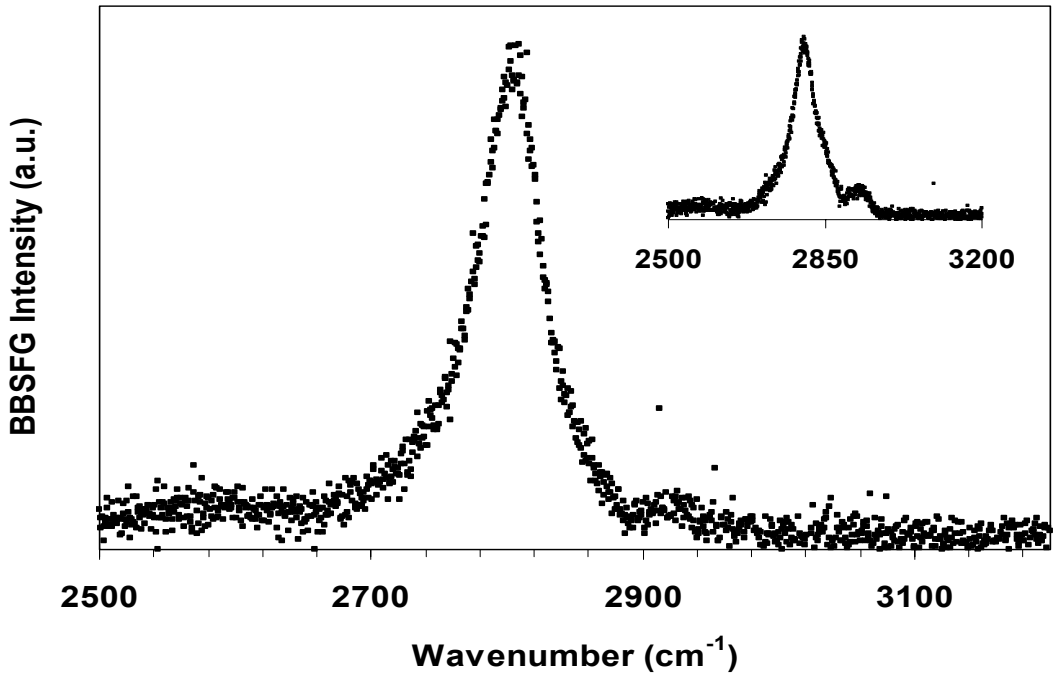

Figure 3.27: BBSFG spectrum (SSP polarization) of PAMAM G1 after deposition on a glass slide using a 5-minute acquisition time. Inset: 36 hours after deposition. ***(G. Ma)***

The structural implications of these measurements were further investigated by comparing the spectrum in figure 3.26 with a BBSFG spectrum taken of a monolayer of sodium dodecyl sulfate (SDS) formed from a 1-mM SDS solution. Shown in figure 3.28 are the spectra from the surface of the SDS solution and from the surface of the PAMAM G0 dendrimer gel. Both spectra were recorded under exactly the same conditions using a 2-minute acquisition time. SDS has been studied extensively using SFG (Gragson and Richmond 1998; Miranda and Shen 1999), and it is interesting to make comparisons with these spectra since SDS is known to form well-ordered monolayers with few CH_2 gauche (skewed) defects where the hydrocarbon chain protrudes out of the liquid.

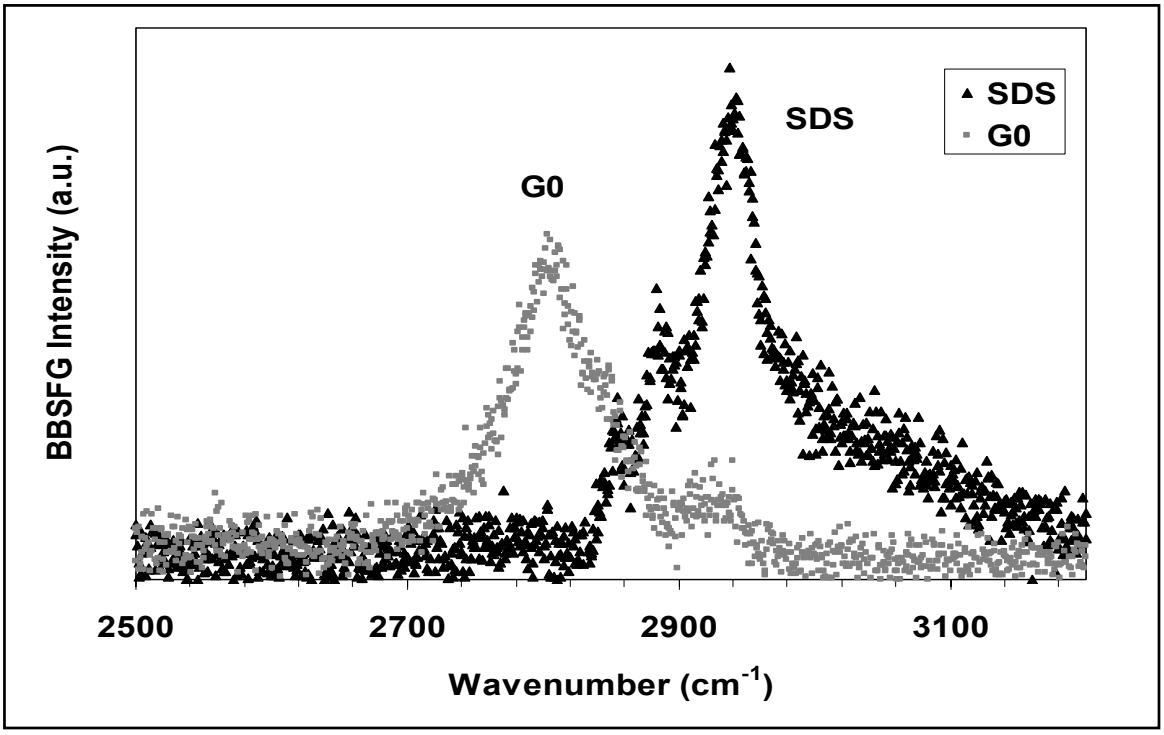

Figure 3.28: BBSFG spectrum (SSP polarization) of a monolayer of sodium dodecyl sulfate (taken from a 1 mM SDS aqueous solution) and a BBSFG spectrum of PAMAM G1 gel using a 2-minute acquisition time. ***(G. Ma)***

The CH_3-fr (2935 cm^{-1}) is the dominant peak in the SDS BBSFG spectrum, the CH_3-ss is much smaller (2872 cm^{-1}), and the CH_2-ss (2844 cm^{-1}) is small relative to the other peaks (CH_2-as is not observed in the SDS spectrum). The intensity of the CH_3-fr and CH_3-ss dominate because the SSP polarization combination couples efficiently with the transition moments that are normal to the surface, in this case, the CH_3-ss. Yet, the CH_2-ss only has a small contribution to the SFG intensity from the SDS since the CH_2-ss on the hydrocarbon chain are in the plane of the surface and since local symmetry cancels their SFG intensities. Therefore, because of local symmetry (the CH_2 groups oppose each other – dominantly s-*trans*-) and because of the lateral direction of the CH_2-SS transition moment, the SFG response is minimal. The small peak that is observed has been attributed to the small number of CH_2 gauche defects in the SDS hydrocarbon chains (Gragson, McCarty et al. 1997). In addition, there are an odd number of methylene groups (eleven) on the SDS hydrocarbon chain, and therefore, even in the instance of a completely s-*trans*- hydrocarbon chain one might expect to observe a CH_2 contribution from the odd CH_2. For the PAMAM G0 spectrum shown with the SDS SFG spectrum in figure 3.28 for comparison, the CH_2-ss peak is substantially larger and broader than that from SDS. One can deduce that the peak broadness is due to the differing chemical environments within the PAMAM G0 dendrimer. The substantial peak intensity implies that there is a net ordering of the CH_2 groups taking place at the surface of the dendrimer gel. This is also confirmed by the facts that the CH_2-as from the PAMAM G0 is relatively small and that the spectrum is dominated by the CH_2-ss. Ordering refers to the net orientation of the methylene groups relative to one another. A purely s-*trans*- configuration would cancel the SFG response. For example: If one CH_2

of the PAMAM pointed out from the surface and another chemically equivalent CH_2 of the PAMAM pointed toward the bulk gel, one would expect cancellation of the SFG response, somewhat similar to that observed for the CH_2-ss in the SDS SFG spectrum of figure 3.28. Any gauche or skewed defects would give rise to a net SFG response from the CH_2-ss modes. Upon examination of PAMAM G0, G1, and AcPAMAM G0, the methylenes occur in groups of two throughout the dendrimer structures. This provides local inversion symmetry only if the two CH_2 groups are exactly s-*trans*- relative to one another. A significant SFG response was observed, which suggests the non-s-*trans* configurations of the adjacent methylene groups. Additionally, since the CH_2-ss are substantially larger than the CH_2-as, it is concluded that the orientations of the CH_2 groups are generally distributed perpendicular to the surface plane. Additional polarization SFG studies are needed to infer the breadth of the distribution about the surface normal. In addition, these findings suggest that the dendritic arms of the PAMAM G0 and G1 extend out in a somewhat planar arrangement, which is consistent with AFM (Hierlemann, Campbell et al. 1998; Lackowski, Campbell et al. 1999; Imae, Ito et al. 2000; Li, Piehler et al. 2000; Sui, Micic et al. 2000; Betley, Holl et al. 2001) and contact angle measurements (Tokuhisa, Zhou et al. 1998; Imae, Ito et al. 2000).

The SFG intensity shown in figures 3.26 and 3.27, and the PAMAM spectrum in figure 3.28 is dominated by the SFG response from the air-dendrimer interface. The reflected visible and infrared beams that interact to produce the SFG intensity can penetrate the dendrimer gel and, in addition to probing the air-dendrimer interface, can also effectively probe the dendrimer-glass interface. However, in the case of the

PAMAM G0 and G1, the thickness of the gel was estimated to encompass multiple layers, so the SFG contribution from the glass surface is not observed.

AcPAMAM G0 at the surface of a glass slide was also studied, and the BBSFG spectrum is shown in figure 3.29. Two BBSFG peaks are observed, 2843 cm^{-1} and 2930 cm^{-1}, and they are attributed to the CH_2–ss modes and CH_3-fr modes, respectively. The shoulder at 2872 cm^{-1} is attributed to the CH_3-ss. One of the major differences between

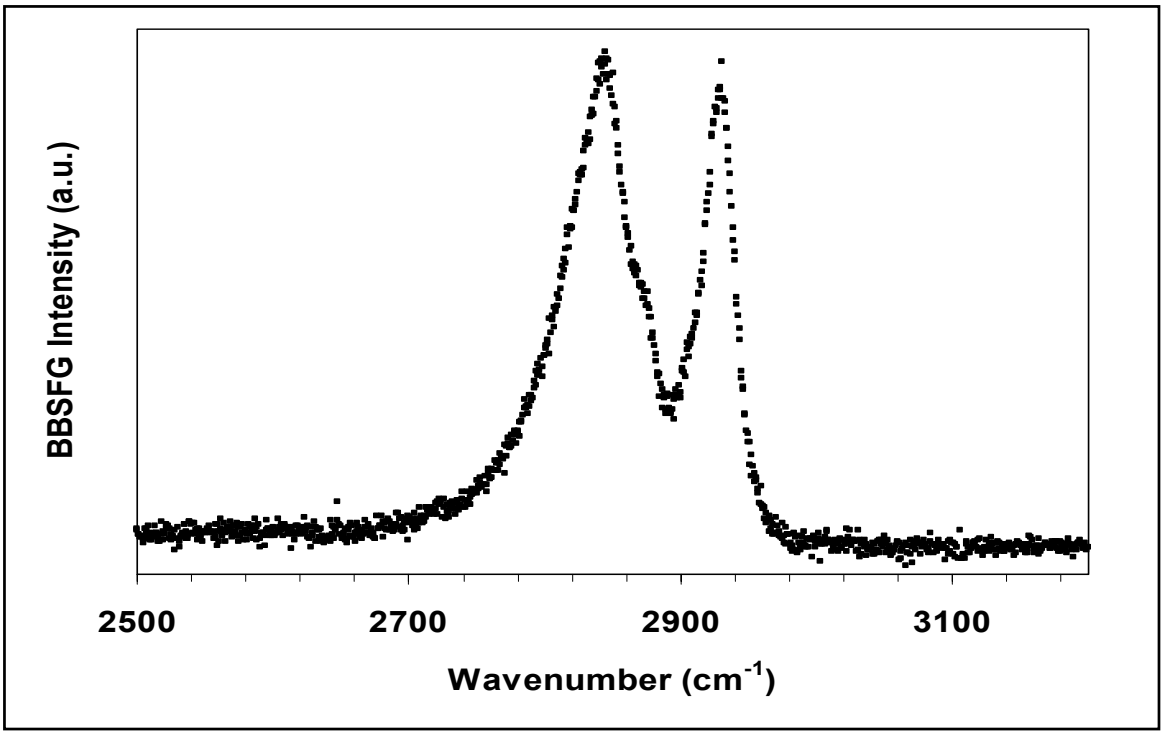

Figure 3.29: BBSFG spectrum (SSP) of AcPAMAM G0 after deposition on a glass slide using a 5-minute acquisition time. ***(G. Ma)***

the SFG spectra of PAMAM G0 and AcPAMAM G0 is that the CH_2-ss peak position has changed. Since SFG responses can interfere constructively or destructively with one another based on their relative phases, the peak position change is not necessarily

significant. These results are preliminary, and fitting the peaks with phase information will help to shed light on the true peak positions. However, it is clear that the CH_3-fr is of significant relative intensity along with the CH_3-ss shoulder on the adjacent peak, and this strongly suggests an ordering of the CH_3 end groups of the dendritic arms. For AcPAMAM G0, each dendrimer contributes four methyl groups and eighteen methylene groups. Since the SFG response arises from a convolution of surface number density and orientation, for similar transition moment strengths, one can infer that a strong SFG response of a low-density moiety suggests a net orientation of this group (*i.e.:* the methyl end groups) relative to the higher density moieties (the methylene groups). This is not necessarily surprising, given the fact that the CH_3 end groups can easily rotate. It is not clear if the CH_3 groups are pointing toward the bulk or toward the air. In addition, the AcPAMAM G0 film is significantly thinner on the glass slide than that used in the PAMAM G0 and G1 BBSFG studies, and it is not as clear if the SFG signal intensity is dominated by the air-dendrimer surface. This is also true for the PAMAM G0 dendrimer film on the gold surface (Figure 3.30). The peaks from the CH_2 stretching modes are observed as dips in the spectrum. The peaks (dips) at 2802 cm^{-1} and at 2943 cm^{-1} are assigned to the CH_2-ss and the CH_2-as respectively and are consistent with the assignments from PAMAM G0 on the glass slide (Figure 3.26) as discussed above. The PAMAM G0 CH_2 peaks are inverted showing that there is a phase mismatch with the nonresonant SFG response from the gold and the resonant response from the dendrimer (Briggman, Stephenson et al. 2001; Lambert, Neivandt et al. 2002). Although the PAMAM G0 dendrimer gel is multilayered on the gold surface (more so than the AcPAMAM G0 on the glass slide), the enhanced reflectivity and recombination of the

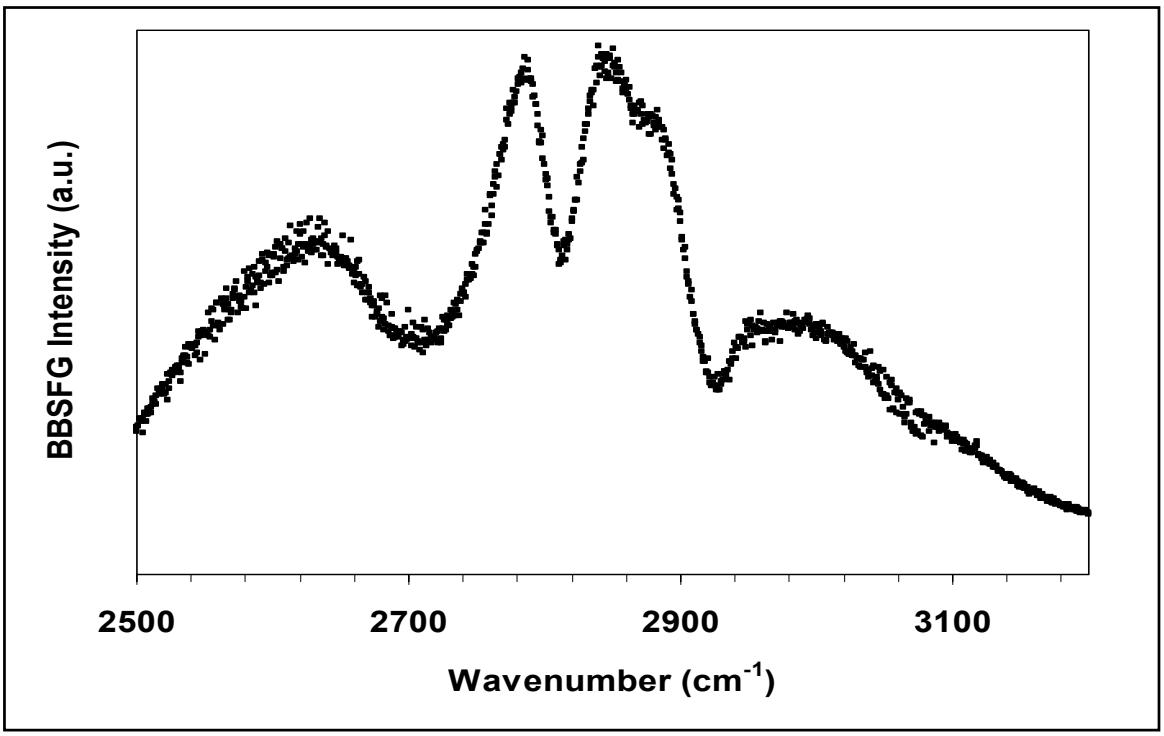

Figure 3.30: BBSFG spectrum (SSP) of PAMAM G0 after deposition on a bare gold surface using a 2-minute acquisition time. ***(G. Ma)***

SFG response from both the air-dendrimer surface and the dendrimer-gold surface will complicate the phase interpretation of this spectrum. This complexity can be deconvoluted upon knowledge of the exact film thickness.

APPENDIX A

VIBSPEC 1.1 COMPUTER PROGRAM

A.1: Introduction. In the computational portion of this study, it became evident that the calculated vibrational frequency and intensity output generated by Gaussian would be more beneficial if it included an observable spectrum to compare with an experimental spectrum. Using the C programming language, a program was written to convert a data text file containing a list of frequencies and relative intensities into another data text file containing x, y coordinates of a spectrum that could be plotted by a program like Microsoft Excel. The Lorentzian profile that was used in the program was of the form:

$$y = \frac{I}{1 + \left(\frac{2 \cdot (\nu - x)}{\Delta \nu} \right)^2} \qquad \text{(A1)}$$

where I represents the calculated intensity, ν represents the calculated frequency, and $\Delta\nu$ represents the broadening factor (Marshall and Verdun 1990). Where more than one Lorentzian profile overlap, VibSpec 1.1 adds the signals to display a combined intensity in the final spectral output. In version 1.0, $\Delta\nu$ was set at 50 cm^{-1}; version 1.1 was updated to allow the user to specify his/her own broadening factor to approximate an observed spectrum. VibSpec 1.1 also prompts the user to enter a scaling factor, the importance of which was documented in work by Scott and Radom (Scott and Radom 1996).

A.2: Program *(written in C programming language)***:**

```
/*  This program will read in a data file containing vibrational
frequencies and intensities calculated from Gaussian, fit them
into Lorentzian profiles, and output a file suitable for graphing
in MS Excel. */

/*  This program is the intellectual property of Anthony P. Davis,
Department of Chemistry, The Ohio State University.  Please do not
distribute, copy, or otherwise alter this program without first
obtaining consent. */

/* Version 1.1 updates allow the user to specify the broadening factor
and a scaling factor to the output spectrum. */

#include <stdio.h>
#include <math.h>
#define NMAX      4096

main()
{
/* Declarations */

      float frequency[NMAX];
      float intensity[NMAX];
      float spectrum[4000];
      float x,y,z;

/* 1.1 update */

      float delta;
      float scale;

/* 1.0 */

      int i,j;
      int modes;
      int nu;

      char filename[32];
      FILE *fp;

/* User interface */

      printf("Vibrational spectrum generation from Gaussian
         calculations:");
      printf("\n\n");

      printf("Name of the file containing the vibrational data?\n");
      scanf("%s",&filename[0]);

      printf("How many vibrational modes are in the file?\n");
      scanf("%d",&modes);
```

```
if((modes<3)||(modes>NMAX)) {
            printf("Number of points must be between 3 and
               %d\n\n",NMAX);
            return(0);
            }

/* 1.1 update */

      printf("What is your scaling factor? (1 is default)\n");
      scanf("%f",&scale);

      printf("What is your broadening factor? (50 is default)\n");
      scanf("%f",&delta);

/* 1.0 */

/* Read in the datafile */

      for(i=1;i<=modes;i++) {
            frequency[i]=0.0;
            intensity[i]=0.0;
            }

      fp = fopen(filename,"r");
      if(fp == 0) {
            printf("Cannot open file %s\n",filename);
            return(0);
            }

      for(i=1;i<=modes;i++) {
            fscanf(fp,"%f     %f",&frequency[i],&intensity[i]);
            }
      fclose(fp);

/* 1.1 update */

      for(i=1;i<=modes;i++)
            frequency[i] = frequency[i] * scale;

/* 1.0 */

      for(i=1;i<=modes;i++) {
            printf("Frequency: %f   Intensity:
               %f\n",frequency[i],intensity[i]);
            }

/* Run Lorentzian function */

      for(i=1;i<=4001;i++) {
            spectrum[i-1]=0.0;
            }
```

```
      for(i=1;i<=modes;i++) {
            nu = frequency[i] - 500.0;
            for(j=1;j<=1000;j++) {
                  nu = nu + 1;
                  if (nu > 0) {
                     x = 2*(frequency[i]-nu)/delta; /* 1.1 update */
                     y = 1+x*x;
                     z = intensity[i]/y;
                     spectrum[nu] = spectrum[nu]+z;
                  }
            }
      }

/* User interface */

      printf("Name of the desired output file?\n");
      scanf("%s",&filename[0]);

/* Generate output file */

      fp = fopen(filename,"w");
      if(fp == 0) {
            printf("Cannot open file %s\n",filename);
            return(0);
            }

      for(i=1;i<=4000;i++) {
            fprintf(fp,"%d \t %f\n",i,spectrum[i]);
            }

      fclose(fp);

      return(0);
}
```

APPENDIX B

VIBRATIONAL MODE FREQUENCY CALCULATIONS

B.1: PAMAM G0.

Ac-En		PAMAM Arm		PAMAM G0	
				2811.064	A s-as
				2816.469	A s-ss
		2865.265	B ss (C/E)	2823.203	Bss/Aas
				2824.615	Bss/Ass
				2828.421	F ss
				2828.444	F ss
2869.2	F ss	2867.563	F ss (B/C)	2865.404	F s-as
				2865.414	F s-ss
				2886.771	B s-as
				2888.887	B s-ss
		2877.397	C ss	2895.023	C s-as
				2895.033	C s-ss
				2904.569	E s-as
				2904.598	E s-ss
				2909.517	C s-ss
				2909.605	C s-as
2911.067	F as (E)	2911.129	F as (E)	2911.859	F a-as
		2919.506	C as (B s)	2911.862	F a-ss
2927.799	E ss	2927.053	E ss (F a)	2929.899	E s-as
				2929.932	E s-ss
				2931.971	C a-as
				2932.123	C a-ss
				2939.642	A as (B/C/E)
				2941.244	C a-as (B)
				2941.552	C a-ss (A/B)
				2950.551	F as (Ea)
				2950.556	F as (Es)
				2951.189	A a-ss (B/C)
				2958.829	B/C a-ss
		2960.771	B as (C)	2959.539	B/C a-as
2975.079	E as (F)	2973.677	E as (F)	2977.556	E a-as
				2977.571	E a-ss

Ac-En		PAMAM Arm		PAMAM G0	
				2983.657	B a-as
				2984.32	B a-ss
				2990.082	E a-ss
				2990.086	E a-ss
3354.759	NH2 ss			3356.007	NH2 ss
		3354.91	NH2 ss (B)	3356.008	NH2 ss
				3359.489	NH2 ss
				3359.493	NH2 ss
3429.81	NH2 as			3431.456	NH2 as
		3429.991	NH2 as (B)	3431.46	NH2 as
				3436.638	NH2 as
				3436.642	NH2 as
3509.863	NH	3499.766	NH	3504.999	NH
				3505.007	NH
				3507.547	NH
				3507.581	NH

B.2: AcPAMAM G0.

diAc-En		AcPAMAM Arm		AcPAMAM G0	
		2860.18	B as	2832.424	B as
				2832.547	B as
				2838.572	Bas/Aas
				2838.768	Bas/Ass
				2846.846	A a-as
2866.31	E ss			2850.698	A a-ss
		2879.92	C ss	2897.016	C s-as
2889.54	E as			2897.156	C s-ss
				2897.729	C s-ss
				2897.764	C s-ss
2891.07	H ss	2900.55	H ss	2898.966	H ss
				2898.97	H ss
				2899.095	H ss
				2899.1	H ss
		2920.22	C as	2927.506	Cas/Aas
				2929.726	C as
				2931.663	C as
				2931.928	C as
		2932.60	E/F sss	2933.446	E/F s-as
				2933.464	E/F s-ss
				2933.618	E/F s-as
				2933.622	E/F s-ss

diAc-En		AcPAMAM Arm		AcPAMAM G0	
		2939.43	E/F s-as	2939.65	E/F s-as
				2939.652	E/F s-as
				2940.445	E/F s-as
				2940.453	E/F s-as
				2941.083	A a-as(Cas)
				2952.969	A a-ss
2942.11	H as	2959.25	H as	2955.929	H as
				2955.93	H as
				2956.087	H as
		2962.71	B as	2956.098	H as
2964.58	F ss	2972.21	E/F a-as	2973.091	E/F a-as
				2973.092	E/F a-as
				2973.125	E/F a-as
				2973.133	E/F a-as
3002.03	H as	2984.96	H as	2989.015	H as
				2989.022	H as
				2989.169	B as
				2989.67	B as
				2989.791	H as
				2989.8	H as
				2992.727	B as
				2993.177	B as
3009.69	F as	2993.36	E/F a-ss	2994.06	E/F a-ss
				2994.095	E/F a-ss
				2994.365	E/F a-ss
				2994.391	E/F a-ss
3483.84	NH	3502.03	NH	3507.517	NH as
				3507.55	NH ss
				3508.357	NH as
				3508.57	NH ss
3494.08	NH	3510.37	NH	3510.308	NH as
				3510.324	NH s-ss
				3510.325	NH ss
				3510.347	NH s-ss

LIST OF REFERENCES

Ahmed, S. M., P. M. Budd, et al. (2001). “Preparation and characterization of a chromophore-bearing dendrimer.” *Polymer* **42**(3): 889-896.

Antonović, D. G., N. D. Stojanović, et al. (1997). "Synthesis and FTIR spectroscopic study of some N-monosubstituted propanamides." *Journal of Molecular Structure* **408/409**(1): 421-423.

Armstrong, J. A., N. Bloembergen, et al. (1962). "Interaction between Light Waves in a Nonlinear Dielectric." *Physical Review* **127**(6): 1918-1939.

Betley, T. A., M. M. B. Holl, et al. (2001). “Tapping Mode Atomic Force Microscopy Investigation of Poly(amidoamine) Dendrimers: Effects of Substrate and pH on Dendrimer Deformation.” *Langmuir* **17**(9): 2768-2773.

Bloembergen, N. and P. S. Pershan (1962). "Light Waves at the Boundary of Nonlinear Media." *Physical Review* **128**(2): 606-622.

Bloembergen, N. (1999). “Surface nonlinear optics: a historical overview.” *Applied Physics. B, Lasers and Optics* **68**(3): 289-293.

Bosman, A. W., H. M. Janssen, et al. (1999). “About Dendrimers: Structure, Physical Properties, and Applications.” *Chemical Reviews* **99**(7): 1665-1688.

Briggman, K. A., J. C. Stephenson, et al. (2001). “Absolute Molecular Orientational Distribution of the Polystyrene Surface.” *Journal of Physical Chemistry. B* **105**(14): 2785-2791.

Chen, H. G. and P. Knochel (1988). “A New Mild Oxidation of Amines to Aldehydes and Ketones. Part II.” *Tetrahedron Letters* **29**(51): 6701-6702.

Chen, W., D. A. Tomalia, et al. (2000). “Unusual pH-Dependent Polarity Changes in PAMAM Dendrimers: Evidence for pH-Responsive Conformational Changes.” *Macromolecules* **33**(25): 9169-9172.

DeJong, R. L., J. G. Davidson, et al. (2001). “The Chemical Development of CI-972 and CI-1000: A Continuous Nitration, A MgCl2/Et3N-Mediated C-Alkylation of a Chloronitropyrimidine, A Catalytic Protodediazotization of a Diazonium Salt, and

an Air Oxidation of an Amine." *Organic Process Research & Development* **5**(3): 216-225.

Dillon, R. E. A. and D. F. Shriver (2001). "Ion Transport and Vibrational Spectra of Branched Polymer and Dendrimer Electrolytes." *Chemistry of Materials* **13**(4): 1369-1373.

Dunn, R. C. (1999). "Near-Field Scanning Optical Microscopy." *Chemical Reviews* **99**(10): 2891-2927.

Dvornic, P. R., A. M. de Leuze-Jallouli, et al. (2000). "Radially Layered Poly(amidoamine-organosilicon) Dendrimers." *Macromolecules* **33**(15): 5366-5378.

Esfand, R. and D. A. Tomalia (2001). "Poly(amidoamine) (PAMAM) dendrimers: from biomimicry to drug delivery and biomedical applications." *Drug Delivery Today* **6**(8): 427-436.

Flörsheimer, M., C. Brillert, et al. (1999). "Chemical imaging of interfaces by sum-frequency generation." *Materials Science and Engineering. C, Biomimetic and supramolecular systems* **8-9**(1): 335-341.

Franken, P. A. and J. F. Ward (1963). "Optical Harmonics and Nonlinear Phenomena." *Reviews of Modern Physics* **35**(1): 23-39.

Ghosh, S. and A. K. Banthia (2001). "Synthesis of photoresponsive polyamidoamine (PAMAM) dendritic architecture." *Tetrahedron Letters* **42**(3): 501-503.

Giorgini, M. G., M. R. Pelletti, et al. (1983). "Vibrational Spectra and Assignments of Ethylene-Diamine and its Deuterated Derivatives." *Journal of Raman Spectroscopy* **14**(1): 16-21.

Gottlieb, H. E., V. Kotlyar, et al. (1997). "NMR Shifts of Common Laboratory Solvents as Trace Impurities." *Journal of Organic Chemistry* **62**(21): 7512-7515.

Gragson, D. E., B. M. McCarty, et al. (1996). "High-power broadly tunable picosecond IR laser system for use in nonlinear spectroscopic applications." *Journal of the Optical Society of America* **13**(9): 2075-2083.

Gragson, D. E., B. M. McCarty, et al. (1997). "Ordering of interfacial water molecules at the charged air/water interface observed by vibrational sum frequency generation." *Journal of the American Chemical Society* **119**(26): 6144-6152.

Gragson, D. E. and G. L. Richmond (1998). "Investigations of the structure and hydrogen bonding of water molecules at liquid surfaces by vibrational sum frequency spectroscopy." *Journal of Physical Chemistry. B* **102**(20): 3847-3861.

Hierlemann, A., J. K. Campbell, et al. (1998). "Structural Distortion of Dendrimers on Gold Surfaces: A Tapping-Mode AFM Investigation." *Journal of the American Chemical Society* **120**(21): 5323-5324.

Hommel, E. L., G. Ma, et al. (2001). "Broadband Vibrational Sum Frequency Generation Spectroscopy of a Liquid Surface." *Analytical Sciences* **17**(11): 1325-1329.

Huang, B. and J. R. Parquette (2000). "Synthesis and Structure of Intramolecularly Hydrogen Bonded Dendrons." *Organic Letters* **2**(3): 239-242.

Imae, T., M. Ito, et al. (2000). "Formation of organized adsorption layers by amphiphilic dendrimers." *Colloids and Surfaces. A, Physicochemical and Engineering Aspects* **175**(3): 225-234.

Ingle, J. D., Jr. and S. R. Crouch (1988). *Spectrochemical Analysis*. Upper Saddle River, NJ, Prentice-Hall, Inc.

Kallos, G. J., D. A. Tomalia, et al. (1991). "Molecular Weight Determination of a Polyamidoamine Starburst Polymer by Electrospray Ionization Mass Spectrometry." *Rapid Communications in Mass Spectrometry* **5**(9): 383-386.

Kovalenko, V. I., V. L. Furer, et al. (2002). "The vibrational spectra of the elementoorganic starburst dendrimers." *Journal of Molecular Structure* **604**(1): 45-56.

Kumar, P., R. K. Pandey, et al. (2000). "Yttria-Zirconia Based Lewis Acid: An Efficient and Chemoselective Catalyst for Acylation Reactions." *Synlett* **2001**(2): 206-209.

Lackowski, W. M., J. K. Campbell, et al. (1999). "Time-Dependent Phase Segregation of Dendrimer/n-Alkylthiol Mixed-Monolayers on Au(111): An Atomic Force Microscopy Study." *Langmuir* **15**(22): 7632-7638.

Lambert, A. G., D. J. Neivandt, et al. (2002). "Interference Effects in Sum Frequency Spectra from Monolayers on Composite Dielectric/Metal Substrates." *Journal of Physical Chemistry. B* **106**(21): 5461-5469.

Larson, C. L. and S. A. Tucker (2001). "Intrinsic Fluorescence of Carboxylate-Terminated Polyamido Amine Dendrimers." *Applied Spectroscopy* **55**(6): 679-683.

Li, J., L. T. Piehler, et al. (2000). "Visualization and Characterization of Poly(amidoamine) Dendrimers by Atomic Force Microscopy." *Langmuir* **16**(13): 5613-5616.

Manna, A., T. Imae, et al. (2001). "Synthesis of Dendrimer-Passivated Noble Metal Nanoparticles in a Polar Medium: Comparison of Size between Silver and Gold Particles." *Chemistry of Materials* **13**(5): 1674-1681.

Marshall, A. G. and F. R. Verdun (1990). *Fourier Transforms in NMR, Optical, and Mass Spectrometry*. New York, NY, Elsevier Science Publishing Company, Inc.

Martin, I. K. and L. J. Twyman (2001). "The synthesis of unsymmetrical PAMAM dendrimers using a divergent/divergent approach." *Tetrahedron Letters* **42**(6): 1119-1121.

Miranda, P. B. and Y. R. Shen (1999). "Liquid Interfaces: A Study by Sum-Frequency Vibrational Spectroscopy." *Journal of Physical Chemistry. B* **103**(17): 3292-3307.

Nagaoka, H. and T. Imae (2001). "Poly(amidoamine) Dendrimer Adsorption onto 3-Mercaptopropionic Acid Self-assembled Monolayer Formed on Au Surface: Investigation by Surface Enhanced Spectroscopy and Surface Plasmon Sensing." *Transactions of the Materials Research Society of Japan* **26**(3): 945-948.

Newkome, G. R., V. V. Narayanan, et al. (1997). "Synthesis and Chemistry of Novel Dendritic Macromolecules Possessing Internal Electroactive Anthraquinoid Moieties." *Macromolecules* **30**(17): 5187-5191.

Noggle, J. H. (1996). *Physical Chemistry, 3rd ed.* New York, NY, Harper Collins College Publishers.

Omura, Y. and T. Shimanouchi (1975). "Skeletal Deformation Vibrations and Rotational Isomerism of Ethylenediamine and Monoethanolamine." *Journal of Molecular Spectroscopy* **57**(3): 480-489.

Pouchert, C. J. (1983). *The Aldrich Library of NMR Spectra, 2nd ed.* Milwaukee, WI, Aldrich Chemical Company, Inc.

Rahman, K. M. A., C. J. Durning, et al. (2000). "Adsorption of Poly(amidoamine) Dendrimers on Gold." *Langmuir* **16**(26): 10154-10160.

Recker, J., D. J. Tomcik, et al. (2000). "Folding Dendrons: The Development of Solvent-, Temperature-, and Generation-Dependent Chiral Conformational Order in Intramolecularly Hydrogen-Bonded Dendrons." *Journal of the American Chemical Society* **122**(42): 10298-10307.

Richter-Egger, D., A. Tesfai, et al. (2001). "Spectroscopic Investigations of Poly(Propyleneimine) Dendrimers Using the Solvatochromic Probe Phenol Blue and Comparisons to Poly(Amidoamine) Dendrimers." *Analytical Chemistry* **73**(23): 5743-5751.

Ruckenstein, E. and W. Yin (2000). "SiO2-Poly(amidoamine) Dendrimer Inorganic/Organic Hybrids." *Journal of Polymer Science. Part A, Polymer Chemistry* **38**(9): 1443-1449.

Sayed-Sweet, Y., D. M. Hedstrand, et al. (1997). "Hydrophobically modified poly(amidoamine) (PAMAM) dendrimers: their properties at the air-water interface and use as nanoscopic container molecules." *Journal of Materials Chemistry* **7**(7): 1199-1205.

Scott, A. P. and L. Radom (1996). "Harmonic Vibrational Frequencies: An Evaluation of Hartree-Fock, Moller-Plesset, Quadratic Configuration Interaction, Density Functional Theory, and Semiempirical Scale Factors." *Journal of Physical Chemistry* **100**(41): 16502-16513.

Service, R. F. (1995). "Dendrimers: Dream Molecules Approach Real Applications." *Science* **267**(5197): 458-459.

Skoog, D. A. and J. J. Leary (1992). *Principles of Instrumental Analysis, 4th ed.* Fort Worth, TX, Saunders College Publishing.

Steglich, W., G. Hoefle (1969). "N,N-Dimethyl-4-pyridinamine, a very effective acylation catalyst." *Angewandte Chemie* **8**(12): 981.

Sui, G., M. Micic, et al. (2000). "Synthesis and Surface Chemistry Study of a New Amphiphilic PAMAM Dendrimer." *Langmuir* **16**(20): 7847-7851.

Tokuhisa, H., M. Zhou, et al. (1998). "Preparation and Characterization of Dendrimer Monolayers and Dendrimer-Alkanethiol Mixed Monolayers Adsorbed to Gold." *Journal of the American Chemical Society* **120**(18): 4492-4501.

Tomalia, D. A. (1995). "Dendrimer Molecules." *Scientific American* **272**(5): 62-66.

Topp, A., B. J. Bauer, et al. (1999). "Probing the Location of the Terminal Groups of Dendrimers in Dilute Solution." *Macromolecules* **32**(21): 7226-7231.

Topp, A., B. J. Bauer, et al. (1999). "Effect of Sovent Quality on the Molecular Dimensions of PAMAM Dendrimers." *Macromolecules* **32**(21): 7232-7237.

Tully, D. C. and J. M. J. Fréchet (2001). "Dendrimers at surfaces and interfaces: chemistry and applications." *Chemical Communications* **2001**(14): 1229-1239.

Wade, D. A., P. A. Torres, et al. (1999). "Spectrochemical investigations in dendritic media: evaluation of nitromethane as a selective fluorescence quenching agent in aqueous carboxylate-terminated polyamido amine (PAMAM) dendrimers." *Analytica Chimica Acta* **397**(1-3): 17-31.

Wade, L. G. J. (1999). *Organic Chemistry, 4th ed.* Upper Saddle River, NJ, Prentice-Hall, Inc.

Wells, M. and R. M. Crooks (1996). "Interactions between Organized, Surface-Confined Monolayers and Vapor-Phase Probe Molecules. 10. Preparation and Properties of Chemically Sensitive Dendrimer Surfaces." *Journal of the American Chemical Society* **118**(16): 3988-3989.

Zeng, F. and S. C. Zimmerman (1997). "Dendrimers in Supramolecular Chemistry: From Molecular Recognition to Self-Assembly." *Chemical Reviews* **97**(5): 1681-1712.

Zhou, R. X., B. Du, et al. (1999). "In vitro release of 5-fluorouracil with cyclic core dendritic polymer." *Journal of Controlled Release* **57**(3): 249-257.